Journal of Scientific Computing (2023) 95:67
https://doi.org/10.1007/s10915-023-02185-7

Modeling and a Domain Decomposition Method with Finite Element Discretization for Coupled Dual-Porosity Flow and Navier–Stokes Flow

Jiangyong Hou[1] · Dan Hu[2] · Xuejian Li[3] · Xiaoming He[3]

Received: 4 October 2022 / Revised: 19 February 2023 / Accepted: 18 March 2023

Abstract
In this paper, we first propose and analyze a steady state Dual-Porosity-Navier–Stokes model, which describes both Dual-Porosity flow and free flow (governed by Navier–Stokes equation) coupled through four interface conditions, including the Beavers–Joseph interface condition. Then we propose a domain decomposition method for efficiently solving such a large complex system. Robin boundary conditions are used to decouple the Dual-Porosity equations from the Navier–Stokes equations in the coupled system. Based on the two decoupled subproblems, a parallel Robin-Robin domain decomposition method is constructed and then discretized by finite elements. We analyze the convergence of the domain decomposition method with the finite element discretization and investigate the effect of Robin parameters on the convergence, which also provide instructions for how to choose the Robin parameters in practice. Three cases of Robin parameters are studied, including a difficult case which was not fully addressed in the literature, and the optimal geometric convergence rate is obtained. Numerical experiments are presented to verify the theoretical conclusions, illustrate how the theory can provide instructions on choosing Robin parameters, and show the features of the proposed model and domain decomposition method.

Keywords Dual-Porosity-Navier–Stokes flow · Interface conditions · Domain decomposition method · Finite elements

1 Introduction

The investigation of fluid flows within a complicated porous medium coupled with conduit system is of significance in many applications, such as groundwater flow system

✉ Xiaoming He
hex@mst.edu

[1] School of Mathematics, Northwest University, Xi'an 710127, Shaanxi, People's Republic of China

[2] School of Sciences, Xi'an University of Technology, Xi'an 710048, Shaanxi, People's Republic of China

[3] Mathematics and Statistics, Missouri University of Science and Technology, Rolla, MO 65409, USA

Published online: 17 April 2023

[1], petroleum extraction [2], industrial filtration [3], etc. It is not an easy job to build a mathematically and physically reasonable model for the coupled flow problem in such coupled system, especially for the problems with complicated porous media including multi-porosity and multi-permeability properties. During the past decades a number of related fluid dynamical models were built by scientists and engineers, including Stokes–Darcy model, Navier–Stokes–Darcy model, Stokes–Darcy-transport model, Dual-Porosity-Stokes model, two-phase Stokes–Darcy models, stochastic Stokes–Darcy model, and so on [4–18]. Meanwhile, there are many numerical methods developed to solve these Stokes–Darcy type systems, which basically include two classes of strategy: the coupled numerical methods [19–22] and the decoupled numerical methods [23–29].

The widely used Darcy model is usually an averaged single porosity/permeability model for the fluid flow in the porous media region. However, it has the limitations to describe complicated geometrical structures of the porous media, especially naturally fractured porous media which contain the multi-porosity/permeability regions [30]. The hydraulically fractured reservoirs, such as shale gas reservioirs, usually have multiscaled pore spaces with different fractures properties, including matrix pores, natural fractures, and vugs. The first multi-porosity model was proposed by Barenblatt for the naturally fractured reservoir where the micro-fracture and matrix systems are formulated by individual but overlapping continua [31]. Based on Barenblatt's model, Warren developed a homogeneous orthotropic Dual-Porosity model in 1963 [32], which was utilized for many applications, such as the geothermal system, hydrogeology, petroleum industry, tight/shale oil/gas reservoirs, and so on. In [33], the authors consider the flow in macro-fractures and vugs and define a kind of triple porosity model for fractured horizontal wells by three sequentially coupled Darcy models. There are other Darcy-type models for describing multi-porosity/permeability media, such as multi-continuum models [34], multiple interacting continua (MINC) models [35], discrete fracture-matrix models [36], mixed-dimensional models [37], mixed-dimensional poromechanical models [38], and so on. However, all these porous media models do not consider the free flow in large conduits, and the wellbore is simplified as the source and sink terms on the right hand side of Darcy equations. On the other hand, the existing Stokes–Darcy or Navier–Stokes–Darcy models do not consider multi-porosity when they couple the porous media flow with the free flow in channels. In practice, there are many real world applications which involve with the coupling between the multi-porosity flow and the free flow in large conduits. For example, the shale oil reservoir simulation with multi-stage fractured horizontal wellbore obviously involve the multi-porosity flow in the shale reservoir and the channel flow in the horizontal wellbore [39].

Therefore, a coupled time-dependent Dual-Porosity-Stokes model with the Beavers-Joseph (BJ) interface condition [40] was recently proposed in [41], where the Dual-Porosity model instead of the single-porosity Darcy model is utilized to govern the flow in the porous media and couples with the Stokes equation via four multi-physical interface conditions. Among these interface conditions, the BJ condition takes into account the coupling between the fracture flow velocity and the free flow velocity along the tangent of interface, which brings an indefinite term to the equation system and requires the BJ constant α to be small enough for the wellposedness of the steady-state model, see [42, 43] for more details about the restriction of α. In [41], the traditional coupled finite element method is utilized to solve and illustrate the new Dual-Porosity-Stokes model. But for such a sophisticated multi-physics model, more efficient decoupled numerical methods are in great needs. Among the existing decoupled algorithms, the domain decomposition methods are very natural to be considered for decoupling the Dual-Porosity-Stokes and Dual-Porosity-Navier–Stokes

models, since the problem domain naturally consists of two different subdomains, see [44–48] and references therein for various domain decomposition works on the Stokes–Darcy model and Navier–Stokes–Darcy model. For the time-dependent Dual-Porosity-Navier–Stokes model, a non-iterative Robin-type decoupled finite element method was studied [49]. For the steady-state Dual-Porosity-Stokes model with the simplified Beavers–Joseph-Saffman (BJS) interface condition [50, 51], the optimized Schwarz method was studied in [52].

However, the convergence analysis of the iterative Robin–Robin domain decomposition methods for steady-state problems in [47, 52, 53] was carried out at the continuous level without considering the finite element discretization. And they did not discuss all the cases, due to a major difficulty for one case, which is important for the realistic parameters as illustrated in [53]. Recently, in [54], this difficult case was analyzed at the discrete level for the steady-state Stokes–Darcy model with the BJ condition, and an almost optimal geometric convergence rate was derived. In the analysis of [54], two inverse inequalities were used to reach complicated and vague Robin parameter restrictions, and the mesh size needs to be larger than the permeability and viscosity. In this paper, we will utilize a different inverse inequality and further improve the analysis directly at the discrete level with the finite element discretization for the more difficult Dual-Porosity-Navier–Stokes model with the BJ condition. Hence we will be able to remove the restriction on the mesh size, reach the optimal geometric convergence rate, and obtain more precise Robin parameter restrictions, which can provide easier instructions on choosing the important Robin parameters. These are the major contributions of this paper for the convergence analysis part, in addition to the other major contributions in the wellposedness of the steady-state Dual-Porosity-Navier–Stokes model with the BJ condition as well as the corresponding algorithm development and validation.

More specifically, we will first analyze the wellposedness of the steady-state Dual-Porosity-Navier–Stokes model with the BJ condition, based on an elegant framework of variational analysis for the Navier–Stokes–Darcy model with the simplified BJS condition in [12]. Then based on two Robin type transmission conditions, we propose the iterative Robin-type domain decomposition method for decoupling Dual-Porosity equations and Navier-Stokes equations. From the investigations about the effect of Robin parameters on the convergence in [26, 52, 53], we know that the Robin-type algorithm is very sensitive to small model parameters and the robustness of the algorithm is significantly affected by the Robin parameters (γ_c and γ_d, see Sect. 3.1 for the detailed definition) under small permeability and viscosity. Therefore, we will analyze the convergence of the proposed method with finite element discretization for all three cases of Robin parameters including $\gamma_c < \gamma_d$, $\gamma_c = \gamma_d$ and $\gamma_c > \gamma_d$, and obtain the optimal geometric convergence rate for the cases $\gamma_c < \gamma_d$ and $\gamma_c > \gamma_d$. For the most difficult case $\gamma_c > \gamma_d$, we present a more accurate and simpler approach than the approach provided in [54] to obtain the optimal geometric convergence rate instead of the almost optimal geometric convergence rate. Specifically, we first prove the inverse inequality for the dual porosity model which is more difficult than the Darcy model. With the help of Young's inequality, we can obtain a more accurate estimate than the estimate for the Darcy model in [26, 54], and can get rid of the lower bound constraints of the mesh size required in [54]. Secondly, by choosing appropriate scaling parameter, we can get rid of the inverse inequality of the Stokes equation that must be used in the proof in [54], so that the unnecessary complexity in the analysis is greatly simplified. More importantly, the optimal geometric convergence rate is obtained due to the two aspects above.

The analysis result provides a general guideline of choice on the Robin parameters to obtain the convergence and geometric convergence rate. The numerical experiments will be provided to illustrate and validate the convergence and applicability of the proposed method.

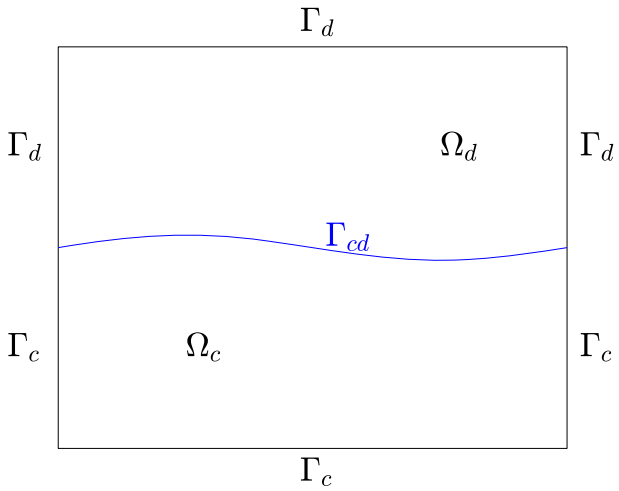

Fig. 1 A sketch of the dual porous media domain Ω_d, the free-flow domain Ω_c, and the interface Γ_{cd}. Define the boundaries $\Gamma_d = \partial\Omega_d / \Gamma_{cd}$ and $\Gamma_c = \partial\Omega_c / \Gamma_{cd}$

In the first experiment, the convergence of all the cases are verified by a mathematical example with known analytic solutions. And the realistic parameters are also considered. In the second and third experiments, we use a more realistic case with more complicated geometries to validate the proposed model and method.

The rest of paper is organized as follows. In Sect. 2, we introduce the Dual-Prosity-Navier–Stokes system and analyze its wellposedness. In Sect. 3, we propose and analyze the Robin type domain decomposition method in three subsections. In Sect. 4, numerical experiments are provided. In Sect. 5, we draw the conclusions.

2 Steady Dual-Porosity-Navier–Stokes Model

2.1 Mathematical Model and Weak Formulation

We consider the coupled Dual-Porosity-Navier–Stokes system on a bounded domain $\Omega = \Omega_d \cup \Omega_c \subset \mathbb{R}^{\mathbf{d}}$, $(\mathbf{d} = 2, 3)$, see Fig. 1.

In the porous media region Ω_d, the flow is governed by the Dual-Porosity system [32]

$$-\nabla \cdot \left(\frac{k_m}{\mu} \nabla p_m \right) = -Q, \tag{2.1}$$

$$-\nabla \cdot \left(\frac{k_f}{\mu} \nabla p_f \right) = Q + q_p. \tag{2.2}$$

Here $Q = \frac{\sigma k_m}{\mu} \left(p_m - p_f \right)$ is a mass exchange term between matrix and micro-fractures porosity, σ is a shape factor associated with the cut rocks and orthogonal fractures, p_m (p_f) is the pressure in matrix (micro-fracture), k_m (k_f) is the intrinsic permeability in matrix (micro-fracture), μ is the dynamic viscosity, and q_p is the sink/source term.

In the fluid region Ω_c, the fluid flow is assumed to satisfy the Navier–Stokes system [55–57]

$$(\mathbf{u}\cdot\nabla)\,\mathbf{u}-\nabla\cdot\mathbb{T}\,(\mathbf{u},\,p)=\mathbf{f}, \tag{2.3}$$

$$\nabla\cdot\mathbf{u}=0, \tag{2.4}$$

where $\mathbf{u}$ is the fluid velocity, p is the kinematic pressure, $\mathbf{f}$ is the external body force, $\mathbb{T}\,(\mathbf{u},\,p)=2\nu\mathbb{D}\,(\mathbf{u})-\frac{1}{\rho}p\mathbb{I}$ is the stress tensor, $\mathbb{D}\,(\mathbf{u})=1/2\left(\nabla\mathbf{u}+(\nabla\mathbf{u})^T\right)$ is the deformation tensor, $\mathbb{I}$ is the identity matrix, ν is the kinematic viscosity of the fluid and ρ is the fluid density, $\nu=\frac{\mu}{\rho}$.

Let $\Gamma_{cd}=\overline{\Omega}_d\cap\overline{\Omega}_c$ denote the interface between the fluid and dual porous media regions. On the interface Γ_{cd}, we consider the following four interface conditions [41]:

$$-\frac{k_m}{\mu}\nabla p_m\cdot(-\mathbf{n}_{cd})=0, \tag{2.5}$$

$$-\frac{k_f}{\mu}\nabla p_f\cdot\mathbf{n}_{cd}=\mathbf{u}\cdot\mathbf{n}_{cd}, \tag{2.6}$$

$$-\mathbf{n}_{cd}^T\mathbb{T}\,(\mathbf{u},\,p)\,\mathbf{n}_{cd}+\frac{1}{2}\mathbf{u}\cdot\mathbf{u}=\frac{1}{\rho}p_f, \tag{2.7}$$

$$-P_\tau\left(\mathbb{T}\,(\mathbf{u},\,p)\,\mathbf{n}_{cd}\right)=\frac{\alpha\nu\sqrt{\mathbf{d}}}{\sqrt{\text{trace}\,(\prod)}}P_\tau\left(\mathbf{u}+\frac{k_f}{\mu}\nabla p_f\right), \tag{2.8}$$

where $\mathbf{n}_{cd}$ denotes the unit outer normal to the fluid region Ω_c on the interface Γ_{cd}, α is a constant parameter, $\prod$ is the intrinsic permeability of fracture media and equal to $\prod=k_f\mathbb{I}$, $\mathbf{d}$ is the spatial dimension, and P_τ denotes the projection onto the local tangent plane on Γ_{cd}, i.e.,

$$P_\tau\mathbf{u}=\sum_{j=1}^{\mathbf{d}-1}(\mathbf{u}\cdot\tau_j)\tau_j,$$

with τ_j $(j=1,\ldots,\mathbf{d}-1)$ being the unit tangential vector on the local tangent planes of Γ_{cd}. The first interface condition (2.5) is a no-exchange condition which means no flux could go across the interface from matrix system directly to the conduits. We refer readers to [41] for more justification of this assumption of the Dual-Porosity model [32]. The interface condition (2.6) stands for the conservation of mass between the micro-fractures and the conduits. The condition (2.7) describes the balance of the forces in the normal direction. The last condition (2.8) is referred to as the Beavers–Joseph interface condition [40].

For simplicity, we assume that the matrix pressure p_m, the fracture pressure p_f and the fluid velocity $\mathbf{u}$ satisfy homogeneous Dirichlet boundary condition except on Γ_{cd}, i.e., $p_m=0$ and $p_f=0$ on the boundary Γ_d and $\mathbf{u}=0$ on the boundary Γ_c.

We define the functional spaces

$$\Psi_0:=\{\psi\in H^1(\Omega_d):\psi=0\text{ on }\Gamma_d\},\quad \mathbf{V}_0:=\{\mathbf{v}\in H^1(\Omega_c)^{\mathbf{d}}:\mathbf{v}=0\text{ on }\Gamma_c\},$$
$$\mathbf{V}_{div}:=\{\mathbf{v}\in\mathbf{V}_0:\nabla\cdot\mathbf{v}=0\},\quad M:=L^2(\Omega_c),\quad \mathbf{X}_0:=\Psi_0\times\Psi_0\times\mathbf{V}_0,\quad \mathbf{Y}_0$$
$$:=\Psi_0\times\Psi_0\times\mathbf{V}_{div},$$

and the corresponding norms

$$\|\psi\|_1 := \|\psi\|_{H^1(\Omega_d)}, \quad \forall \psi \in \Psi_0, \tag{2.9}$$

$$\|\mathbf{v}\|_1 := \left(\sum_{i=1}^{\mathbf{d}} \|v_i\|^2_{H^1(\Omega_c)}\right)^{1/2}, \quad \forall \mathbf{v} = \{v_i\}_{i=1}^{\mathbf{d}} \in \mathbf{V}_0, \tag{2.10}$$

$$\|q\|_0 := \|q\|_{L^2(\Omega_c)}, \quad \forall q \in M, \tag{2.11}$$

$$\left\|\overrightarrow{\mathbf{v}}\right\|_{\mathbf{X}_0} := \left(\|\psi_m\|_1^2 + \left\|\psi_f\right\|_1^2 + \|\mathbf{v}\|_1^2\right)^{1/2}, \quad \forall \overrightarrow{\mathbf{v}} = (\psi_m, \psi_f, \mathbf{v}) \in \mathbf{X}_0, \tag{2.12}$$

$$\left\|\overrightarrow{\mathbf{v}}\right\|_{\mathbf{L}^2} := \left(\|\psi_m\|^2_{L^2(\Omega_d)} + \left\|\psi_f\right\|^2_{L^2(\Omega_d)} + \|\mathbf{v}\|^2_{L^2(\Omega_c)}\right)^{1/2}, \quad \forall \overrightarrow{\mathbf{v}} = (\psi_m, \psi_f, \mathbf{v}) \in \mathbf{X}_0, \tag{2.13}$$

$$\left\|\overrightarrow{\mathbf{v}}\right\|_{\mathbf{Y}_0} := \left(\frac{k_m}{\rho\mu}\|\nabla\psi_m\|^2_{L^2(\Omega_d)} + \frac{k_f}{\rho\mu}\left\|\nabla\psi_f\right\|^2_{L^2(\Omega_d)} + 2\nu\|\mathbb{D}(\mathbf{v})\|^2_{L^2(\Omega_c)}\right)^{1/2}, \quad \forall \overrightarrow{\mathbf{v}} = (\psi_m, \psi_f, \mathbf{v}) \in \mathbf{Y}_0. \tag{2.14}$$

We also need the trace space defined as $\mathbf{H}_{00}^{\frac{1}{2}}(\Gamma_{cd}) := \mathbf{V}_0|_{\Gamma_{cd}}$, which is a non-closed subspace of $\mathbf{H}^{\frac{1}{2}}(\Gamma_{cd})$ and has a continuous zero extension to $\mathbf{H}^{\frac{1}{2}}(\partial\Omega_c)$, see [42, 43].

For the domain D ($D = \Omega_c$ or Ω_d), $(\cdot,\cdot)_D$ denotes the L^2 inner product on the domain D, and $\langle\cdot,\cdot\rangle$ denotes the L^2 inner product on the interface Γ_{cd} or the duality pairing between $\left(\mathbf{H}_{00}^{\frac{1}{2}}(\Gamma_{cd})\right)'$ and $\mathbf{H}_{00}^{\frac{1}{2}}(\Gamma_{cd})$. With these notations, the weak formulation of the coupled steady-state Dual-Porosity-Navier–Stokes problem is given as follows: find $\left(\overrightarrow{\mathbf{u}}, p\right) \in \mathbf{X}_0 \times M$, such that

$$c\left(\overrightarrow{\mathbf{u}}, \overrightarrow{\mathbf{u}}, \overrightarrow{\mathbf{v}}\right) + a\left(\overrightarrow{\mathbf{u}}, \overrightarrow{\mathbf{v}}\right) + b\left(\overrightarrow{\mathbf{v}}, p\right) = \ell\left(\overrightarrow{\mathbf{v}}\right), \quad \forall \overrightarrow{\mathbf{v}} \in \mathbf{X}_0, \tag{2.15}$$

$$b\left(\overrightarrow{\mathbf{u}}, q\right) = 0, \quad \forall q \in M. \tag{2.16}$$

The trilinear form is defined as

$$c\left(\overrightarrow{\mathbf{w}}, \overrightarrow{\mathbf{u}}, \overrightarrow{\mathbf{v}}\right) = ((\mathbf{w}\cdot\nabla)\mathbf{u}, \mathbf{v})_{\Omega_c} - \frac{1}{2}\langle\mathbf{w}\cdot\mathbf{u}, \mathbf{v}\cdot\mathbf{n}_{cd}\rangle, \tag{2.17}$$

for arbitrary $\overrightarrow{\mathbf{u}} = \left(p_m, p_f, \mathbf{u}\right)$, $\overrightarrow{\mathbf{v}} = \left(\psi_m, \psi_f, \mathbf{v}\right)$ and $\overrightarrow{\mathbf{w}} = \left(\phi_m, \phi_f, \mathbf{w}\right)$ in $\mathbf{X}_0$. Based on (3.3) in [47], we have

$$c\left(\overrightarrow{\mathbf{v}}, \overrightarrow{\mathbf{v}}, \overrightarrow{\mathbf{v}}\right) = 0. \tag{2.18}$$

The bilinear forms and linear form are defined respectively as,

$$\begin{aligned} a\left(\overrightarrow{\mathbf{u}}, \overrightarrow{\mathbf{v}}\right) =& \eta\left(\frac{k_m}{\mu}\nabla p_m, \nabla\psi_m\right)_{\Omega_d} \\ &+ \eta\left(\frac{k_f}{\mu}\nabla p_f, \nabla\psi_f\right)_{\Omega_d} \\ &+ 2\nu\left(\mathbb{D}(\mathbf{u}), \mathbb{D}(\mathbf{v})\right)_{\Omega_c} \\ &+ \eta\left(\frac{\sigma k_m}{\mu}\left(p_m - p_f\right), \psi_m\right)_{\Omega_d} \\ &+ \eta\left(\frac{\sigma k_m}{\mu}\left(p_f - p_m\right), \psi_f\right)_{\Omega_d} + \left\langle\frac{1}{\rho}p_f, \mathbf{v}\cdot\mathbf{n}_{cd}\right\rangle \end{aligned}$$

$$- \eta \left\langle \mathbf{u} \cdot \mathbf{n}_{cd}, \psi_f \right\rangle + \frac{\alpha \nu \sqrt{\mathbf{d}}}{\sqrt{\text{trace}\left(\prod\right)}} \left\langle P_\tau \left(\mathbf{u} + \frac{k_f}{\mu} \nabla p_f \right), P_\tau \mathbf{v} \right\rangle, \tag{2.19}$$

$$b\left(\overrightarrow{\mathbf{v}}, p\right) = -\frac{1}{\rho} \left(\nabla \cdot \mathbf{v}, p\right)_{\Omega_c}, \tag{2.20}$$

$$\ell\left(\overrightarrow{\mathbf{v}}\right) = \left(\mathbf{f}, \mathbf{v}\right)_{\Omega_c} + \eta \left(q_p, \psi_f\right)_{\Omega_d}, \tag{2.21}$$

for arbitrary $\overrightarrow{\mathbf{u}} = \left(p_m, p_f, \mathbf{u}\right)$ and $\overrightarrow{\mathbf{v}} = \left(\psi_m, \psi_f, \mathbf{v}\right)$ in $\mathbf{X}_0$. The integral $\left\langle P_\tau \left(\frac{k_f}{\mu} \nabla \psi_f \right), P_\tau \mathbf{v} \right\rangle$ on Γ_{cd} is understood to be the value of the functional $P_\tau \left(\frac{k_f}{\mu} \nabla \psi_f \right) |_{\Gamma_{cd}} \in \left(\mathbf{H}_{00}^{\frac{1}{2}} \left(\Gamma_{cd}\right) \right)'$ applied to $\mathbf{v}|_{\Gamma_{cd}} \in \mathbf{H}_{00}^{\frac{1}{2}} \left(\Gamma_{cd}\right)$, which is well defined when $k_f \mathbb{I}$ is isotropic, see [43] and the references cited therein. We remark that for simplicity the scaling factor η multiplied to the Dual-Porosity equations is set to $1/\rho$ in the later proof.

2.2 Well-Posedness of the Model

To prepare for the analysis, we recall the following Poincaré inequality, Korn's inequality, trace inequality, and Sobolev inequalities: there exist constants $C_p, C_k, C_t, C_s, D_t, E_t$, which only depend on the domain Ω_c, and $\tilde{C}_p, \tilde{C}_t, \tilde{C}_\tau, \tilde{D}_t$, which only depend on the domain Ω_d, such that for all $\psi \in \Psi_0$ and $\mathbf{v} \in \mathbf{V}_0$,

$$\begin{aligned} \|\mathbf{v}\|_{L^2(\Omega_c)} &\leq C_p \|\nabla \mathbf{v}\|_{L^2(\Omega_c)}, \\ \|\psi\|_{L^2(\Omega_d)} &\leq \tilde{C}_p \|\nabla \psi\|_{L^2(\Omega_d)}, \end{aligned} \tag{2.22}$$

$$\|\nabla \mathbf{v}\|_{L^2(\Omega_c)} \leq C_k \|\mathbb{D}(\mathbf{v})\|_{L^2(\Omega_c)}, \tag{2.23}$$

$$\begin{aligned} &\|\mathbf{v}\|_{1/2,\Gamma_{cd}} \leq C_t \|\nabla \mathbf{v}\|_{L^2(\Omega_c)}, \\ &\|\psi\|_{1/2,\Gamma_{cd}} \leq \tilde{C}_t \|\nabla \psi\|_{L^2(\Omega_d)}, \quad \|\nabla_\tau \psi\|_{-1/2,\Gamma_{cd}} \leq \tilde{C}_\tau \|\nabla \psi\|_{L^2(\Omega_d)}, \end{aligned} \tag{2.24}$$

$$\|\mathbf{v}\|_{L^2(\Gamma_{cd})} \leq D_t \|\nabla \mathbf{v}\|_{L^2(\Omega_c)}, \quad \|\psi\|_{L^2(\Gamma_{cd})} \leq \tilde{D}_t \|\nabla \psi\|_{L^2(\Omega_d)}, \tag{2.25}$$

$$\|\mathbf{v}\|_{L^4(\Gamma_{cd})} \leq E_t \|\nabla \mathbf{v}\|_{L^2(\Omega_c)}, \quad \|\mathbf{v}\|_{L^4(\Omega_c)} \leq C_s \|\nabla \mathbf{v}\|_{L^2(\Omega_c)}, \tag{2.26}$$

where $\nabla_\tau \psi$ stands for the tangential derivative of ψ and is defined in the dual space of $\mathbf{H}_{00}^{1/2} \left(\Gamma_{cd}\right)$, see [42] and the references therein for more details.

Lemma 2.1 *The bilinear functional $b(\cdot, \cdot)$ is continuous on $\mathbf{X}_0 \times M$ and satisfies the inf-sup condition, that is, there exists a constant $\beta > 0$ such that*

$$\inf_{0 \neq q \in M} \sup_{\mathbf{0} \neq \overrightarrow{\mathbf{v}} \in \mathbf{X}_0} \frac{|b\left(\overrightarrow{\mathbf{v}}, q\right)|}{\|q\|_M \left\| \overrightarrow{\mathbf{v}} \right\|_{\mathbf{X}_0}} \geq \beta. \tag{2.27}$$

By the similar arguments in [41], we can obtain the following lemma.

Lemma 2.2 *Assume that $\mathbf{f} \in L^2(\Omega_c)^{\mathbf{d}}$, $q_p \in L^2(\Omega_d)$. Then the solution $\left(\overrightarrow{\mathbf{u}}, p\right) \in \mathbf{X}_0 \times M$ of (2.1)-(2.8) is equivalent to the solution of the weak problem (2.15)-(2.16).*

Next, we follow the framework in [12] for the Navier–Stokes–Darcy model to obtain the existence of the weak solution of (2.15)-(2.16). By restricting the test functions $\mathbf{v}$ in (2.15)-(2.16) on the divergence-free subspace $\mathbf{V}_{div}$, we have the following variational equations:

find $\overrightarrow{\mathbf{u}} \in \mathbf{Y}_0$, such that

$$c\left(\overrightarrow{\mathbf{u}}, \overrightarrow{\mathbf{u}}, \overrightarrow{\mathbf{v}}\right) + a\left(\overrightarrow{\mathbf{u}}, \overrightarrow{\mathbf{v}}\right) = \ell\left(\overrightarrow{\mathbf{v}}\right), \quad \forall \overrightarrow{\mathbf{v}} \in \mathbf{Y}_0. \tag{2.28}$$

Based on Lemma 2.1, the reduced problem (2.28) and the problem (2.15)-(2.16) are equivalent, therefore it suffices to prove the existence and uniqueness of a weak solution of problem (2.28).

The following theorems concern the existence and uniqueness of solution to the problem (2.28). Since the proof is pretty standard [12], we omit it here due to the page limitation.

Theorem 2.3 *Let α be small enough so that $\alpha \tilde{C}_\tau C_t C_k \leq 1$, and $\mathcal{R}$ be the following constant*

$$\mathcal{R} = \left(\frac{2C_p^2 C_k^2}{\nu} \|\mathbf{f}\|^2_{L^2(\Omega_c)} + \frac{2\nu \tilde{C}_p^2}{k_f} \|q_p\|^2_{L^2(\Omega_d)} \right)^{\frac{1}{2}} \tag{2.29}$$

which only depends on the viscosity, micro-fracture permeability, domain and sink/source term. Then there exists a solution to the problem (2.28) satisfying

$$\frac{k_m}{\rho\mu} \|\nabla \psi_m\|^2_{L^2(\Omega_d)} + \frac{k_f}{\rho\mu} \|\nabla \psi_f\|^2_{L^2(\Omega_d)} + 2\nu \|\mathbb{D}(\mathbf{v})\|^2_{L^2(\Omega_c)} \leq \mathcal{R}^2. \tag{2.30}$$

Theorem 2.4 *Under the assumption of Theorem 2.3, and the data satisfying*

$$\nu^3 > 2\left(C_s^2 C_k^3 + \frac{1}{2} D_t E_t^2 C_k^3 \right)^2 \mathcal{R}^2, \tag{2.31}$$

the problem (2.28) has a unique weak solution.

3 Robin–Robin Domain Decomposition Method

In this section, we follow the idea in [47], which was for the Navier–Stokes–Darcy model, to propose the domain decomposition approach for decoupling the Dual-Porosity-Navier–Stokes system with Beavers–Joseph interface condition. Instead of the convergence analysis based on the continuous formulation, which was discussed only for two cases in [47], in this section we will carry out the convergence analysis based on the finite element discretization formulation for all the three cases.

3.1 Domain Decomposition with Robin Boundary Conditions

Based on the idea in [47], we consider the following Robin conditions to decouple the Dual-Porosity model and Navier-Stokes equation: for given constants $\gamma_d > 0$ and $\gamma_c > 0$, and given functions η_d, η_c and $\overrightarrow{\eta}_{c\tau}$ defined on Γ_{cd},

$$\gamma_d \frac{k_f}{\mu} \nabla \widehat{p}_f \cdot (-\mathbf{n}_{cd}) + \frac{1}{\rho} \widehat{p}_f = \eta_d \qquad \text{on } \Gamma_{cd}, \tag{3.1}$$

$$\mathbf{n}_{cd} \cdot (\mathbb{T}(\widehat{\mathbf{u}}, \widehat{p}) \cdot \mathbf{n}_{cd}) - \frac{1}{2} \widehat{\mathbf{u}} \cdot \widehat{\mathbf{u}} + \gamma_c \widehat{\mathbf{u}} \cdot \mathbf{n}_{cd} = \eta_c \qquad \text{on } \Gamma_{cd}, \tag{3.2}$$

$$-P_\tau (\mathbb{T}(\widehat{\mathbf{u}}, \widehat{p}) \cdot \mathbf{n}_{cd}) - \frac{\alpha\nu\sqrt{\mathbf{d}}}{\sqrt{\text{trace}(\prod)}} P_\tau \widehat{\mathbf{u}} = \overrightarrow{\eta}_{c\tau} \qquad \text{on } \Gamma_{cd}, \tag{3.3}$$

together with (2.5). Then the weak formulation for the decoupled Dual-Porosity-Navier–Stokes system reads: for $\eta_d,\ \eta_c,\ \overrightarrow{\eta}_{c\tau} \in L^2(\Gamma_{cd})$, find $\left(\widehat{p}_m, \widehat{p}_f, \widehat{\mathbf{u}}, \widehat{p}\right) \in \mathbf{X}_0 \times M$, such that

$$\begin{aligned}
&\left(\frac{k_m}{\mu}\nabla\widehat{p}_m, \nabla\psi_m\right)_{\Omega_d} + \left(\frac{k_f}{\mu}\nabla\widehat{p}_f, \nabla\psi_f\right)_{\Omega_d} \\
&\quad + \left(\frac{\sigma k_m}{\mu}\left(\widehat{p}_m - \widehat{p}_f\right), \psi_m\right)_{\Omega_d} + \left(\frac{\sigma k_m}{\mu}\left(\widehat{p}_f - \widehat{p}_m\right), \psi_f\right)_{\Omega_d} \\
&\quad + \left((\widehat{\mathbf{u}}\cdot\nabla)\,\widehat{\mathbf{u}}, \mathbf{v}\right)_{\Omega_c} - \frac{1}{2}\left\langle\widehat{\mathbf{u}}\cdot\widehat{\mathbf{u}}, \mathbf{v}\cdot\mathbf{n}_{cd}\right\rangle + 2\nu\left(\mathbb{D}\left(\widehat{\mathbf{u}}\right), \mathbb{D}\left(\mathbf{v}\right)\right)_{\Omega_c} - \left(\nabla\cdot\mathbf{v}, \widehat{p}\right)_{\Omega_c} + \left(\nabla\cdot\widehat{\mathbf{u}}, q\right)_{\Omega_c} \\
&\quad + \left\langle\frac{\widehat{p}_f}{\gamma_d\rho}, \psi_f\right\rangle + \gamma_c\left\langle\widehat{\mathbf{u}}\cdot\mathbf{n}_{cd}, \mathbf{v}\cdot\mathbf{n}_{cd}\right\rangle + \frac{\alpha\nu\sqrt{\mathbf{d}}}{\sqrt{\text{trace}\left(\prod\right)}}\left\langle P_\tau\widehat{\mathbf{u}}, P_\tau\mathbf{v}\right\rangle \\
&= \left(q_p, \psi_f\right)_{\Omega_d} + \left(\mathbf{f}, \mathbf{v}\right)_{\Omega_c} + \left\langle\frac{\eta_d}{\gamma_d}, \psi_f\right\rangle + \left\langle\eta_c, \mathbf{v}\cdot\mathbf{n}_{cd}\right\rangle \\
&\quad - \left\langle\overrightarrow{\eta}_{c\tau}, P_\tau\mathbf{v}\right\rangle, \quad \forall\ \left(\psi_m, \psi_f, \mathbf{v}, q\right) \in \mathbf{X}_0 \times M.
\end{aligned} \tag{3.4}$$

Next we show that, for appropriate choices of γ_c, γ_d, η_c, η_d, and $\overrightarrow{\eta}_{c\tau}$, the solution of coupled Dual-Porosity-Navier–Stokes system (2.15)-(2.16) are equivalent to the solution of decoupled system (3.4).

Lemma 3.1 *Under the assumptions of Theorem 2.3 and Theorem 2.4, let* $\left(p_m, p_f, \mathbf{u}, p\right)$ *be the solution of the coupled Dual-Porosity-Navier–Stokes system (2.15)–(2.16) and let* $\left(\widehat{p}_m, \widehat{p}_f, \widehat{\mathbf{u}}, \widehat{p}\right)$ *be the solution of the decoupled Dual-Porosity and Navier–Stokes system (3.4) with Robin boundary conditions (3.1)–(3.3) at the interface. Then,* $\left(\widehat{p}_m, \widehat{p}_f, \widehat{\mathbf{u}}, \widehat{p}\right) = \left(p_m, p_f, \mathbf{u}, p\right)$ *if and only if* γ_c, γ_d, η_c, $\overrightarrow{\eta}_{c\tau}$, *and* η_d *satisfy the following compatibility conditions:*

$$\eta_d = \gamma_d\widehat{\mathbf{u}}\cdot\mathbf{n}_{cd} + \frac{1}{\rho}\widehat{p}_f, \tag{3.5}$$

$$\eta_c = \gamma_c\widehat{\mathbf{u}}\cdot\mathbf{n}_{cd} - \frac{1}{\rho}\widehat{p}_f, \tag{3.6}$$

$$\overrightarrow{\eta}_{c\tau} = \frac{\alpha\nu\sqrt{\boldsymbol{d}}}{\sqrt{trace\left(\prod\right)}}P_\tau\left(\frac{k_f}{\mu}\nabla\widehat{p}_f\right). \tag{3.7}$$

Proof For the necessity, we pick $\psi_m = \psi_f = 0$ and $\mathbf{v}$ such that $P_\tau\mathbf{v} = 0$ in (2.15) and (3.4), then by subtracting (3.4) from (2.15), we get

$$\left\langle\eta_c - \gamma_c\mathbf{u}_f\cdot\mathbf{n}_{cd} + \frac{1}{\rho}p_f, \mathbf{v}\cdot\mathbf{n}_{cd}\right\rangle = 0, \forall\,\mathbf{v} \in \mathbf{V}_0 \text{ with } P_\tau\mathbf{v} = 0$$

which implies (3.6). The necessity of (3.5) and (3.7) can be derived in a similar fashion.

As for the sufficiency, by substituting the compatibility conditions (3.5)–(3.7) into (3.4), we can easily see that $\left(\widehat{p}_m, \widehat{p}_f, \widehat{\mathbf{u}}, \widehat{p}\right)$ solves the coupled Dual-Porosity-Navier–Stokes system (2.15)–(2.16). Since the solution to the Dual-Porosity-Navier–Stokes system is unique under the assumptions in Theorems 2.3 and 2.4, we have $\left(\widehat{p}_m, \widehat{p}_f, \widehat{\mathbf{u}}, \widehat{p}\right) = \left(p_m, p_f, \mathbf{u}, p\right)$. □

For convenience, we define the following bilinear forms for the two independent systems respectively.

$$a_m\left(p_m, \psi_m\right) = \left(\frac{k_m}{\mu}\nabla p_m, \nabla\psi_m\right)_{\Omega_d}, \quad a_f\left(p_f, \psi_f\right) = \left(\frac{k_f}{\mu}\nabla p_f, \nabla\psi_f\right)_{\Omega_d}, \tag{3.8}$$

$$a_c(\mathbf{u},\mathbf{v}) = 2\nu\left(\mathbb{D}(\mathbf{u}),\mathbb{D}(\mathbf{v})\right)_{\Omega_c}, \quad b_c(\mathbf{v},p) = -\frac{1}{\rho}\left(\nabla\cdot\mathbf{v},p\right)_{\Omega_c}. \tag{3.9}$$

Then we propose the parallel Robin–Robin domain decomposition algorithm for the Dual-Porosity-Navier–Stokes system.

Algorithm 3.1 (parallel DDM):

1. Initial values of η_d^0, η_c^0 and $\overrightarrow{\eta}_{c\tau}^0$ are guessed.
2. For $k = 0, 1, 2, \ldots$, independently solve the Navier–Stokes equation and Dual-Porosity equation with Robin boundary conditions. More precisely, $\left(p_m^k, p_f^k\right) \in \Psi_0 \times \Psi_0$ is computed from

$$\begin{aligned} &a_m\left(p_m^k,\psi_m\right) + a_f\left(p_f^k,\psi_f\right) + \left(\frac{\sigma k_m}{\mu}\left(p_m^k - p_f^k\right),\psi_m\right)_{\Omega_d} + \\ &\left(\frac{\sigma k_m}{\mu}\left(p_f^k - p_m^k\right),\psi_f\right)_{\Omega_d} + \left\langle\frac{p_f^k}{\gamma_d\rho},\psi_f\right\rangle = \left(q_p,\psi_f\right)_{\Omega_d} + \left\langle\frac{\eta_d^k}{\gamma_d},\psi_f\right\rangle \\ &\forall\,\psi_m,\psi_f \in \Psi_0, \end{aligned} \tag{3.10}$$

and $\mathbf{u}^k \in \mathbf{V}_0$ and $p^k \in M$ are computed from

$$\begin{aligned} &c\left(\mathbf{u}^k,\mathbf{u}^k,\mathbf{v}\right) + a_c\left(\mathbf{u}^k,\mathbf{v}\right) + b_c\left(\mathbf{v},p^k\right) \\ &+\gamma_c\left\langle\mathbf{u}^k\cdot\mathbf{n}_{cd},\mathbf{v}\cdot\mathbf{n}_{cd}\right\rangle + \frac{\alpha\nu\sqrt{\mathbf{d}}}{\sqrt{\operatorname{trace}\left(\prod\right)}}\left\langle P_\tau\mathbf{u}^k, P_\tau\mathbf{v}\right\rangle \\ &\quad = \left\langle\eta_c^k,\mathbf{v}\cdot\mathbf{n}_{cd}\right\rangle + (\mathbf{f},\mathbf{v})_{\Omega_c} - \left\langle\overrightarrow{\eta}_{c\tau}^k, P_\tau\mathbf{v}\right\rangle \qquad \forall\,\mathbf{v}\in\mathbf{V}_0, \end{aligned} \tag{3.11}$$

$$b_c\left(\mathbf{u}^k,q\right) = 0 \qquad \forall\, q \in M. \tag{3.12}$$

3. η_d^{k+1}, η_c^{k+1} and $\overrightarrow{\eta}_{c\tau}^{k+1}$ are updated in the following manner:

$$\eta_c^{k+1} = a\eta_d^k + \frac{b}{\rho}p_f^k, \tag{3.13}$$

$$\eta_d^{k+1} = c\eta_c^k + d\mathbf{u}^k\cdot\mathbf{n}_{cd}, \tag{3.14}$$

$$\overrightarrow{\eta}_{c\tau}^{k+1} = \frac{\alpha\nu\sqrt{\mathbf{d}}}{\sqrt{\operatorname{trace}\left(\prod\right)}}P_\tau\left(\frac{k_f}{\mu}\nabla p_f^k\right), \tag{3.15}$$

where the coefficients a, b, c, d are chosen as follows:

$$a = \frac{\gamma_c}{\gamma_d}, \quad b = -1-a, \quad c = -1, \quad d = \gamma_c + \gamma_d. \tag{3.16}$$

The relations in (3.16) are necessary to ensure the convergence of the scheme. Suppose that above algorithm is convergent, and η_c^k, η_d^k, p_m^k, p_f^k and $\mathbf{u}^k$ converge to η_c^*, η_d^*, p_m^*, p_f^* and $\mathbf{u}^*$, respectively. Then, by (3.13)-(3.14) and Lemma 3.1, it can be easily seen that η_c^*, η_d^*, p_m^*, p_f^* and $\mathbf{u}^*$ satisfy the consistency equations (3.5)-(3.6),

For the comparison purpose, we also present a serial scheme as follows.

Algorithm 3.2 (serial DDM):

1. Initial values of η_d^0, η_c^0 and $\overrightarrow{\eta}_{c\tau}^0$ are guessed.

2. Firstly, for $k = 0, 1, 2, \ldots$, solve the Dual-Porosity model with Robin boundary conditions to find $\left(p_m^k, p_f^k\right) \in \Psi_0 \times \Psi_0$ satisfying (3.10).
3. η_c^{k+1} and $\overrightarrow{\eta}_{c\tau}^{k+1}$ can be updated by (3.13) and (3.15).
4. Then, for $k = 0, 1, 2, \ldots$, solve the Navier–Stokes equation with Robin boundary conditions to find $\mathbf{u}^k \in \mathbf{V}_0$ and $p^k \in M$ satisfying (3.11)-(3.12).
5. η_d^{k+1} is updated in the following manner:

$$\eta_d^{k+1} = c\eta_c^{k+1} + d\mathbf{u}^k \cdot \mathbf{n}_{cd}, \tag{3.17}$$

where the coefficients a, b, c, d are defined in (3.16).

In the following we consider finite element discretization of the Robin-Robin domain decomposition method. Let $\mathcal{T}_{c,h}$ and $\mathcal{T}_{d,h}$ be the partitions of Ω_c and Ω_d respectively, and they are compatible on the interface Γ_{cd}. Upon the partitions, the conforming finite element spaces Ψ_h^0, $\mathbf{V}_h^0$, and M_h are defined by

$$\Psi_h^0 := \{\psi_h \in C^0\left(\overline{\Omega}_d\right) \mid \psi_h|_K \in \mathbb{P}_2(K) \ \ \forall K \in \mathcal{T}_{d,h}, \psi_h|_{\Gamma_d} = 0\}, \tag{3.18}$$

$$\mathbf{V}_h^0 := \{\mathbf{v}_h \in \left(C^0\left(\overline{\Omega}_c\right)\right)^{\mathbf{d}} \mid \mathbf{v}_h|_K \in (\mathbb{P}_2(K))^{\mathbf{d}} \ \ \forall K \in \mathcal{T}_{c,h}, \mathbf{v}_h|_{\Gamma_c} = 0\}, \tag{3.19}$$

$$M_h := \{q_h \in C^0\left(\overline{\Omega}_c\right) \mid q_h|_K \in \mathbb{P}_1(K) \ \ \forall K \in \mathcal{T}_{c,h}\}, \tag{3.20}$$

where $\mathbb{P}_2(K)$ and $\mathbb{P}_1(K)$ denote the space of quadratic and linear finite elements respectively. Thus, $\mathbf{X}_h^0 = \Psi_h^0 \times \Psi_h^0 \times \mathbf{V}_h^0$ is the subspace of $\mathbf{X}_0$. Furthermore, we define the finite element space on the interface Γ_{cd},

$$\Lambda_h := \{\eta_h \in C^0(\Gamma_{cd}) \mid \eta_h|_e \in \mathbb{P}_2(e) \ \ \forall e \in \mathcal{I}_h, \ \eta_h|_{\partial\Gamma_{cd}} = 0\}, \tag{3.21}$$

where $\mathcal{I}_h$ is the induced partition by $\mathcal{T}_{c,h}$ and $\mathcal{T}_{d,h}$ on Γ_{cd}. It is easy to see that Λ_h is the trace space in the sense that

$$\Lambda_{d,h} := \Psi_h^0|_{\Gamma_{cd}} = \Lambda_h, \tag{3.22}$$

$$\Lambda_{c,h} := \mathbf{V}_h^0|_{\Gamma_{cd}} \cdot \mathbf{n}_{cd} = \Lambda_h. \tag{3.23}$$

We recall the standard conforming finite element method for the coupled Dual-Porosity-Navier–Stokes system (2.15)-(2.16): find $\overrightarrow{\mathbf{u}}_h = \left(p_{m,h}, p_{f,h}, \mathbf{u}_h\right) \in \mathbf{X}_h^0$ and $p_h \in M_h$, such that

$$c\left(\overrightarrow{\mathbf{u}}_h, \overrightarrow{\mathbf{u}}_h, \overrightarrow{\mathbf{v}}_h\right) + a\left(\overrightarrow{\mathbf{u}}_h, \overrightarrow{\mathbf{v}}_h\right) + b\left(\overrightarrow{\mathbf{v}}_h, p_h\right) = \ell\left(\overrightarrow{\mathbf{v}}_h\right), \ \ \forall \overrightarrow{\mathbf{v}}_h \in \mathbf{X}_h^0, \tag{3.24}$$

$$b\left(\overrightarrow{\mathbf{u}}_h, q_h\right) = 0, \ \ \forall q_h \in M_h. \tag{3.25}$$

Remark 3.2 The well-posedness and convergence analysis of (3.24)-(3.25) can be obtained by combing the corresponding analysis techniques for the steady-state Dual-Porosity-Navier–Stokes model [49, 58] and the Navier–Stokes–Darcy model [47, 59, 60]. In this work, we focus on the decoupled domain decomposition schemes instead of the above coupled scheme.

The decoupled Dual-Porosity-Navier–Stokes system with the Robin-Robin domain decomposition conditions (3.1)-(3.3) can be discretized by the finite element approximation: for given $\eta_{d,h}^k, \eta_{c,h}^k, \overrightarrow{\eta}_{c\tau,h}^k \in \Lambda_h$, find $\left(p_{m,h}^k, p_{f,h}^k, \mathbf{u}_h^k, p_h^k\right) \in \Psi_h^0 \times \Psi_h^0 \times \mathbf{V}_h^0 \times M_h$ such that

$$
\begin{aligned}
&c\left(\mathbf{u}_h^k, \mathbf{u}_h^k, \mathbf{v}\right) + a_c\left(\mathbf{u}_h^k, \mathbf{v}\right) + b_c\left(\mathbf{v}, p_h^k\right) + a_m\left(p_{m,h}^k, \psi_m\right) \\
&+a_f\left(p_{f,h}^k, \psi_f\right) + \left(\frac{\sigma k_m}{\mu}\left(p_{m,h}^k - p_{f,h}^k\right), \psi_m\right)_{\Omega_d} \\
&+\left(\frac{\sigma k_m}{\mu}\left(p_{f,h}^k - p_{m,h}^k\right), \psi_f\right)_{\Omega_d} + \gamma_c\left\langle \mathbf{u}_h^k \cdot \mathbf{n}_{cd}, \mathbf{v} \cdot \mathbf{n}_{cd}\right\rangle \\
&+\left\langle \frac{p_{f,h}^k}{\gamma_d \rho}, \psi_f\right\rangle + \frac{\alpha \nu \sqrt{\mathbf{d}}}{\sqrt{\text{trace}\left(\prod\right)}}\left\langle P_\tau \mathbf{u}_h^k, P_\tau \mathbf{v}\right\rangle \\
&= \left(\mathbf{f}^k, \mathbf{v}\right)_{\Omega_c} + \left\langle \eta_{c,h}^k, \mathbf{v} \cdot \mathbf{n}_{cd}\right\rangle + \left\langle \frac{\eta_{d,h}^k}{\gamma_d}, \psi_f\right\rangle - \left\langle \overrightarrow{\eta}_{c\tau,h}^k, P_\tau \mathbf{v}\right\rangle \\
&\forall\, \psi_m, \psi_f \in \Psi_h^0, \mathbf{v} \in \mathbf{V}_h^0, \qquad (3.26)\\
&b_c\left(\mathbf{u}_h^k, q\right) = 0 \qquad \forall\, q \in M_h. \qquad (3.27)
\end{aligned}
$$

3.2 Convergence of the Robin–Robin Domain Decomposition Method

In this section, we follow the elegant energy method proposed in to demonstrate the convergence of the parallel Robin–Robin domain decomposition method with finite element discretization. Three cases of Robin parameters γ_c and γ_d are discussed and the analysis result provides a general guideline of choice on the relevant parameters to obtain the convergence and geometric convergence rate.

Let $\left(p_{m,h}, p_{f,h}, \mathbf{u}_h, p_h\right)$ denote the corresponding finite element solution of the Dual-Porosity-Navier–Stokes system (3.24)-(3.25), and $\left(p_{m,h}^k, p_{f,h}^k, \mathbf{u}_h^k, p_h^k\right)$ denote the solution of the decoupled system (3.26)-(3.27) with $\eta_{d,h}^k$, $\eta_{c,h}^k$, $\overrightarrow{\eta}_{c\tau,h}^k$ satisfying the discrete counterpart of compatibility conditions (3.13)-(3.15). Next, we define the error functions

$$
\begin{aligned}
&\varepsilon_{d,h}^k = \eta_{d,h} - \eta_{d,h}^k \quad \varepsilon_{c,h}^k = \eta_{c,h} - \eta_{c,h}^k \qquad \overrightarrow{\varepsilon}_{c\tau,h}^k = \overrightarrow{\eta}_{c\tau,h} - \overrightarrow{\eta}_{c\tau,h}^k \\
&e_{m,h}^k = p_{m,h} - p_{m,h}^k \quad e_{f,h}^k = p_{f,h} - p_{f,h}^k \quad \mathbf{e}_{u,h}^k = \mathbf{u}_h - \mathbf{u}_h^k \quad e_{p,h}^k = p_h - p_h^k.
\end{aligned}
$$

Thus, the error functions satisfy the following error equations:

$$
\begin{aligned}
&a_m\left(e_{m,h}^k, \psi_m\right) + a_f\left(e_{f,h}^k, \psi_f\right) + \left(\frac{\sigma k_m}{\mu}\left(e_{m,h}^k - e_{f,h}^k\right), \psi_m - \psi_f\right)_{\Omega_d} \\
&+\left\langle \frac{e_{f,h}^k}{\gamma_d \rho}, \psi_f\right\rangle = \left\langle \frac{\varepsilon_{d,h}^k}{\gamma_d}, \psi_f\right\rangle \qquad \forall\, \psi_m, \psi_f \in \Psi_h^0, \qquad (3.28)\\
&c\left(\mathbf{u}_h, \mathbf{u}_h, \mathbf{v}\right) - c\left(\mathbf{u}_h^k, \mathbf{u}_h^k, \mathbf{v}\right) + a_c\left(\mathbf{e}_{u,h}^k, \mathbf{v}\right) + b_c\left(\mathbf{v}, e_{p,h}^k\right) + \gamma_c\left\langle \mathbf{e}_{u,h}^k \cdot \mathbf{n}_{cd}, \mathbf{v} \cdot \mathbf{n}_{cd}\right\rangle \\
&+\frac{\alpha \nu \sqrt{\mathbf{d}}}{\sqrt{\text{trace}\left(\prod\right)}}\left\langle P_\tau \mathbf{e}_{u,h}^k, P_\tau \mathbf{v}\right\rangle = \left\langle \varepsilon_{c,h}^k, \mathbf{v} \cdot \mathbf{n}_{cd}\right\rangle - \left\langle \overrightarrow{\varepsilon}_{c\tau,h}^k, P_\tau \mathbf{v}\right\rangle \qquad \forall\, \mathbf{v} \in \mathbf{V}_h^0, \\
&\qquad (3.29)\\
&b_c\left(\mathbf{e}_{u,h}^k, q\right) = 0 \qquad \forall\, q \in M_h, \qquad (3.30)
\end{aligned}
$$

and, along the interface Γ_{cd},

$$\varepsilon_{c,h}^{k+1} = a\varepsilon_{d,h}^{k} + \frac{b}{\rho} e_{f,h}^{k}, \tag{3.31}$$

$$\varepsilon_{d,h}^{k+1} = c\varepsilon_{c,h}^{k} + d\mathbf{e}_{u,h}^{k} \cdot \mathbf{n}_{cd}, \tag{3.32}$$

$$\overrightarrow{\varepsilon}_{c\tau,h}^{k+1} = \frac{\alpha\nu\sqrt{\mathbf{d}}}{\sqrt{\text{trace}\left(\prod\right)}} P_\tau \left(\frac{k_f}{\mu}\nabla e_{f,h}^{k}\right). \tag{3.33}$$

Lemma 3.3 *The error functions satisfy*

$$\begin{aligned}\left\|\varepsilon_{c,h}^{k+1}\right\|_{L^2(\Gamma_{cd})}^2 &= \left(\frac{\gamma_c}{\gamma_d}\right)^2 \left\|\varepsilon_{d,h}^{k}\right\|_{L^2(\Gamma_{cd})}^2 + \frac{1}{\rho^2}\left(1 - \left(\frac{\gamma_c}{\gamma_d}\right)^2\right) \left\|e_{f,h}^{k}\right\|_{L^2(\Gamma_{cd})}^2 \\ &\quad - \frac{2\gamma_c}{\rho}\left(1 + \frac{\gamma_c}{\gamma_d}\right)\left(a_m\left(e_{m,h}^{k}, e_{m,h}^{k}\right)\right. \\ &\quad \left. + a_f\left(e_{f,h}^{k}, e_{f,h}^{k}\right) + \left(\frac{\sigma k_m}{\mu}\left(e_{m,h}^{k} - e_{f,h}^{k}\right), e_{m,h}^{k} - e_{f,h}^{k}\right)_{\Omega_d}\right),\end{aligned} \tag{3.34}$$

$$\begin{aligned}\left\|\varepsilon_{d,h}^{k+1}\right\|_{L^2(\Gamma_{cd})}^2 &= \left\|\varepsilon_{c,h}^{k}\right\|_{L^2(\Gamma_{cd})}^2 + \left(\gamma_d^2 - \gamma_c^2\right)\left\|\mathbf{e}_{u,h}^{k} \cdot \mathbf{n}_{cd}\right\|_{L^2(\Gamma_{cd})}^2 \\ &\quad - 2\left(\gamma_c + \gamma_d\right)\left(c\left(\mathbf{e}_{u,h}^{k}, \mathbf{u}_h, \mathbf{e}_{u,h}^{k}\right) + c\left(\mathbf{u}_h, \mathbf{e}_{u,h}^{k}, \mathbf{e}_{u,h}^{k}\right)\right) \\ &\quad - 2\left(\gamma_c + \gamma_d\right) a_c\left(\mathbf{e}_{u,h}^{k}, \mathbf{e}_{u,h}^{k}\right) - 2\left(\gamma_c + \gamma_d\right) \\ &\quad \frac{\alpha\nu\sqrt{\boldsymbol{d}}}{\sqrt{trace\left(\prod\right)}}\left\langle P_\tau\left(\mathbf{e}_{u,h}^{k} + \frac{k_f}{\mu}\nabla e_{f,h}^{k-1}\right), P_\tau \mathbf{e}_{u,h}^{k}\right\rangle.\end{aligned} \tag{3.35}$$

Proof Equation (3.31) leads to

$$\left\|\varepsilon_{c,h}^{k+1}\right\|_{L^2(\Gamma_{cd})}^2 = a^2\left\|\varepsilon_{d,h}^{k}\right\|_{L^2(\Gamma_{cd})}^2 + b^2\left\|\frac{1}{\rho}e_{f,h}^{k}\right\|_{L^2(\Gamma_{cd})}^2 + 2ab\left\langle\varepsilon_{d,h}^{k}, \frac{1}{\rho}e_{f,h}^{k}\right\rangle. \tag{3.36}$$

Setting $\psi_m = \frac{1}{\rho}e_{m,h}^{k}$ and $\psi_f = \frac{1}{\rho}e_{f,h}^{k}$ in (3.28), we have

$$\begin{aligned}\left\langle\varepsilon_{d,h}^{k}, \frac{1}{\rho}e_{f,h}^{k}\right\rangle &= \frac{\gamma_d}{\rho}\left(a_m\left(e_{m,h}^{k}, e_{m,h}^{k}\right) + a_f\left(e_{f,h}^{k}, e_{f,h}^{k}\right)\right. \\ &\quad \left. + \left(\frac{\sigma k_m}{\mu}\left(e_{m,h}^{k} - e_{f,h}^{k}\right), e_{m,h}^{k} - e_{f,h}^{k}\right)_{\Omega_d}\right) \\ &\quad + \frac{1}{\rho^2}\left\langle e_{f,h}^{k}, e_{f,h}^{k}\right\rangle.\end{aligned} \tag{3.37}$$

Substituting (3.37) into (3.36), we have

$$\begin{aligned}\left\|\varepsilon_{c,h}^{k+1}\right\|_{L^2(\Gamma_{cd})}^2 &= a^2\left\|\varepsilon_{d,h}^{k}\right\|_{L^2(\Gamma_{cd})}^2 + \frac{\left(b^2 + 2ab\right)}{\rho^2}\left\|e_{f,h}^{k}\right\|_{L^2(\Gamma_{cd})} \\ &\quad + \frac{2ab\gamma_d}{\rho}\left(a_m\left(e_{m,h}^{k}, e_{m,h}^{k}\right) + a_f\left(e_{f,h}^{k}, e_{f,h}^{k}\right) + \left(\frac{\sigma k_m}{\mu}\left(e_{m,h}^{k} - e_{f,h}^{k}\right), e_{m,h}^{k} - e_{f,h}^{k}\right)_{\Omega_d}\right).\end{aligned} \tag{3.38}$$

With a and b defined in (3.16) the error function (3.34) is obtained.

The error function (3.35) can be similarly obtained. □

We are now ready to demonstrate the convergence of Robin–Robin domain decomposition method. The convergence analysis for $\gamma_c < \gamma_d$, $\gamma_c = \gamma_d$ and $\gamma_c > \gamma_d$ will be treated separately.

3.2.1 Case 1: $\gamma_c < \gamma_d$

Theorem 3.4 *Under the assumptions of Theorem 2.3 and Theorem 2.4, if γ_c and γ_d satisfy*

$$0 < \gamma_d - \gamma_c \le \frac{\nu}{D_t^2 C_k^2} \text{ and } 0 < \frac{1}{\gamma_c} - \frac{1}{\gamma_d} \le \frac{1}{\tilde{D}_t^2 \frac{\nu}{k_f}}, \tag{3.39}$$

then the domain decomposition solution $(p_{m,h}^k,\ p_{f,h}^k,\ \mathbf{u}_h^k,\ p_h^k)$ converges to the finite element solution of the coupled system $(p_{m,h},\ p_{f,h},\ \mathbf{u}_h,\ p_h)$. Specifically, if γ_c and γ_d further satisfy

$$0 < \gamma_d - \gamma_c \le \frac{\nu}{D_t^2 C_k^2} \text{ and } \frac{1}{\gamma_c} - \frac{1}{\gamma_d} \le \frac{1}{\tilde{D}_t^2 \frac{\nu}{k_f} + \gamma_d}, \tag{3.40}$$

then the algorithm has geometric convergence rate $\sqrt{\frac{\gamma_c}{\gamma_d}}$.

Remark 3.5 It is noticeable that for very small viscosity ν and permeability k_f in practise, the upper bounds of the constraints in (3.39) will be very close to 0. Hence γ_c and γ_d need to be very close to each other in order to satisfy (3.39). Therefore, if ν and k_f are very small, then it is very difficult for the choice of $\gamma_c < \gamma_d$ to reach convergence. In fact, even though the convergence is reached with extraordinary effort, the convergence will be very slow with a rate $\sqrt{\frac{\gamma_c}{\gamma_d}}$ close to 1 in such situation. We will need the Case 3 ($\gamma_c > \gamma_d$) in Subsection 3.2.3 to deal with this difficulty. On the other hand, when viscosity ν and permeability k_f are not small and γ_d is not too big, it is much easier for the choice of $\gamma_c < \gamma_d$ to satisfy the constraints (3.39) and (3.40), hence guarantee the convergence and geometric convergence rate. These observations provide theoretical instructions for selecting γ_c and γ_d and will be numerically demonstrated in Sect. 4.

Proof Multiplying (3.35) by $\frac{\gamma_c}{\gamma_d}$ and adding it to (3.34), we obtain

$$\begin{aligned}
&\frac{\gamma_c}{\gamma_d}\left\|\varepsilon_{d,h}^{k+1}\right\|_{L^2(\Gamma_{cd})}^2 + \left\|\varepsilon_{c,h}^{k+1}\right\|_{L^2(\Gamma_{cd})}^2 \\
&= \left(\frac{\gamma_c}{\gamma_d}\right)^2 \left\|\varepsilon_{d,h}^{k}\right\|_{L^2(\Gamma_{cd})}^2 + \frac{\gamma_c}{\gamma_d}\left\|\varepsilon_{c,h}^{k}\right\|_{L^2(\Gamma_{cd})}^2 \\
&\quad + \frac{\gamma_c}{\gamma_d}\left(\gamma_d^2 - \gamma_c^2\right)\left\|\mathbf{e}_{u,h}^k \cdot \mathbf{n}_{cd}\right\|_{L^2(\Gamma_{cd})}^2 + \frac{1}{\rho^2}\left(1 - \left(\frac{\gamma_c}{\gamma_d}\right)^2\right)\left\|e_{f,h}^k\right\|_{L^2(\Gamma_{cd})}^2 \\
&\quad - 2\frac{\gamma_c}{\gamma_d}\left(\gamma_c + \gamma_d\right)\left(c\left(\mathbf{e}_{u,h}^k, \mathbf{u}_h, \mathbf{e}_{u,h}^k\right) + c\left(\mathbf{u}_h, \mathbf{e}_{u,h}^k, \mathbf{e}_{u,h}^k\right) + a_c\left(\mathbf{e}_{u,h}^k, \mathbf{e}_{u,h}^k\right)\right) \\
&\quad - 2\frac{\gamma_c}{\gamma_d}\left(\gamma_c + \gamma_d\right)\frac{1}{\rho}\left(a_m\left(e_{m,h}^k, e_{m,h}^k\right) + a_f\left(e_{f,h}^k, e_{f,h}^k\right) + \frac{\sigma k_m}{\mu}\left\|e_{m,h}^k - e_{f,h}^k\right\|_{L^2(\Omega_d)}^2\right) \\
&\quad - 2\frac{\gamma_c}{\gamma_d}\left(\gamma_c + \gamma_d\right)\frac{\alpha\nu\sqrt{\mathbf{d}}}{\sqrt{\operatorname{trace}\left(\prod\right)}}\left\langle P_\tau\left(\mathbf{e}_{u,h}^k + \frac{k_f}{\mu}\nabla e_{f,h}^{k-1}\right), P_\tau \mathbf{e}_{u,h}^k\right\rangle.
\end{aligned} \tag{3.41}$$

For the trilinear form in the right hand side of (3.41), we have

$$\begin{aligned} & c\left(\mathbf{e}_{u,h}^k, \mathbf{u}_h, \mathbf{e}_{u,h}^k\right)+c\left(\mathbf{u}_h, \mathbf{e}_{u,h}^k, \mathbf{e}_{u,h}^k\right) \\ = & \left(\left(\mathbf{e}_{u,h}^k \cdot \nabla\right) \mathbf{u}_h, \mathbf{e}_{u,h}^k\right)_{\Omega_c}+\left(\left(\mathbf{u}_h \cdot \nabla\right) \mathbf{e}_{u,h}^k, \mathbf{e}_{u,h}^k\right)_{\Omega_c}-\left\langle \mathbf{u}_h \cdot \mathbf{e}_{u,h}^k, \mathbf{e}_{u,h}^k \cdot \mathbf{n}_{cd}\right\rangle . \end{aligned} \tag{3.42}$$

Using Hölder, Korn, Sobolev and trace inequalities, the three terms in the last line in (3.42) are bounded as follows,

$$\begin{aligned} & \left|\left(\left(\mathbf{e}_{u,h}^k \cdot \nabla\right) \mathbf{u}_h, \mathbf{e}_{u,h}^k\right)_{\Omega_c}\right| \leq\left\|\mathbf{e}_{u,h}^k\right\|_{L^4(\Omega_c)}^2\|\nabla \mathbf{u}_h\|_{L^2(\Omega_c)} \\ & \leq C_s^2 C_k^3\left\|\mathbb{D}(\mathbf{e}_{u,h}^k)\right\|_{L^2(\Omega_c)}^2\|\mathbb{D}(\mathbf{u}_h)\|_{L^2(\Omega_c)}, \end{aligned} \tag{3.43}$$

$$\begin{aligned} & \left|\left(\left(\mathbf{u}_h \cdot \nabla\right) \mathbf{e}_{u,h}^k, \mathbf{e}_{u,h}^k\right)_{\Omega_c}\right| \leq\|\mathbf{u}_h\|_{L^4(\Omega_c)}\left\|\nabla \mathbf{e}_{u,h}^k\right\|_{L^2(\Omega_c)}\left\|\mathbf{e}_{u,h}^k\right\|_{L^4(\Omega_c)} \\ & \leq C_s^2 C_k^3\left\|\mathbb{D}(\mathbf{e}_{u,h}^k)\right\|_{L^2(\Omega_c)}^2\|\mathbb{D}(\mathbf{u}_h)\|_{L^2(\Omega_c)}, \end{aligned} \tag{3.44}$$

$$\begin{aligned} & \left|\left\langle \mathbf{u}_h \cdot \mathbf{e}_{u,h}^k, \mathbf{e}_{u,h}^k \cdot \mathbf{n}_{cd}\right\rangle\right| \leq\left\|\mathbf{e}_{u,h}^k\right\|_{L^2(\Gamma_{cd})}\|\mathbf{u}_h\|_{L^4(\Gamma_{cd})}\left\|\mathbf{e}_{u,h}^k\right\|_{L^4(\Gamma_{cd})} \\ & \leq D_t E_t^2 C_k^3\left\|\mathbb{D}(\mathbf{e}_{u,h}^k)\right\|_{L^2(\Omega_c)}^2\|\mathbb{D}(\mathbf{u}_h)\|_{L^2(\Omega_c)}. \end{aligned} \tag{3.45}$$

By the constraint (2.30) in Theorem 2.3, we know that the discrete solution $\mathbf{u}_h$ is uniformly bounded by

$$\|\mathbb{D}\left(\mathbf{u}_h\right)\|_{L^2(\Omega_c)} \leq \frac{1}{\sqrt{2\nu}}\mathcal{R}. \tag{3.46}$$

Then, substituting (3.46) into (3.43)-(3.45), we obtain

$$\begin{aligned} & \left|c\left(\mathbf{e}_{u,h}^k, \mathbf{u}_h, \mathbf{e}_{u,h}^k\right)+c\left(\mathbf{u}_h, \mathbf{e}_{u,h}^k, \mathbf{e}_{u,h}^k\right)\right| \\ & \leq\left(2C_s^2 C_k^3+D_t E_t^2 C_k^3\right)\left\|\mathbb{D}(\mathbf{e}_{u,h}^k)\right\|_{L^2(\Omega_c)}^2\|\mathbb{D}(\mathbf{u}_h)\|_{L^2(\Omega_c)} \\ & \leq \frac{1}{\sqrt{2\nu}}\mathcal{R}(2C_s^2+D_t E_t^2)C_k^3\left\|\mathbb{D}(\mathbf{e}_{u,h}^k)\right\|_{L^2(\Omega_c)}^2 \\ & \leq \nu\left\|\mathbb{D}(\mathbf{e}_{u,h}^k)\right\|_{L^2(\Omega_c)}^2, \end{aligned} \tag{3.47}$$

where the last inequality in (3.47) holds due to the assumption (2.31) in Theorem 2.4.

For the BJ condition in the right hand side of (3.41), using Hölder, trace, Korn and Young's inequalities, we have

$$\begin{aligned} & \left|\frac{\alpha \nu \sqrt{\mathbf{d}}}{\sqrt{\operatorname{trace}\left(\prod\right)}}\left\langle P_\tau\left(\frac{k_f}{\mu}\nabla e_{f,h}^k\right), P_\tau \mathbf{e}_{u,h}^k\right\rangle\right| \\ & =\left|\frac{\alpha\sqrt{k_f}}{\rho}\left\langle P_\tau\left(\nabla e_{f,h}^k\right), P_\tau \mathbf{e}_{u,h}^k\right\rangle\right| \\ & \leq \frac{\alpha\sqrt{k_f}}{\rho}\left\|\nabla_\tau e_{f,h}^k\right\|_{-1/2,\Gamma_{cd}}\left\|P_\tau \mathbf{e}_{u,h}^k\right\|_{1/2,\Gamma_{cd}} \end{aligned}$$

$$\leq \frac{1}{2}\alpha\tilde{C}_\tau C_t C_k 2\frac{\sqrt{k_f}}{\rho}\left\|\nabla e^k_{f,h}\right\|_{L^2(\Omega_d)}\left\|\mathbb{D}\left(\mathbf{e}^k_{u,h}\right)\right\|_{L^2(\Omega_c)}$$
$$\leq \frac{1}{2}\alpha\tilde{C}_\tau C_t C_k\left(\epsilon\left\|\mathbb{D}\left(\mathbf{e}^k_{u,h}\right)\right\|^2_{L^2(\Omega_c)}+\frac{k_f}{\rho^2\epsilon}\left\|\nabla e^k_{f,h}\right\|^2_{L^2(\Omega_d)}\right)$$
$$\leq \frac{\nu}{2}\left\|\mathbb{D}\left(\mathbf{e}^k_{u,h}\right)\right\|^2_{L^2(\Omega_c)}+\frac{k_f}{2\rho\mu}\left\|\nabla e^k_{f,h}\right\|^2_{L^2(\Omega_d)}. \tag{3.48}$$

In the last inequality in (3.48), we use $\epsilon=\nu$ in the Young's inequality, the relationship $\rho\nu=\mu$, and the assumption $\alpha\tilde{C}_\tau C_t C_k\leq 1$ in Theorem 2.3.

By the trace inequality (2.25) and the Korn inequality (2.23), we have

$$\left\|\mathbf{e}^k_{u,h}\cdot\mathbf{n}_{cd}\right\|^2_{L^2(\Gamma_{cd})}\leq D_t^2C_k^2\left\|\mathbb{D}(\mathbf{e}^k_{u,h})\right\|^2_{L^2(\Omega_c)}, \tag{3.49}$$
$$\left\|e^k_{f,h}\right\|^2_{L^2(\Gamma_{cd})}\leq \tilde{D}_t^2\left\|\nabla e^k_{f,h}\right\|^2_{L^2(\Omega_d)}. \tag{3.50}$$

Summing (3.41) over k from $k=1$ to N, combining (3.47), (3.48), (3.49) and (3.50), then we deduce

$$\frac{\gamma_c}{\gamma_d}\left\|\varepsilon^{N+1}_{d,h}\right\|^2_{L^2(\Gamma_{cd})}+\sum_{k=2}^{N}\left(\frac{\gamma_c}{\gamma_d}-\left(\frac{\gamma_c}{\gamma_d}\right)^2\right)\left\|\varepsilon^k_{d,h}\right\|^2_{L^2(\Gamma_{cd})}$$
$$+\left\|\varepsilon^{N+1}_{c,h}\right\|^2_{L^2(\Gamma_{cd})}+\sum_{k=2}^{N}\left(1-\frac{\gamma_c}{\gamma_d}\right)\left\|\varepsilon^k_{c,h}\right\|^2_{L^2(\Gamma_{cd})}$$
$$=\left(\frac{\gamma_c}{\gamma_d}\right)^2\left\|\varepsilon^1_{d,h}\right\|^2_{L^2(\Gamma_{cd})}+\frac{\gamma_c}{\gamma_d}\left\|\varepsilon^1_{c,h}\right\|^2_{L^2(\Gamma_{cd})}$$
$$+\frac{\gamma_c}{\gamma_d}\left(\gamma_d^2-\gamma_c^2\right)\sum_{k=1}^{N}\left\|\mathbf{e}^k_{u,h}\cdot\mathbf{n}_{cd}\right\|^2_{L^2(\Gamma_{cd})}+\frac{1}{\rho^2}\left(1-\left(\frac{\gamma_c}{\gamma_d}\right)^2\right)\sum_{k=1}^{N}\left\|e^k_{f,h}\right\|^2_{L^2(\Gamma_{cd})}$$
$$-2\frac{\gamma_c}{\gamma_d}(\gamma_c+\gamma_d)\sum_{k=1}^{N}\left(c\left(\mathbf{e}^k_{u,h},\mathbf{u}_h,\mathbf{e}^k_{u,h}\right)+c\left(\mathbf{u}_h,\mathbf{e}^k_{u,h},\mathbf{e}^k_{u,h}\right)+a_c\left(\mathbf{e}^k_{u,h},\mathbf{e}^k_{u,h}\right)\right.$$
$$\left.+\frac{1}{\rho}a_m\left(e^k_{m,h},e^k_{m,h}\right)+\frac{1}{\rho}a_f\left(e^k_{f,h},e^k_{f,h}\right)\right)$$
$$+\frac{1}{\rho}\left(\frac{\sigma k_m}{\mu}\left(e^k_{m,h}-e^k_{f,h}\right),e^k_{m,h}-e^k_{f,h}\right)_{\Omega_d}+\frac{\alpha\nu\sqrt{\mathbf{d}}}{\sqrt{\text{trace}\left(\prod\right)}}$$
$$\left\langle P_\tau\left(\mathbf{e}^k_{u,h}+\frac{k_f}{\mu}\nabla e^{k-1}_{f,h}\right),P_\tau\mathbf{e}^k_{u,h}\right\rangle\Big)$$
$$\leq\left(\frac{\gamma_c}{\gamma_d}\right)^2\left\|\varepsilon^1_{d,h}\right\|^2_{L^2(\Gamma_{cd})}+\frac{\gamma_c}{\gamma_d}\left\|\varepsilon^1_{c,h}\right\|^2_{L^2(\Gamma_{cd})}$$
$$+\frac{\gamma_c}{\gamma_d}\left(\gamma_d^2-\gamma_c^2\right)D_t^2C_k^2\sum_{k=1}^{N}\left\|\mathbb{D}(\mathbf{e}^k_{u,h})\right\|^2_{L^2(\Omega_c)}$$
$$+\frac{1}{\rho^2}\left(1-\left(\frac{\gamma_c}{\gamma_d}\right)^2\right)\tilde{D}_t^2\sum_{k=1}^{N}\left\|\nabla e^k_{f,h}\right\|^2_{L^2(\Omega_d)}$$

$$
\begin{aligned}
&- 2\frac{\gamma_c}{\gamma_d}\left(\gamma_c+\gamma_d\right)\sum_{k=1}^{N}\Bigg(-\nu\left\|\mathbb{D}(\mathbf{e}_{u,h}^{k})\right\|_{L^2(\Omega_c)}^2+2\nu\left\|\mathbb{D}(\mathbf{e}_{u,h}^{k})\right\|_{L^2(\Omega_c)}^2\\
&\quad+\frac{k_m}{\rho\mu}\left\|\nabla e_{m,h}^{k}\right\|_{L^2(\Omega_d)}^2+\frac{k_f}{\rho\mu}\left\|\nabla e_{f,h}^{k}\right\|_{L^2(\Omega_d)}^2\\
&+\frac{\sigma k_m}{\rho\mu}\left\|e_{m,h}^{k}-e_{f,h}^{k}\right\|_{L^2(\Omega_d)}^2+\frac{\alpha\nu\sqrt{\mathbf{d}}}{\sqrt{\operatorname{trace}\left(\prod\right)}}\left\|P_\tau\mathbf{e}_{u,h}^{k}\right\|_{L^2(\Gamma_{cd})}^2\\
&\quad-\frac{\nu}{2}\left\|\mathbb{D}\left(\mathbf{e}_{u,h}^{k}\right)\right\|_{L^2(\Omega_c)}^2-\frac{k_f}{2\rho\mu}\left\|\nabla e_{f,h}^{k-1}\right\|_{L^2(\Omega_d)}^2\Bigg)\\
\le&\left(\frac{\gamma_c}{\gamma_d}\right)^2\left\|\varepsilon_{d,h}^{1}\right\|_{L^2(\Gamma_{cd})}^2+\frac{\gamma_c}{\gamma_d}\left\|\varepsilon_{c,h}^{1}\right\|_{L^2(\Gamma_{cd})}^2\\
&-2\frac{\gamma_c}{\gamma_d}\left(\gamma_c+\gamma_d\right)\frac{k_m}{\rho\mu}\sum_{k=1}^{N}\left\|\nabla e_{m,h}^{k}\right\|_{L^2(\Omega_d)}^2\\
&-\frac{\gamma_c}{\gamma_d}\left(\gamma_c+\gamma_d\right)\frac{k_f}{\rho\mu}\left(\left\|\nabla e_{f,h}^{N}\right\|_{L^2(\Omega_d)}^2\right.\\
&\quad\left.-\left\|\nabla e_{f,h}^{0}\right\|_{L^2(\Omega_d)}^2\right)\\
&+\left(\frac{\gamma_c}{\gamma_d}\left(\gamma_d^2-\gamma_c^2\right)D_t^2C_k^2-\frac{\gamma_c}{\gamma_d}\left(\gamma_c+\gamma_d\right)\nu\right)\sum_{k=1}^{N}\left\|\mathbb{D}(\mathbf{e}_{u,h})^k\right\|_{L^2(\Omega_c)}^2\\
&+\left(\frac{1}{\rho^2}\left(1-\left(\frac{\gamma_c}{\gamma_d}\right)^2\right)\tilde{D}_t^2-\frac{\gamma_c}{\gamma_d}\left(\gamma_c+\gamma_d\right)\frac{k_f}{\rho\mu}\right)\sum_{k=1}^{N}\left\|\nabla e_{f,h}^{k}\right\|_{L^2(\Omega_d)}^2
\end{aligned}
\tag{3.51}
$$

Suppose γ_c and γ_d are chosen such that

$$
\begin{aligned}
&\frac{\gamma_c}{\gamma_d}\left(\gamma_d^2-\gamma_c^2\right)D_t^2C_k^2-\frac{\gamma_c}{\gamma_d}\left(\gamma_c+\gamma_d\right)\nu\le 0,\\
&\frac{1}{\rho^2}\left(1-\left(\frac{\gamma_c}{\gamma_d}\right)^2\right)\tilde{D}_t^2-\frac{\gamma_c}{\gamma_d}\left(\gamma_c+\gamma_d\right)\frac{k_f}{\rho\mu}\le 0,
\end{aligned}
$$

which are equivalent to

$$
\gamma_d-\gamma_c\le\frac{\nu}{D_t^2C_k^2},
\tag{3.52}
$$

$$
\frac{1}{\gamma_c}-\frac{1}{\gamma_d}\le\frac{1}{\tilde{D}_t^2\frac{\nu}{k_f}}.
\tag{3.53}
$$

Then, from (3.51)-(3.53), we derive

$$
\begin{aligned}
&\frac{\gamma_c}{\gamma_d}\left\|\varepsilon_{d,h}^{N+1}\right\|_{L^2(\Gamma_{cd})}^2+\sum_{k=2}^{N}\left(\frac{\gamma_c}{\gamma_d}-\left(\frac{\gamma_c}{\gamma_d}\right)^2\right)\left\|\varepsilon_{d,h}^{k}\right\|_{L^2(\Gamma_{cd})}^2\\
&\quad+\left\|\varepsilon_{c,h}^{N+1}\right\|_{L^2(\Gamma_{cd})}^2+\sum_{k=2}^{N}\left(1-\frac{\gamma_c}{\gamma_d}\right)\left\|\varepsilon_{c,h}^{k}\right\|_{L^2(\Gamma_{cd})}^2
\end{aligned}
$$

$$
\begin{aligned}
&+2\frac{\gamma_c}{\gamma_d}\left(\gamma_c+\gamma_d\right)\frac{k_m}{\rho\mu}\sum_{k=1}^{N}\left\|\nabla e_{m,h}^{k}\right\|_{L^2(\Omega_d)}^2+\frac{\gamma_c}{\gamma_d}\left(\gamma_c+\gamma_d\right)\frac{k_f}{\rho\mu}\left\|\nabla e_{f,h}^{N}\right\|_{L^2(\Omega_d)}^2\\
&+\left(\frac{\gamma_c}{\gamma_d}\left(\gamma_c+\gamma_d\right)\nu-\frac{\gamma_c}{\gamma_d}\left(\gamma_d^2-\gamma_c^2\right)D_t^2C_k^2\right)\sum_{k=1}^{N}\left\|\mathbb{D}(\mathbf{e}_{u,h}^{k})\right\|_{L^2(\Omega_c)}^2\\
&+\left(\frac{\gamma_c}{\gamma_d}\left(\gamma_c+\gamma_d\right)\frac{k_f}{\rho\mu}-\frac{1}{\rho^2}\left(1-\left(\frac{\gamma_c}{\gamma_d}\right)^2\right)\tilde{D}_t^2\right)\sum_{k=1}^{N}\left\|\nabla e_{f,h}^{k}\right\|_{L^2(\Omega_d)}^2\\
&\leq\left(\frac{\gamma_c}{\gamma_d}\right)^2\left\|\varepsilon_{d,h}^{1}\right\|_{L^2(\Gamma_{cd})}^2+\frac{\gamma_c}{\gamma_d}\left\|\varepsilon_{c,h}^{1}\right\|_{L^2(\Gamma_{cd})}^2+\frac{\gamma_c}{\gamma_d}\left(\gamma_c+\gamma_d\right)\frac{k_f}{\rho\mu}\left\|\nabla e_{f,h}^{0}\right\|_{L^2(\Omega_d)}^2
\end{aligned}
\tag{3.54}
$$

which implies $\left\|\varepsilon_{d,h}^{k}\right\|_{L^2(\Gamma_{cd})}^2$, $\left\|\varepsilon_{c,h}^{k}\right\|_{L^2(\Gamma_{cd})}^2$, $\left\|\mathbf{e}_{u,h}^{k}\right\|_1$, $\left\|e_{m,h}^{k}\right\|_1$ and $\left\|e_{f,h}^{k}\right\|_1$ tend to zero as $k\longrightarrow\infty$.

Next we derive a geometric convergence rate for Case 1. Plugging (3.34) into (3.35), using trace and Korn inequalities, and combining (3.47) and (3.48), we have

$$
\begin{aligned}
&\left\|\varepsilon_{d,h}^{k+1}\right\|_{L^2(\Gamma_{cd})}^2=\left(\frac{\gamma_c}{\gamma_d}\right)^2\left\|\varepsilon_{d,h}^{k-1}\right\|_{L^2(\Gamma_{cd})}^2\\
&\quad+\frac{1}{\rho^2}\left(1-\left(\frac{\gamma_c}{\gamma_d}\right)^2\right)\left\|e_{f,h}^{k-1}\right\|_{L^2(\Gamma_{cd})}^2\\
&\quad+\left(\gamma_d^2-\gamma_c^2\right)\left\|\mathbf{e}_{u,h}^{k}\cdot\mathbf{n}_{cd}\right\|_{L^2(\Gamma_{cd})}^2\\
&\quad-\frac{2\gamma_c}{\rho}\left(1+\frac{\gamma_c}{\gamma_d}\right)\left(a_m\left(e_{m,h}^{k-1},e_{m,h}^{k-1}\right)+a_f\left(e_{f,h}^{k-1},e_{f,h}^{k-1}\right)\right.\\
&\quad\left.+\left(\frac{\sigma k_m}{\mu}\left(e_{m,h}^{k-1}-e_{f,h}^{k-1}\right),e_{m,h}^{k-1}-e_{f,h}^{k-1}\right)_{\Omega_d}\right)\\
&\quad-2\left(\gamma_c+\gamma_d\right)\left(c\left(\mathbf{e}_{u,h}^{k},\mathbf{u}_h,\mathbf{e}_{u,h}^{k}\right)+c\left(\mathbf{u}_h,\mathbf{e}_{u,h}^{k},\mathbf{e}_{u,h}^{k}\right)\right)\\
&\quad-2\left(\gamma_c+\gamma_d\right)a_c\left(\mathbf{e}_{u,h}^{k},\mathbf{e}_{u,h}^{k}\right)\\
&\quad-2\left(\gamma_c+\gamma_d\right)\frac{\alpha\nu\sqrt{\mathbf{d}}}{\sqrt{\operatorname{trace}\left(\prod\right)}}\\
&\quad\left\langle P_\tau\left(\mathbf{e}_{u,h}^{k}+\frac{k_f}{\mu}\nabla e_{f,h}^{k-1}\right),P_\tau\mathbf{e}_{u,h}^{k}\right\rangle\\
&=\left(\frac{\gamma_c}{\gamma_d}\right)^2\left\|\varepsilon_{d,h}^{k-1}\right\|_{L^2(\Gamma_{cd})}^2+\frac{1}{\rho^2}\left(1-\left(\frac{\gamma_c}{\gamma_d}\right)^2\right)\left\|e_{f,h}^{k-1}\right\|_{L^2(\Gamma_{cd})}^2\\
&\quad+\left(\gamma_d^2-\gamma_c^2\right)\left\|\mathbf{e}_{u,h}^{k}\cdot\mathbf{n}_{cd}\right\|_{L^2(\Gamma_{cd})}^2\\
&\quad-\frac{2\gamma_c}{\rho}\left(1+\frac{\gamma_c}{\gamma_d}\right)\left(\frac{k_m}{\mu}\|\nabla e_{m,h}^{k-1}\|_{L^2(\Omega_d)}^2+\frac{k_f}{\mu}\|\nabla e_{f,h}^{k-1}\|_{L^2(\Omega_d)}^2\right.\\
&\quad\left.+\frac{\sigma k_m}{\mu}\left\|e_{m,h}^{k-1}-e_{f,h}^{k-1}\right\|_{L^2(\Omega_d)}^2\right)\\
&\quad-2\left(\gamma_c+\gamma_d\right)\left(c\left(\mathbf{e}_{u,h}^{k},\mathbf{u}_h,\mathbf{e}_{u,h}^{k}\right)+c\left(\mathbf{u}_h,\mathbf{e}_{u,h}^{k},\mathbf{e}_{u,h}^{k}\right)2\nu\left\|\mathbb{D}(\mathbf{e}_{u,h}^{k})\right\|_{\Omega_c}^2\right)
\end{aligned}
$$

$$
\begin{aligned}
&-2\left(\gamma_c+\gamma_d\right)\frac{\alpha\nu\sqrt{\mathbf{d}}}{\sqrt{\operatorname{trace}\left(\prod\right)}}\left\|P_\tau\mathbf{e}_{u,h}^k\right\|_{L^2(\Gamma_{cd})}^2-2\left(\gamma_c+\gamma_d\right)\frac{\alpha\nu\sqrt{\mathbf{d}}}{\sqrt{\operatorname{trace}\left(\prod\right)}}\\
&\left\langle P_\tau\left(\frac{k_f}{\mu}\nabla e_{f,h}^{k-1}\right),P_\tau\mathbf{e}_{u,h}^k\right\rangle\\
\le&\left(\frac{\gamma_c}{\gamma_d}\right)^2\left\|\varepsilon_{d,h}^{k-1}\right\|_{L^2(\Gamma_{cd})}^2+\frac{1}{\rho^2}\left(1-\left(\frac{\gamma_c}{\gamma_d}\right)^2\right)\tilde{D}_t^2\left\|\nabla e_{f,h}^{k-1}\right\|_{L^2(\Omega_{cd})}^2\\
&+\left(\gamma_d^2-\gamma_c^2\right)D_t^2C_k^2\left\|\mathbb{D}\left(\mathbf{e}_{u,h}^k\right)\right\|_{L^2(\Omega_c)}^2\\
&-\frac{2\gamma_c}{\rho}\left(1+\frac{\gamma_c}{\gamma_d}\right)\left(\frac{k_m}{\mu}\|\nabla e_{m,h}^{k-1}\|_{L^2(\Omega_d)}^2\right.\\
&\left.+\frac{k_f}{\mu}\|\nabla e_{f,h}^{k-1}\|_{L^2(\Omega_d)}^2+\frac{\sigma k_m}{\mu}\left\|e_{m,h}^{k-1}-e_{f,h}^{k-1}\right\|_{L^2(\Omega_d)}^2\right)\\
&-2\left(\gamma_c+\gamma_d\right)\left(-\nu\|\mathbb{D}(\mathbf{e}_{u,h}^k)\|_{L^2(\Omega_c)}^2+2\nu\left\|\mathbb{D}(\mathbf{e}_{u,h}^k)\right\|_{L^2(\Omega_c)}^2\right)\\
&-2\left(\gamma_c+\gamma_d\right)\frac{\alpha\nu\sqrt{\mathbf{d}}}{\sqrt{\operatorname{trace}\left(\prod\right)}}\left\|P_\tau\mathbf{e}_{u,h}^k\right\|_{L^2(\Gamma_{cd})}^2\\
&+2\left(\gamma_c+\gamma_d\right)\frac{\nu}{2}\left\|\mathbb{D}\left(\mathbf{e}_{u,h}^k\right)\right\|_{L^2(\Omega_c)}^2+2\left(\gamma_c+\gamma_d\right)\frac{k_f}{2\rho\mu}\left\|\nabla e_{f,h}^{k-1}\right\|_{L^2(\Omega_d)}^2\\
\le&\left(\frac{\gamma_c}{\gamma_d}\right)^2\left\|\varepsilon_{d,h}^{k-1}\right\|_{L^2(\Gamma_{cd})}^2-\frac{2\gamma_c}{\rho}\left(1+\frac{\gamma_c}{\gamma_d}\right)\left(\frac{k_m}{\mu}\|\nabla e_{m,h}^{k-1}\|_{L^2(\Omega_d)}^2+\frac{\sigma k_m}{\mu}\left\|e_{m,h}^{k-1}-e_{f,h}^{k-1}\right\|_{L^2(\Omega_d)}^2\right)\\
&+\frac{1}{\rho^2}\left(1-\left(\frac{\gamma_c}{\gamma_d}\right)^2\right)\tilde{D}_t^2\left\|\nabla e_{f,h}^{k-1}\right\|_{L^2(\Omega_{cd})}^2-\left(\gamma_c+\gamma_d\right)\frac{k_f}{\rho\mu}\left(\frac{2\gamma_c}{\gamma_d}-1\right)\left\|\nabla e_{f,h}^{k-1}\right\|_{L^2(\Omega_d)}^2\\
&+\left(\gamma_d^2-\gamma_c^2\right)D_t^2C_k^2\left\|\mathbb{D}\left(\mathbf{e}_{u,h}^k\right)\right\|_{L^2(\Omega_c)}^2-\left(\gamma_c+\gamma_d\right)\nu\|\mathbb{D}(\mathbf{e}_{u,h}^k)\|_{L^2(\Omega_c)}^2\\
&-2\left(\gamma_c+\gamma_d\right)\frac{\alpha\nu\sqrt{\mathbf{d}}}{\sqrt{\operatorname{trace}\left(\prod\right)}}\left\|P_\tau\mathbf{e}_{u,h}^k\right\|_{L^2(\Gamma_{cd})}^2
\end{aligned}
\tag{3.55}
$$

Suppose γ_c and γ_d are chosen such that

$$
\begin{aligned}
&\left(\gamma_d^2-\gamma_c^2\right)D_t^2C_k^2-\left(\gamma_c+\gamma_d\right)\nu\le 0,\\
&\frac{1}{\rho^2}\left(1-\left(\frac{\gamma_c}{\gamma_d}\right)^2\right)\tilde{D}_t^2-\left(\gamma_c+\gamma_d\right)\frac{k_f}{\rho\mu}\left(\frac{2\gamma_c}{\gamma_d}-1\right)\le 0,
\end{aligned}
$$

which are equivalent to

$$
\gamma_d-\gamma_c\le\frac{\nu}{D_t^2C_k^2},\tag{3.56}
$$

$$
\frac{1}{\gamma_c}-\frac{1}{\gamma_d}\le\frac{1}{\tilde{D}_t^2\frac{\nu}{k_f}+\gamma_d}.\tag{3.57}
$$

Noting that the constraints (3.56) and (3.52) are the same, but the upper bound of constraint (3.57) is smaller than that of constraint (3.53).

Then, from (3.55)-(3.57), we obtain

$$\left\|\varepsilon_{d,h}^{k+1}\right\|_{L^2(\Gamma_{cd})}^2 \leq \left(\frac{\gamma_c}{\gamma_d}\right)^2 \left\|\varepsilon_{d,h}^{k-1}\right\|_{L^2(\Gamma_{cd})}^2,$$

which implies the geometric convergence rate $\sqrt{\frac{\gamma_c}{\gamma_d}}$ for $\varepsilon_{d,h}^k$.

Setting $\psi_m = e_{m,h}^k$ and $\psi_f = e_{f,h}^k$ in (3.28), we have

$$\frac{k_m}{\mu}\left\|\nabla e_{m,h}^k\right\|_{L^2(\Omega_d)}^2 + \frac{k_f}{\mu}\left\|\nabla e_{f,h}^k\right\|_{L^2(\Omega_d)}^2 + \frac{\sigma k_m}{\mu}\left\|e_{m,h}^k - e_{f,h}^k\right\|_{L^2(\Omega_d)}^2 + \frac{1}{\rho\gamma_d}\left\|e_{f,h}^k\right\|_{L^2(\Gamma_{cd})}^2 = \frac{1}{\gamma_d}\left\langle \varepsilon_{d,h}^k, e_{f,h}^k\right\rangle. \tag{3.58}$$

Using Hölder's and Young's inequalities, we estimate the right hand side of (3.58) as follows,

$$\begin{aligned}\frac{1}{\gamma_d}\left\langle \varepsilon_{d,h}^k, e_{f,h}^k\right\rangle &\leq \frac{1}{\gamma_d}\left\|\varepsilon_{d,h}^k\right\|_{L^2(\Gamma_{cd})}\left\|e_{f,h}^k\right\|_{L^2(\Gamma_{cd})} \leq \frac{1}{2\gamma_d}\left(\epsilon\left\|e_{f,h}^k\right\|_{L^2(\Gamma_{cd})}^2 + \frac{1}{\epsilon}\left\|\varepsilon_{d,h}^k\right\|_{L^2(\Gamma_{cd})}^2\right)\\ &\leq \frac{1}{\rho\gamma_d}\left\|e_{f,h}^k\right\|_{L^2(\Gamma_{cd})}^2 + \frac{\rho}{4\gamma_d}\left\|\varepsilon_{d,h}^k\right\|_{L^2(\Gamma_{cd})}^2\end{aligned} \tag{3.59}$$

where $\epsilon = \frac{2}{\rho}$ in the Young's inequality. From (3.58) and (3.59), it is easily seen that

$$\frac{k_m}{\rho\mu}\left\|\nabla e_{m,h}^k\right\|_{L^2(\Omega_d)}^2 + \frac{k_f}{\rho\mu}\left\|\nabla e_{f,h}^k\right\|_{L^2(\Omega_d)}^2 + \frac{\sigma k_m}{\rho\mu}\left\|e_{m,h}^k - e_{f,h}^k\right\|_{L^2(\Omega_d)}^2 \leq \frac{1}{4\gamma_d}\left\|\varepsilon_{d,h}^k\right\|_{L^2(\Gamma_{cd})}^2 \tag{3.60}$$

which implies the convergence rate for $\left\|e_{m,h}^k\right\|_1$ and $\left\|e_{f,h}^k\right\|_1$ is at least $\sqrt{\frac{\gamma_c}{\gamma_d}}$. From (3.31) and the convergence of $e_{f,h}^k$ and $\varepsilon_{d,h}^k$, we can obtain the geometric convergence rate for $\varepsilon_{c,h}^k$. Through (3.29)-(3.30) and (3.32) -(3.33), we can similarly obtain the geometric convergence rate for the rest variables. □

3.2.2 Case 2: $\gamma_c = \gamma_d$

In the case $\gamma_d = \gamma_c = \gamma$, by Lemma 3.3, we have

$$\begin{aligned}\left\|\varepsilon_{c,h}^{k+1}\right\|_{L^2(\Gamma_{cd})}^2 = \left\|\varepsilon_{d,h}^k\right\|_{L^2(\Gamma_{cd})}^2 - \frac{4\gamma}{\rho}\Big(&a_m\left(e_{m,h}^k, e_{m,h}^k\right)\\ &+a_f\left(e_{f,h}^k, e_{f,h}^k\right) + \left(\frac{\sigma k_m}{\mu}\left(e_{m,h}^k - e_{f,h}^k\right), e_{m,h}^k - e_{f,h}^k\right)_{\Omega_d}\Big).\end{aligned} \tag{3.61}$$

$$\begin{aligned}\left\|\varepsilon_{d,h}^{k+1}\right\|_{L^2(\Gamma_{cd})}^2 = \left\|\varepsilon_{c,h}^k\right\|_{L^2(\Gamma_{cd})}^2 &- 4\gamma\left(c\left(\mathbf{e}_{u,h}^k, \mathbf{u}_h, \mathbf{e}_{u,h}^k\right) + c\left(\mathbf{u}_h, \mathbf{e}_{u,h}^k, \mathbf{e}_{u,h}^k\right) + a_c\left(\mathbf{e}_{u,h}^k, \mathbf{e}_{u,h}^k\right)\right)\\ &- 4\gamma\frac{\alpha\nu\sqrt{\mathbf{d}}}{\sqrt{\text{trace}\left(\prod\right)}}\left\langle P_\tau\left(\mathbf{e}_{u,h}^k + \frac{k_f}{\mu}\nabla e_{f,h}^{k-1}\right), P_\tau\mathbf{e}_{u,h}^k\right\rangle,\end{aligned} \tag{3.62}$$

Theorem 3.6 *Under the assumptions of Theorem 2.3 and Theorem 2.4, if $\gamma_c = \gamma_d = \gamma$, then the domain decomposition solution $(p_{m,h}^k, p_{f,h}^k, \mathbf{u}_h^k, p_h^k)$ converges to the finite element solution of the coupled system.*

Proof Adding (3.61) and (3.62) and summing over k from 1 to N, we derive

$$\left\|\varepsilon_{d,h}^{N+1}\right\|_{L^2(\Gamma_{cd})}^2 + \left\|\varepsilon_{c,h}^{N+1}\right\|_{L^2(\Gamma_{cd})}^2$$

$$
\begin{aligned}
&= \left\|\varepsilon_{d,h}^{1}\right\|_{L^2(\Gamma_{cd})}^2 + \left\|\varepsilon_{c,h}^{1}\right\|_{L^2(\Gamma_{cd})}^2 - 4\gamma \sum_{k=1}^{N} \Bigg(c\left(\mathbf{e}_{u,h}^{k}, \mathbf{u}_h, \mathbf{e}_{u,h}^{k}\right) \\
&\quad + c\left(\mathbf{u}_h, \mathbf{e}_{u,h}^{k}, \mathbf{e}_{u,h}^{k}\right) + a_c\left(\mathbf{e}_{u,h}^{k}, \mathbf{e}_{u,h}^{k}\right) + \frac{1}{\rho} a_m\left(e_{m,h}^{k}, e_{m,h}^{k}\right) \\
&\quad + \frac{1}{\rho} a_f\left(e_{f,h}^{k}, e_{f,h}^{k}\right) + \frac{1}{\rho}\left(\frac{\sigma k_m}{\mu}\left(e_{m,h}^{k} - e_{f,h}^{k}\right), e_{m,h}^{k} - e_{f,h}^{k}\right)_{\Omega_d} \\
&\quad + \frac{\alpha \nu \sqrt{\mathbf{d}}}{\sqrt{\operatorname{trace}\left(\prod\right)}}\left\langle P_\tau\left(\mathbf{e}_{u,h}^{k} + \frac{k_f}{\mu}\nabla e_{f,h}^{k-1}\right), P_\tau \mathbf{e}_{u,h}^{k}\right\rangle\Bigg).
\end{aligned} \tag{3.63}
$$

By (3.47) and (3.48), we have

$$
\begin{aligned}
&c\left(\mathbf{e}_{u,h}^{k}, \mathbf{u}_h, \mathbf{e}_{u,h}^{k}\right) + c\left(\mathbf{u}_h, \mathbf{e}_{u,h}^{k}, \mathbf{e}_{u,h}^{k}\right) + a_c\left(\mathbf{e}_{u,h}^{k}, \mathbf{e}_{u,h}^{k}\right) \\
&\quad + \frac{1}{\rho} a_m\left(e_{m,h}^{k}, e_{m,h}^{k}\right) + \frac{1}{\rho} a_f\left(e_{f,h}^{k}, e_{f,h}^{k}\right) \\
&\quad + \frac{1}{\rho}\left(\frac{\sigma k_m}{\mu}\left(e_{m,h}^{k} - e_{f,h}^{k}\right), e_{m,h}^{k} - e_{f,h}^{k}\right)_{\Omega_d} \\
&\quad + \frac{\alpha \nu \sqrt{\mathbf{d}}}{\sqrt{\operatorname{trace}\left(\prod\right)}}\left\langle P_\tau\left(\mathbf{e}_{u,h}^{k} + \frac{k_f}{\mu}\nabla e_{f,h}^{k-1}\right), P_\tau \mathbf{e}_{u,h}^{k}\right\rangle \\
&\geq 2\nu \left\|\mathbb{D}\left(\mathbf{e}_{u,h}^{k}\right)\right\|_{L^2(\Omega_c)}^2 + \frac{k_m}{\rho\mu}\left\|\nabla e_{m,h}^{k}\right\|_{L^2(\Omega_d)}^2 + \frac{k_f}{\rho\mu}\left\|\nabla e_{f,h}^{k}\right\|_{L^2(\Omega_d)}^2 \\
&\quad + \frac{\sigma k_m}{\rho\mu}\left\|\nabla e_{m,h}^{k} - \nabla e_{f,h}^{k}\right\|_{L^2(\Omega_d)}^2 \\
&\quad + \frac{\alpha \nu \sqrt{\mathbf{d}}}{\sqrt{\operatorname{trace}\left(\prod\right)}}\left\|P_\tau \mathbf{e}_{u,h}^{k}\right\|_{L^2(\Gamma_{cd})}^2 - \nu\left\|\mathbb{D}\left(\mathbf{e}_{u,h}^{k}\right)\right\|_{L^2(\Omega_c)}^2 \\
&\quad - \frac{\nu}{2}\left\|\mathbb{D}\left(\mathbf{e}_{u,h}^{k}\right)\right\|_{L^2(\Omega_c)}^2 - \frac{k_f}{2\rho\mu}\left\|\nabla e_{f,h}^{k-1}\right\|_{L^2(\Omega_d)}^2 \\
&\geq \frac{\nu}{2}\left\|\mathbb{D}\left(\mathbf{e}_{u,h}^{k}\right)\right\|_{L^2(\Omega_c)}^2 + \frac{k_m}{\rho\mu}\left\|\nabla e_{m,h}^{k}\right\|_{L^2(\Omega_d)}^2 + \frac{k_f}{2\rho\mu}\left\|\nabla e_{f,h}^{k}\right\|_{L^2(\Omega_d)}^2 \\
&\quad + \frac{\sigma k_m}{\rho\mu}\left\|\nabla e_{m,h}^{k} - \nabla e_{f,h}^{k}\right\|_{L^2(\Omega_d)}^2 \\
&\quad + \frac{\alpha \nu \sqrt{\mathbf{d}}}{\sqrt{\operatorname{trace}\left(\prod\right)}}\left\|P_\tau \mathbf{e}_{u,h}^{k}\right\|_{L^2(\Gamma_{cd})}^2 \\
&\quad + \frac{k_f}{2\rho\mu}\left(\left\|\nabla e_{f,h}^{k}\right\|_{L^2(\Omega_d)}^2 - \left\|\nabla e_{f,h}^{k-1}\right\|_{L^2(\Omega_d)}^2\right).
\end{aligned} \tag{3.64}
$$

Considering (3.64) into (3.63), we deduce

$$
\begin{aligned}
&\left\|\varepsilon_{d,h}^{N+1}\right\|_{L^2(\Gamma_{cd})}^2 + \left\|\varepsilon_{c,h}^{N+1}\right\|_{L^2(\Gamma_{cd})}^2 \\
&= \left\|\varepsilon_{d,h}^{1}\right\|_{L^2(\Gamma_{cd})}^2 + \left\|\varepsilon_{c,h}^{1}\right\|_{L^2(\Gamma_{cd})}^2 - 4\gamma \sum_{k=1}^{N} \Bigg(c\left(\mathbf{e}_{u,h}^{k}, \mathbf{u}_h, \mathbf{e}_{u,h}^{k}\right)
\end{aligned}
$$

$$
\begin{aligned}
&+c\left(\mathbf{u}_h,\mathbf{e}_{u,h}^k,\mathbf{e}_{u,h}^k\right)+a_c\left(\mathbf{e}_{u,h}^k,\mathbf{e}_{u,h}^k\right)+\frac{1}{\rho}a_m\left(e_{m,h}^k,e_{m,h}^k\right)\\
&+\frac{1}{\rho}a_f\left(e_{f,h}^k,e_{f,h}^k\right)+\frac{1}{\rho}\left(\frac{\sigma k_m}{\mu}\left(e_{m,h}^k-e_{f,h}^k\right),e_{m,h}^k-e_{f,h}^k\right)_{\Omega_d}\\
&+\frac{\alpha\nu\sqrt{\mathbf{d}}}{\sqrt{\operatorname{trace}\left(\prod\right)}}\left\langle P_\tau\left(\mathbf{e}_{u,h}^k+\frac{k_f}{\mu}\nabla e_{f,h}^{k-1}\right),P_\tau\mathbf{e}_{u,h}^k\right\rangle\Big)\\
\le&\left\|\varepsilon_{d,h}^1\right\|_{L^2(\Gamma_{cd})}^2+\left\|\varepsilon_{c,h}^1\right\|_{L^2(\Gamma_{cd})}^2-4\gamma\sum_{k=1}^{N}\left(\frac{\nu}{2}\left\|\mathbb{D}\left(\mathbf{e}_{u,h}^k\right)\right\|_{L^2(\Omega_c)}^2\right.\\
&\left.+\frac{k_m}{\rho\mu}\left\|\nabla e_{m,h}^k\right\|_{L^2(\Omega_d)}^2+\frac{k_f}{2\rho\mu}\left\|\nabla e_{f,h}^k\right\|_{L^2(\Omega_d)}^2\right)\\
&-4\gamma\sum_{k=1}^{N}\left(\frac{\sigma k_m}{\rho\mu}\left\|\nabla e_{m,h}^k-\nabla e_{f,h}^k\right\|_{L^2(\Omega_d)}^2+\frac{\alpha\nu\sqrt{\mathbf{d}}}{\sqrt{\operatorname{trace}\left(\prod\right)}}\left\|P_\tau\mathbf{e}_{u,h}^k\right\|_{L^2(\Gamma_{cd})}^2\right)\\
&-2\gamma\frac{k_f}{\rho\mu}\left(\left\|\nabla e_{f,h}^N\right\|_{L^2(\Omega_d)}^2-\left\|\nabla e_{f,h}^0\right\|_{L^2(\Omega_d)}^2\right).
\end{aligned}
\tag{3.65}
$$

Moving the negative terms on the right hand side of (3.65) to the left hand side, then we get

$$
\begin{aligned}
&\left\|\varepsilon_{d,h}^{N+1}\right\|_{L^2(\Gamma_{cd})}^2+\left\|\varepsilon_{c,h}^{N+1}\right\|_{L^2(\Gamma_{cd})}^2+4\gamma\sum_{k=1}^{N}\left(\frac{\nu}{2}\left\|\mathbb{D}\left(\mathbf{e}_{u,h}^k\right)\right\|_{L^2(\Omega_c)}^2\right.\\
&\left.+\frac{k_m}{\rho\mu}\left\|\nabla e_{m,h}^k\right\|_{L^2(\Omega_d)}^2+\frac{k_f}{2\rho\mu}\left\|\nabla e_{f,h}^k\right\|_{L^2(\Omega_d)}^2\right)\\
&+2\gamma\frac{k_f}{\rho\mu}\left\|\nabla e_{f,h}^N\right\|_{L^2(\Omega_d)}^2+4\gamma\sum_{k=1}^{N}\left(\frac{\sigma k_m}{\rho\mu}\left\|\nabla e_{m,h}^k-\nabla e_{f,h}^k\right\|_{L^2(\Omega_d)}^2\right.\\
&\left.+\frac{\alpha\nu\sqrt{\mathbf{d}}}{\sqrt{\operatorname{trace}\left(\prod\right)}}\left\|P_\tau\mathbf{e}_{u,h}^k\right\|_{L^2(\Gamma_{cd})}^2\right)\\
&\le\left\|\varepsilon_{d,h}^0\right\|_{L^2(\Gamma_{cd})}^2+\left\|\varepsilon_{c,h}^0\right\|_{L^2(\Gamma_{cd})}^2+2\gamma\frac{k_f}{\rho\mu}\left\|\nabla e_{f,h}^0\right\|_{L^2(\Omega_d)}^2
\end{aligned}
\tag{3.66}
$$

which implies $\mathbf{e}_{u,h}^k$ tends to zero in $\left(H^1\left(\Omega_c\right)\right)^{\mathbf{d}}$, and $e_{m,h}^k$ and $e_{f,h}^k$ tend to zero in $H^1\left(\Omega_d\right)$, respectively. The convergence of $e_{m,h}^k$ and $e_{f,h}^k$ together with the error equation (3.28) implies the convergence of $\varepsilon_{d,h}^k$ in $H^{-\frac{1}{2}}\left(\Gamma_{cd}\right)$. Combining the convergence of $\varepsilon_{d,h}^k$ and $e_{f,h}^k$ and the error equation (3.31), we deduce the convergence of $\varepsilon_{c,h}^k$ in $H^{-\frac{1}{2}}\left(\Gamma_{cd}\right)$. Combining the convergence of $e_{f,h}^k$ and the error equation on the interface (3.33), we deduce the convergence of $\overrightarrow{\varepsilon}_{c\tau,h}^k$ in $H^{-\frac{1}{2}}\left(\Gamma_{cd}\right)$. The convergence of the pressure then follows from error equation (3.29) and the discrete counterpart of the inf-sup condition (2.27). Hence we have proved the theorem. □

In order to obtain an explicit convergence rate for the case $\gamma_c=\gamma_d$ and the case $\gamma_c>\gamma_d$ in next subsection, we introduce the inverse inequality for the Dual-Porosity model in the lemma below. One of the key ingredients in the following estimation is an extension technique

which was used in [26] for the Stokes–Darcy model. An alternate extension technique is the discrete harmonic extension used in [54] and can provide equivalent results. Here we will use the extension technique in [26] and prove the inverse inequality for the Dual-Porosity model where two coupled Darcy equations need to be handled properly. Particularly, we obtain a more precise result with the help of Young's inequality than that in [26, 54], and get rid of the lower bound constraints of the mesh size required in [54].

Based on the inverse inequality for finite element spaces, see Lemma 4.5.3 in [61], we reduce the quasi-uniform assumption on the entire partition to a local quasi-uniform assumption only for the elements near the interface Γ_{cd}:

Lemma 3.7 *(**Local inverse inequality**) Let $\Psi_h^0 \subset H^1(\Omega_d)$ be the finite element space with shape regular and local quasi-uniform triangulation $\mathcal{T}_{d,h}$. Then, we have*

$$\|\nabla \psi_h\|_{L^2(K)} \leq C_I h^{-1} \|\psi_h\|_{L^2(K)} \quad \forall \psi_h \in \Psi_h^0, \tag{3.67}$$

for all $K \in \mathcal{T}_{d,h}$ along the interface Γ_{cd} and $Ch \leq \text{diam } K \leq h$.

Lemma 3.8 *Under the assumption of Lemma 3.7, then we have*

$$\begin{aligned}\left\|\varepsilon_{d,h}^k\right\|_{L^2(\Gamma_{cd})}^2 \leq 4\gamma_d^2 C_I^2 h^{-1} &\left(\frac{k_m^2}{\mu^2}\left\|\nabla e_{m,h}^k\right\|_{L^2(\Omega_d)}^2 + \frac{k_f^2}{\mu^2}\left\|\nabla e_{f,h}^k\right\|_{L^2(\Omega_d)}^2\right) \\ &+ \frac{2}{\rho^2}\left\|e_{f,h}^k\right\|_{L^2(\Gamma_{cd})}^2.\end{aligned} \tag{3.68}$$

Remark 3.9 This inverse inequality is critical to the analysis of convergence rate for the cases $\gamma_c = \gamma_d$ and $\gamma_c > \gamma_d$ below. By several techniques different from those of [54], we obtain a more precise estimate and get rid of the lower bound constraints of mesh size in Lemma 2.3 of [54]. Moreover, we use the local inverse inequality on the elements along the interface (see Lemma 3.7) instead of the inverse inequality on the boundary in Lemma 2.2 of [54], and avoid using any inverse inequality for the Stokes equation, in order to simplify the analysis of the case $\gamma_c > \gamma_d$.

Proof First, we introduce the zero extension operator $\mathcal{E}_{d,h}$ from Λ_h to Ψ_h^0 as follows,

$$\mathcal{E}_{d,h}\varepsilon_{d,h}^k(N) = \begin{cases} \varepsilon_{d,h}^k(N) & \text{if } N \in \mathcal{N}_{d,h}|_{\Gamma_{cd}}, \\ 0 & \text{if } N \in \mathcal{N}_{d,h} \setminus \mathcal{N}_{d,h}|_{\Gamma_{cd}}, \end{cases} \tag{3.69}$$

where $\mathcal{N}_{d,h}$ denotes the set of nodes for global basis functions on the finite element triangulation on Ω_d. We directly recall the following conclusion (see Lemma 5.4 in [26] for more details):

$$\left\|\mathcal{E}_{d,h}\varepsilon_{d,h}^k\right\|_{L^2(\Omega_d)}^2 \approx h^{\mathbf{d}} \sum_{N \in \mathcal{N}_{d,h}} \left(\mathcal{E}_{d,h}\varepsilon_{d,h}^k(N)\right)^2 \approx h^{\mathbf{d}} \sum_{N \in \mathcal{N}_{d,h}|_{\Gamma_{cd}}} \left(\varepsilon_{d,h}^k(N)\right)^2 \approx h\left\|\varepsilon_{d,h}^k\right\|_{L^2(\Gamma_{cd})}^2. \tag{3.70}$$

Setting $\psi_m = \psi_f = \mathcal{E}_{d,h}\varepsilon_{d,h}^k$ in (3.28)

$$a_m\left(e_{m,h}^k, \mathcal{E}_{d,h}\varepsilon_{d,h}^k\right) + a_f\left(e_{f,h}^k, \mathcal{E}_{d,h}\varepsilon_{d,h}^k\right) + \left\langle \frac{e_{f,h}^k}{\gamma_d \rho}, \varepsilon_{d,h}^k \right\rangle = \left\langle \frac{\varepsilon_{d,h}^k}{\gamma_d}, \varepsilon_{d,h}^k \right\rangle, \tag{3.71}$$

and using the Cauchy-Schwarz inequality and Young's inequality, we get

$$\left\|\varepsilon_{d,h}^k\right\|_{L^2(\Gamma_{cd})}^2 = \gamma_d a_m\left(e_{m,h}^k, \mathcal{E}_{d,h}\varepsilon_{d,h}^k\right) + \gamma_d a_f\left(e_{f,h}^k, \mathcal{E}_{d,h}\varepsilon_{d,h}^k\right) + \left\langle \frac{e_{f,h}^k}{\rho}, \varepsilon_{d,h}^k \right\rangle$$

$$
\begin{aligned}
&\leq \gamma_d \frac{k_m}{\mu} \left\| \nabla e^k_{m,h} \right\|_{L^2(\Omega_d)} \left\| \nabla \mathcal{E}_{d,h} \varepsilon^k_{d,h} \right\|_{L^2(\Omega_d)} \\
&\quad + \gamma_d \frac{k_f}{\mu} \left\| \nabla e^k_{f,h} \right\|_{L^2(\Omega_d)} \left\| \nabla \mathcal{E}_{d,h} \varepsilon^k_{d,h} \right\|_{L^2(\Omega_d)} \\
&\quad + \frac{1}{\rho} \left\| e^k_{f,h} \right\|_{L^2(\Gamma_{cd})} \left\| \varepsilon^k_{d,h} \right\|_{L^2(\Gamma_{cd})} \\
&\leq \frac{1}{2} \gamma_d \frac{k_m}{\mu} \left(\epsilon_1 \left\| \nabla \mathcal{E}_{d,h} \varepsilon^k_{d,h} \right\|^2_{L^2(\Omega_d)} + \frac{1}{\epsilon_1} \left\| \nabla e^k_{m,h} \right\|^2_{L^2(\Omega_d)} \right) \\
&\quad + \frac{1}{2} \gamma_d \frac{k_f}{\mu} \left(\epsilon_2 \left\| \nabla \mathcal{E}_{d,h} \varepsilon^k_{d,h} \right\|^2_{L^2(\Omega_d)} + \frac{1}{\epsilon_2} \left\| \nabla e^k_{f,h} \right\|^2_{L^2(\Omega_d)} \right) \\
&\quad + \frac{1}{2\rho} \left(\epsilon_3 \left\| \varepsilon^k_{d,h} \right\|^2_{L^2(\Gamma_{cd})} + \frac{1}{\epsilon_3} \left\| e^k_{f,h} \right\|^2_{L^2(\Gamma_{cd})} \right).
\end{aligned} \tag{3.72}
$$

Let $\mathcal{F}_{d,h}$ be the subset of the partition $\mathcal{T}_{d,h}$ containing only elements along the interface Γ_{cd}. Since $\mathcal{E}_{d,h}\varepsilon^k_{d,h}|_K$ vanishes for the element K not close to the interface Γ_{cd}, then we have

$$
\left\| \mathcal{E}_{d,h} \varepsilon^k_{d,h} \right\|^2_{L^2(\Omega_d)} = \sum_{K \in \mathcal{F}_{d,h}} \left\| \mathcal{E}_{d,h} \varepsilon^k_{d,h} \right\|^2_{L^2(K)}, \tag{3.73}
$$

$$
\left\| \nabla \mathcal{E}_{d,h} \varepsilon^k_{d,h} \right\|^2_{L^2(\Omega_d)} = \sum_{K \in \mathcal{F}_{d,h}} \left\| \nabla \mathcal{E}_{d,h} \varepsilon^k_{d,h} \right\|^2_{L^2(K)}. \tag{3.74}
$$

From (3.73), (3.74) and Lemma 3.7, we deduce

$$
\left\| \nabla \mathcal{E}_{d,h} \varepsilon^k_{d,h} \right\|_{L^2(\Omega_d)} \leq C_I h^{-1} \left\| \mathcal{E}_{d,h} \varepsilon^k_{d,h} \right\|_{L^2(\Omega_d)}. \tag{3.75}
$$

Substituting (3.75) into (3.72), and considering (3.70), then we obtain

$$
\begin{aligned}
\left\| \varepsilon^k_{d,h} \right\|^2_{L^2(\Gamma_{cd})} &\leq \frac{1}{2} \gamma_d \frac{k_m}{\mu} \left(\epsilon_1 C_I^2 h^{-1} \left\| \varepsilon^k_{d,h} \right\|^2_{L^2(\Gamma_{cd})} + \frac{1}{\epsilon_1} \left\| \nabla e^k_{m,h} \right\|^2_{L^2(\Omega_d)} \right) \\
&\quad + \frac{1}{2} \gamma_d \frac{k_f}{\mu} \left(\epsilon_2 C_I^2 h^{-1} \left\| \varepsilon^k_{d,h} \right\|^2_{L^2(\Gamma_{cd})} + \frac{1}{\epsilon_2} \left\| \nabla e^k_{f,h} \right\|^2_{L^2(\Omega_d)} \right) \\
&\quad + \frac{1}{2\rho} \left(\epsilon_3 \left\| \varepsilon^k_{d,h} \right\|^2_{L^2(\Gamma_{cd})} + \frac{1}{\epsilon_3} \left\| e^k_{f,h} \right\|^2_{L^2(\Gamma_{cd})} \right).
\end{aligned} \tag{3.76}
$$

Merging the same terms, we have

$$
\begin{aligned}
&\left(1 - \frac{\gamma_d}{2\mu} \frac{C_I^2}{h} \left(k_m \epsilon_1 + k_f \epsilon_2 \right) - \frac{\epsilon_3}{2\rho} \right) \left\| \varepsilon^k_{d,h} \right\|^2_{L^2(\Gamma_{cd})} \\
&\quad \leq \frac{1}{2} \gamma_d \frac{k_m}{\mu} \frac{1}{\epsilon_1} \left\| \nabla e^k_{m,h} \right\|^2_{L^2(\Omega_d)} + \frac{1}{2} \gamma_d \frac{k_f}{\mu} \frac{1}{\epsilon_2} \left\| \nabla e^k_{f,h} \right\|^2_{L^2(\Omega_d)} \\
&\quad + \frac{1}{2\rho} \frac{1}{\epsilon_3} \left\| e^k_{f,h} \right\|^2_{L^2(\Gamma_{cd})},
\end{aligned} \tag{3.77}
$$

and setting $\epsilon_1 = \frac{1}{4\gamma_d} \frac{\mu}{k_m} \frac{h}{C_I^2}$, $\epsilon_2 = \frac{1}{4\gamma_d} \frac{\mu}{k_f} \frac{h}{C_I^2}$ and $\epsilon_3 = \frac{\rho}{2}$, we have

$$
\frac{1}{2} \left\| \varepsilon^k_{d,h} \right\|^2_{L^2(\Gamma_{cd})} \leq 2\gamma_d^2 \frac{C_I^2}{h} \frac{k_m^2}{\mu^2} \left\| \nabla e^k_{m,h} \right\|^2_{L^2(\Omega_d)} + 2\gamma_d^2 \frac{C_I^2}{h} \frac{k_f^2}{\mu^2} \left\| \nabla e^k_{f,h} \right\|^2_{L^2(\Omega_d)}
$$

$$+\frac{1}{\rho^2}\left\|e_{f,h}^k\right\|_{L^2(\Gamma_{cd})}^2. \tag{3.78}$$

Hence we have

$$\begin{aligned}\left\|\varepsilon_{d,h}^k\right\|_{L^2(\Gamma_{cd})}^2 &\le 4\gamma_d^2 C_I^2 h^{-1}\left(\frac{k_m^2}{\mu^2}\left\|\nabla e_{m,h}^k\right\|_{L^2(\Omega_d)}^2+\frac{k_f^2}{\mu^2}\left\|\nabla e_{f,h}^k\right\|_{L^2(\Omega_d)}^2\right)\\ &+\frac{2}{\rho^2}\left\|e_{f,h}^k\right\|_{L^2(\Gamma_{cd})}^2\end{aligned} \tag{3.79}$$

which proves the lemma. □

Theorem 3.10 *Under the assumptions of Theorem 2.3 and Theorem 2.4, if* $\gamma_c=\gamma_d=\gamma$ *and* $\gamma\ge\max\left\{\frac{k_m}{4\nu},\frac{k_f}{\nu}\right\}$, *then the domain decomposition algorithm has convergence rate proportional to* $1-O(h)$.

Proof Substituting (3.47), (3.48) and (3.61) into (3.62), we obtain

$$\begin{aligned}&\left\|\varepsilon_{d,h}^{k+1}\right\|_{L^2(\Gamma_{cd})}^2\\ &=\left\|\varepsilon_{d,h}^{k-1}\right\|_{L^2(\Gamma_{cd})}^2-\frac{4\gamma}{\rho}\left(a_m\left(e_{m,h}^{k-1},e_{m,h}^{k-1}\right)+a_f\left(e_{f,h}^{k-1},e_{f,h}^{k-1}\right)\right.\\ &\quad\left.+\left(\frac{\sigma k_m}{\mu}\left(e_{m,h}^{k-1}-e_{f,h}^{k-1}\right),e_{m,h}^{k-1}-e_{f,h}^{k-1}\right)_{\Omega_d}\right)\\ &\quad-4\gamma\left(c\left(\mathbf{e}_{u,h}^k,\mathbf{u}_h,\mathbf{e}_{u,h}^k\right)+c\left(\mathbf{u}_h,\mathbf{e}_{u,h}^k,\mathbf{e}_{u,h}^k\right)+a_c\left(\mathbf{e}_{u,h}^k,\mathbf{e}_{u,h}^k\right)\right.\\ &\quad\left.+\frac{\alpha\nu\sqrt{\mathbf{d}}}{\sqrt{\operatorname{trace}\left(\prod\right)}}\left\langle P_\tau\left(\mathbf{e}_{u,h}^k+\frac{k_f}{\mu}\nabla e_{f,h}^{k-1}\right),P_\tau\mathbf{e}_{u,h}^k\right\rangle\right)\\ &\le\left\|\varepsilon_{d,h}^{k-1}\right\|_{L^2(\Gamma_{cd})}^2-\frac{4\gamma}{\rho}\left(\frac{k_m}{\mu}\|\nabla e_{m,h}^{k-1}\|_{L^2(\Omega_d)}^2\right.\\ &\quad\left.+\frac{k_f}{\mu}\|\nabla e_{f,h}^{k-1}\|_{L^2(\Omega_d)}^2+\frac{\sigma k_m}{\mu}\left\|e_{m,h}^{k-1}-e_{f,h}^{k-1}\right\|_{L^2(\Omega_d)}^2\right)\\ &\quad-4\gamma\left(-\nu\left\|\mathbb{D}\left(\mathbf{e}_{u,h}^k\right)\right\|_{L^2(\Omega_c)}^2+2\nu\left\|\mathbb{D}\left(\mathbf{e}_{u,h}^k\right)\right\|_{L^2(\Omega_c)}^2\right)\\ &\quad-4\gamma\frac{\alpha\nu\sqrt{\mathbf{d}}}{\sqrt{\operatorname{trace}\left(\prod\right)}}\left\|P_\tau\mathbf{e}_{u,h}^k\right\|_{L^2(\Gamma_{cd})}^2\\ &\quad-4\gamma\left(-\frac{\nu}{2}\left\|\mathbb{D}\left(\mathbf{e}_{u,h}^k\right)\right\|_{L^2(\Omega_c)}^2-\frac{k_f}{2\rho\mu}\left\|\nabla e_{f,h}^{k-1}\right\|_{L^2(\Omega_d)}^2\right)\\ &\le\left\|\varepsilon_{d,h}^{k-1}\right\|_{L^2(\Gamma_{cd})}^2-\frac{4\gamma}{\rho}\frac{k_m}{\mu}\|\nabla e_{m,h}^{k-1}\|_{L^2(\Omega_d)}^2-\frac{2\gamma}{\rho}\frac{k_f}{\mu}\|\nabla e_{f,h}^{k-1}\|_{L^2(\Omega_d)}^2\\ &\quad-2\gamma\nu\left\|\mathbb{D}\left(\mathbf{e}_{u,h}^k\right)\right\|_{L^2(\Omega_c)}^2-\frac{4\gamma}{\rho}\frac{\sigma k_m}{\mu}\left\|e_{m,h}^{k-1}-e_{f,h}^{k-1}\right\|_{L^2(\Omega_d)}^2\\ &\quad-4\gamma\frac{\alpha\nu\sqrt{\mathbf{d}}}{\sqrt{\operatorname{trace}\left(\prod\right)}}\left\|P_\tau\mathbf{e}_{u,h}^k\right\|_{L^2(\Gamma_{cd})}^2.\end{aligned} \tag{3.80}$$

By the inverse inequality (3.68), we have

$$\frac{h}{4\gamma^2 C_I^2}\left\|\varepsilon_{d,h}^{k-1}\right\|^2_{L^2(\Gamma_{cd})} \leq \frac{k_m^2}{\mu^2}\left\|\nabla e_{m,h}^{k-1}\right\|^2_{L^2(\Omega_d)} + \frac{k_f^2}{\mu^2}\left\|\nabla e_{f,h}^{k-1}\right\|^2_{L^2(\Omega_d)} + \frac{h}{2\rho^2\gamma^2 C_I^2}\left\|e_{f,h}^{k-1}\right\|^2_{L^2(\Gamma_{cd})}. \tag{3.81}$$

For the last term in above inequality, using the trace inequality (2.25), we deduce

$$\frac{h}{2\rho^2\gamma^2 C_I^2}\left\|e_{f,h}^{k-1}\right\|^2_{L^2(\Gamma_{cd})} \leq \frac{h\tilde{D}_t^2}{2\rho^2\gamma^2 C_I^2}\left\|\nabla e_{f,h}^{k-1}\right\|^2_{L^2(\Omega_d)} \leq \frac{k_f^2}{\mu^2}\left\|\nabla e_{f,h}^{k-1}\right\|^2_{L^2(\Omega_d)} \tag{3.82}$$

where the last inequality holds if the mesh size is small enough such that $h \leq \frac{2C_I^2}{\tilde{D}_t^2}\frac{k_f^2}{\nu^2}\gamma^2$. Combining (3.81) and (3.82), we have

$$\begin{aligned}\frac{h}{4\gamma^2 C_I^2}\left\|\varepsilon_{d,h}^{k-1}\right\|^2_{L^2(\Gamma_{cd})} &\leq \frac{k_m^2}{\mu^2}\left\|\nabla e_{m,h}^{k-1}\right\|^2_{L^2(\Omega_d)} + 2\frac{k_f^2}{\mu^2}\left\|\nabla e_{f,h}^{k-1}\right\|^2_{L^2(\Omega_d)} \\ &\leq \frac{4\gamma}{\rho}\frac{k_m}{\mu}\|\nabla e_{m,h}^{k-1}\|^2_{L^2(\Omega_d)} + \frac{2\gamma}{\rho}\frac{k_f}{\mu}\|\nabla e_{f,h}^{k-1}\|^2_{L^2(\Omega_d)}\end{aligned} \tag{3.83}$$

where the last inequality uses the assumption $\gamma \geq \max\left\{\frac{k_m}{4\nu}, \frac{k_f}{\nu}\right\}$. The restriction $\gamma \geq \max\left\{\frac{k_m}{4\nu}, \frac{k_f}{\nu}\right\}$ is actually $\gamma \geq \frac{k_f}{\nu}$, since the matrix permeability k_m is much smaller than the micro-fracture permeability k_f in the Dual-Porosity model.

Finally, substituting (3.83) into (3.80) and dropping the last three terms in the right hand side of (3.80), then we obtain

$$\begin{aligned}\left\|\varepsilon_{d,h}^{k+1}\right\|^2_{L^2(\Gamma_{cd})} &\leq \left\|\varepsilon_{d,h}^{k-1}\right\|^2_{L^2(\Gamma_{cd})} - 4\gamma\frac{k_m}{\rho\mu}\|\nabla e_{m,h}^{k-1}\|^2_{L^2(\Omega_d)} - 2\gamma\frac{k_f}{\rho\mu}\|\nabla e_{f,h}^{k-1}\|^2_{L^2(\Omega_d)} \\ &\leq \left(1 - \frac{h}{4\gamma^2 C_I^2}\right)\left\|\varepsilon_{d,h}^{k-1}\right\|^2_{L^2(\Gamma_{cd})}\end{aligned} \tag{3.84}$$

which implies that the rate of convergence depends on the mesh size h and is proportional to $1 - O(h)$ for small h. The same convergence rate can be obtained for the rest variables through arguments at the end of proof in Theorem 3.4. □

3.2.3 Case 3: $\gamma_c > \gamma_d$

In this subsection we consider the case $\gamma_c > \gamma_d$. In [26], this case was analyzed for the steady-state Stokes–Darcy model with BJSJ interface condition, which is much easier than the steady-state Dual-porosity-Navier–Stokes model with BJ interface condition in this paper, and they derived a convergence rate of 1-$O(h)$ provided that γ_c and γ_d are close enough. Recently, in [54], this case was also analyzed for the steady-state Stokes–Darcy model with BJ interface condition and an almost optimal geometric convergence rate was derived. For the analysis in this recent work, the techniques of the discrete harmonic extension and discrete Stokes extension were used to obtain two important inverse inequalities one for Darcy model and the other for the Stokes equation, and the mesh size h was required to be bigger than the viscosity and hydraulic conductivity. In our analysis below, simpler and more precise constrains are presented to obtain the optimal geometric convergence rate. Hence the theoretical analysis results in this section are more practically useful for providing instructions to select γ_c and γ_d, see the remark below and the numerical experiments in Sect. 4. Specifically, the inverse

inequality (3.68) for the Dual-Porosity model is enough in the analysis by properly selecting the scaling parameter, and no particular lower bound constraints are required for the mesh size h.

Theorem 3.11 *Under the assumptions of Theorem 2.3 and Theorem 2.4, if γ_c and γ_d satisfy*

$$0 < \left(\frac{\gamma_c}{\gamma_d} - 1\right)\left(2\frac{C_I^2}{h}\frac{k_m}{\nu}\gamma_d - 1\right) \le 1, \tag{3.85}$$

$$0 < \left(\frac{\gamma_c}{\gamma_d} - 1\right)\left(4\frac{C_I^2}{h}\frac{k_f}{\nu}\gamma_d + \tilde{D}_t^2\frac{\nu}{k_f}\frac{1}{\gamma_d} - 2\right) \le 1, \tag{3.86}$$

then the domain decomposition solution $(p_{m,h}^k,\ p_{f,h}^k,\ \mathbf{u}_h^k,\ p_h^k)$ converges to the finite element solution of the coupled system $(p_{m,h},\ p_{f,h},\ \mathbf{u}_h,\ p_h)$. Specifically, if γ_c and γ_d further satisfy

$$0 < \left(\frac{\gamma_c}{\gamma_d} - 1\right)\left(2\frac{C_I^2}{h}\frac{k_m}{\nu}\gamma_d - \frac{\gamma_c^2}{\gamma_c^2+\gamma_d^2}\right) \le \frac{\gamma_c^2}{\gamma_c^2+\gamma_d^2}, \tag{3.87}$$

$$0 < \left(\frac{\gamma_c}{\gamma_d} - 1\right)\left(4\frac{C_I^2}{h}\frac{k_f}{\nu}\gamma_d + \tilde{D}_t^2\frac{\nu}{k_f}\frac{1}{\gamma_d} - 2\frac{\gamma_c^2}{\gamma_c^2+\gamma_d^2}\right) \le \frac{\gamma_c^2}{\gamma_c^2+\gamma_d^2}, \tag{3.88}$$

then the algorithm has geometric convergence rate $\sqrt{\frac{\gamma_d}{\gamma_c}}$.

Remark 3.12 In Remark 3.5, we noted that, for low permeability the conditions (3.39) and (3.40) are hard to be satisfied unless γ_c is close to γ_d. However, Theorem 3.11 indicates that for low permeability the conditions (3.85) and (3.86) are easier to be satisfied with properly selected $\gamma_c > \gamma_d$. It is also noted that the constraints of Robin parameters in Theorem 3.11 depend on both the model parameters (permeability and viscosity) and the mesh size. From the analysis of Theorem 3.11 and the numerical experiments, we have the following general observations about how to properly choose Robin parameters in the case of small permeability and viscosity. If the permeability is much smaller than ν, then $\gamma_c > \gamma_d$ should be considered and γ_d should be accordingly increased to counteract the effect of small permeability. If the value of ν is very small, the value of γ_d should be accordingly reduced to counteract the effect of small ν, while the choice of $\gamma_c > \gamma_d$ or $\gamma_c < \gamma_d$ depends on the the permeability value. There is another possible way to decide the Robin parameters, that is the optimized Schwarz method discussed in [44, 48, 52]. It works well for the Stokes–Darcy model and Dual-Porosity-Stokes models, but more refined future works are needed for the Navier–Stokes–Darcy and Dual-Porosity-Navier–Stokes models.

Proof Multiplying (3.35) by δ and adding it to (3.34), we obtain

$$\begin{aligned}
&\delta\left\|\varepsilon_{d,h}^{k+1}\right\|_{L^2(\Gamma_{cd})}^2 + \left\|\varepsilon_{c,h}^{k+1}\right\|_{L^2(\Gamma_{cd})}^2 \\
&= \left(\frac{\gamma_c}{\gamma_d}\right)^2\left\|\varepsilon_{d,h}^{k}\right\|_{L^2(\Gamma_{cd})}^2 + \delta\left\|\varepsilon_{c,h}^{k}\right\|_{L^2(\Gamma_{cd})}^2 \\
&\quad +\delta\left(\gamma_d^2-\gamma_c^2\right)\left\|\mathbf{e}_{u,h}^k\cdot\mathbf{n}_{cd}\right\|_{L^2(\Gamma_{cd})}^2 + \frac{1}{\rho^2}\left(1-\left(\frac{\gamma_c}{\gamma_d}\right)^2\right)\left\|e_{f,h}^k\right\|_{L^2(\Gamma_{cd})}^2 \\
&\quad -2\delta\left(\gamma_c+\gamma_d\right)\left(c\left(\mathbf{e}_{u,h}^k,\mathbf{u}_h,\mathbf{e}_{u,h}^k\right)+c\left(\mathbf{u}_h,\mathbf{e}_{u,h}^k,\mathbf{e}_{u,h}^k\right)+a_c\left(\mathbf{e}_{u,h}^k,\mathbf{e}_{u,h}^k\right)\right)
\end{aligned}$$

$$
\begin{aligned}
&-2\delta\left(\gamma_c+\gamma_d\right)\frac{\alpha\nu\sqrt{\mathbf{d}}}{\sqrt{\operatorname{trace}\left(\prod\right)}}\left\langle P_\tau\left(\mathbf{e}_{u,h}^k+\frac{k_f}{\mu}\nabla e_{f,h}^{k-1}\right),P_\tau\mathbf{e}_{u,h}^k\right\rangle\\
&-\frac{2\gamma_c}{\rho\gamma_d}\left(\gamma_c+\gamma_d\right)\left(a_m\left(e_{m,h}^k,e_{m,h}^k\right)+a_f\left(e_{f,h}^k,e_{f,h}^k\right)\right.\\
&\left.+\left(\frac{\sigma k_m}{\mu}\left(e_{m,h}^k-e_{f,h}^k\right),e_{m,h}^k-e_{f,h}^k\right)_{\Omega_d}\right).
\end{aligned}
\tag{3.89}
$$

Summing (3.89) over k from $k=1$ to N, using trace and Korn inequalities, and combining (3.47) and (3.48), then we deduce

$$
\begin{aligned}
&\delta\left\|\varepsilon_{d,h}^{N+1}\right\|_{L^2(\Gamma_{cd})}^2+\left\|\varepsilon_{c,h}^{N+1}\right\|_{L^2(\Gamma_{cd})}^2+\left(\delta-\left(\frac{\gamma_c}{\gamma_d}\right)^2\right)\sum_{k=2}^N\left\|\varepsilon_{d,h}^k\right\|_{L^2(\Gamma_{cd})}^2+(1-\delta)\sum_{k=2}^N\left\|\varepsilon_{c,h}^k\right\|_{L^2(\Gamma_{cd})}^2\\
&+\delta\left(\gamma_c^2-\gamma_d^2\right)\sum_{k=1}^N\left\|\mathbf{e}_{u,h}^k\cdot\mathbf{n}_{cd}\right\|_{L^2(\Gamma_{cd})}^2+\frac{1}{\rho^2}\left(\left(\frac{\gamma_c}{\gamma_d}\right)^2-1\right)\sum_{k=1}^N\left\|e_{f,h}^k\right\|_{L^2(\Gamma_{cd})}^2\\
=&\left(\frac{\gamma_c}{\gamma_d}\right)^2\left\|\varepsilon_{d,h}^1\right\|_{L^2(\Gamma_{cd})}^2+\delta\left\|\varepsilon_{c,h}^1\right\|_{L^2(\Gamma_{cd})}^2\\
&-2\delta\left(\gamma_c+\gamma_d\right)\sum_{k=1}^N\left(c\left(\mathbf{e}_{u,h}^k,\mathbf{u}_h,\mathbf{e}_{u,h}^k\right)+c\left(\mathbf{u}_h,\mathbf{e}_{u,h}^k,\mathbf{e}_{u,h}^k\right)+a_c\left(\mathbf{e}_{u,h}^k,\mathbf{e}_{u,h}^k\right)\right)\\
&-2\delta\left(\gamma_c+\gamma_d\right)\frac{\alpha\nu\sqrt{\mathbf{d}}}{\sqrt{\operatorname{trace}\left(\prod\right)}}\sum_{k=1}^N\left\langle P_\tau\left(\mathbf{e}_{u,h}^k+\frac{k_f}{\mu}\nabla e_{f,h}^{k-1}\right),P_\tau\mathbf{e}_{u,h}^k\right\rangle\\
&-\frac{2\gamma_c}{\rho\gamma_d}\left(\gamma_c+\gamma_d\right)\sum_{k=1}^N\left(a_m\left(e_{m,h}^k,e_{m,h}^k\right)+a_f\left(e_{f,h}^k,e_{f,h}^k\right)\right.\\
&\left.+\left(\frac{\sigma k_m}{\mu}\left(e_{m,h}^k-e_{f,h}^k\right),e_{m,h}^k-e_{f,h}^k\right)_{\Omega_d}\right)\\
\le&\left(\frac{\gamma_c}{\gamma_d}\right)^2\left\|\varepsilon_{d,h}^1\right\|_{L^2(\Gamma_{cd})}^2+\delta\left\|\varepsilon_{c,h}^1\right\|_{L^2(\Gamma_{cd})}^2\\
&-2\delta\left(\gamma_c+\gamma_d\right)\sum_{k=1}^N\left(-\nu\left\|\mathbb{D}\left(\mathbf{e}_{u,h}^k\right)\right\|_{L^2(\Omega_c)}^2+2\nu\left\|\mathbb{D}\left(\mathbf{e}_{u,h}^k\right)\right\|_{L^2(\Omega_c)}^2\right)\\
&-2\delta\left(\gamma_c+\gamma_d\right)\frac{\alpha\nu\sqrt{\mathbf{d}}}{\sqrt{\operatorname{trace}\left(\prod\right)}}\\
&\sum_{k=1}^N\left\|P_\tau\mathbf{e}_{u,h}^k\right\|_{L^2(\Gamma_{cd})}^2-2\delta\left(\gamma_c+\gamma_d\right)\sum_{k=1}^N\left(-\frac{\nu}{2}\left\|\mathbb{D}\left(\mathbf{e}_{u,h}^k\right)\right\|_{L^2(\Omega_c)}^2-\frac{k_f}{2\rho\mu}\left\|\nabla e_{f,h}^{k-1}\right\|_{L^2(\Omega_d)}^2\right)\\
&-\frac{2\gamma_c}{\gamma_d}\left(\gamma_c+\gamma_d\right)\sum_{k=1}^N\left(\frac{k_m}{\rho\mu}\left\|\nabla e_{m,h}^k\right\|^2+\frac{k_f}{\rho\mu}\left\|\nabla e_{f,h}^k\right\|^2+\frac{\sigma k_m}{\rho\mu}\left\|e_{m,h}^k-e_{f,h}^k\right\|_{L^2(\Omega_d)}^2\right)\\
\le&\left(\frac{\gamma_c}{\gamma_d}\right)^2\left\|\varepsilon_{d,h}^1\right\|_{L^2(\Gamma_{cd})}^2+\delta\left\|\varepsilon_{c,h}^1\right\|_{L^2(\Gamma_{cd})}^2\\
&-2\delta\left(\gamma_c+\gamma_d\right)\sum_{k=1}^N\left(\frac{\nu}{2}\left\|\mathbb{D}\left(\mathbf{e}_{u,h}^k\right)\right\|_{L^2(\Omega_c)}^2+\frac{\alpha\nu\sqrt{\mathbf{d}}}{\sqrt{\operatorname{trace}\left(\prod\right)}}\left\|P_\tau\mathbf{e}_{u,h}^k\right\|_{L^2(\Gamma_{cd})}^2\right)
\end{aligned}
$$

$$
\begin{aligned}
&-\frac{2\gamma_c}{\gamma_d}(\gamma_c+\gamma_d)\sum_{k=1}^{N}\left(\frac{k_m}{\rho\mu}\left\|\nabla e_{m,h}^{k}\right\|_{L^2(\Omega_d)}^2+\frac{\sigma k_m}{\rho\mu}\left\|e_{m,h}^{k}-e_{f,h}^{k}\right\|_{L^2(\Omega_d)}^2\right)\\
&+\delta(\gamma_c+\gamma_d)\sum_{k=1}^{N}\frac{k_f}{\rho\mu}\left(\left\|\nabla e_{f,h}^{k-1}\right\|_{L^2(\Omega_d)}^2-\left\|\nabla e_{f,h}^{k}\right\|_{L^2(\Omega_d)}^2\right)\\
&-\left(\frac{2\gamma_c}{\gamma_d}-\delta\right)(\gamma_c+\gamma_d)\sum_{k=1}^{N}\left(\frac{k_f}{\rho\mu}\left\|\nabla e_{f,h}^{k}\right\|_{L^2(\Omega_d)}^2\right).
\end{aligned}
\tag{3.90}
$$

Setting $\delta=1$ in above inequality, moving the term $\sum_{k=2}^{N}\left\|\varepsilon_{d,h}^{k}\right\|_{L^2(\Gamma_{cd})}^2$ to the right hand side and using the inverse inequality (3.68) and trace inequality, then we derive

$$
\begin{aligned}
&\left\|\varepsilon_{d,h}^{N+1}\right\|_{L^2(\Gamma_{cd})}^2+\left\|\varepsilon_{c,h}^{N+1}\right\|_{L^2(\Gamma_{cd})}^2+(\gamma_c+\gamma_d)\frac{k_f}{\rho\mu}\left\|\nabla e_{f,h}^{N}\right\|_{L^2(\Omega_d)}^2\\
&+2(\gamma_c+\gamma_d)\sum_{k=1}^{N}\left(\frac{\nu}{2}\left\|\mathbb{D}\left(\mathbf{e}_{u,h}^{k}\right)\right\|_{L^2(\Omega_c)}^2+\frac{\alpha\nu\sqrt{\mathbf{d}}}{\sqrt{\operatorname{trace}\left(\prod\right)}}\left\|P_\tau\mathbf{e}_{u,h}^{k}\right\|_{L^2(\Gamma_{cd})}^2\right)\\
&+\left(\gamma_c^2-\gamma_d^2\right)\sum_{k=1}^{N}\left\|\mathbf{e}_{u,h}^{k}\cdot\mathbf{n}_{cd}\right\|_{L^2(\Gamma_{cd})}^2+\frac{2\gamma_c}{\gamma_d}(\gamma_c+\gamma_d)\sum_{k=1}^{N}\frac{\sigma k_m}{\rho\mu}\left\|e_{m,h}^{k}-e_{f,h}^{k}\right\|_{L^2(\Omega_d)}^2\\
&\le\left(\frac{\gamma_c}{\gamma_d}\right)^2\left\|\varepsilon_{d,h}^{1}\right\|_{L^2(\Gamma_{cd})}^2+\left\|\varepsilon_{c,h}^{1}\right\|_{L^2(\Gamma_{cd})}^2+(\gamma_c+\gamma_d)\frac{k_f}{\rho\mu}\left\|\nabla e_{f,h}^{0}\right\|_{L^2(\Omega_d)}^2\\
&-\frac{2\gamma_c}{\gamma_d}(\gamma_c+\gamma_d)\sum_{k=1}^{N}\frac{k_m}{\rho\mu}\left\|\nabla e_{m,h}^{k}\right\|_{L^2(\Omega_d)}^2-\left(\frac{2\gamma_c}{\gamma_d}-1\right)(\gamma_c+\gamma_d)\sum_{k=1}^{N}\frac{k_f}{\rho\mu}\left\|\nabla e_{f,h}^{k}\right\|_{L^2(\Omega_d)}^2\\
&-\frac{1}{\rho^2}\left(\left(\frac{\gamma_c}{\gamma_d}\right)^2-1\right)\sum_{k=1}^{N}\left\|e_{f,h}^{k}\right\|_{L^2(\Gamma_{cd})}^2+\left(\left(\frac{\gamma_c}{\gamma_d}\right)^2-1\right)\sum_{k=2}^{N}\left\|\varepsilon_{d,h}^{k}\right\|_{L^2(\Gamma_{cd})}^2\\
&\le\left(\frac{\gamma_c}{\gamma_d}\right)^2\left\|\varepsilon_{d,h}^{1}\right\|_{L^2(\Gamma_{cd})}^2+\left\|\varepsilon_{c,h}^{1}\right\|_{L^2(\Gamma_{cd})}^2+(\gamma_c+\gamma_d)\frac{k_f}{\rho\mu}\left\|\nabla e_{f,h}^{0}\right\|_{L^2(\Omega_d)}^2\\
&-\left[\frac{2\gamma_c}{\gamma_d}(\gamma_c+\gamma_d)\frac{k_m}{\rho\mu}-\left(\left(\frac{\gamma_c}{\gamma_d}\right)^2-1\right)4\gamma_d^2C_I^2h^{-1}\frac{k_m^2}{\mu^2}\right]\sum_{k=1}^{N}\left\|\nabla e_{m,h}^{k}\right\|_{L^2(\Omega_d)}^2\\
&-\left[\left(\frac{2\gamma_c}{\gamma_d}-1\right)(\gamma_c+\gamma_d)\frac{k_f}{\rho\mu}-\left(\left(\frac{\gamma_c}{\gamma_d}\right)^2-1\right)4\gamma_d^2C_I^2h^{-1}\frac{k_f^2}{\mu^2}\right]\sum_{k=1}^{N}\left\|\nabla e_{f,h}^{k}\right\|_{L^2(\Omega_d)}^2\\
&+\frac{1}{\rho^2}\left(\left(\frac{\gamma_c}{\gamma_d}\right)^2-1\right)\tilde{D}_t^2\sum_{k=1}^{N}\left\|\nabla e_{f,h}^{k}\right\|_{L^2(\Omega_d)}^2.
\end{aligned}
\tag{3.91}
$$

Assuming that

$$
\left[\frac{2\gamma_c}{\gamma_d}(\gamma_c+\gamma_d)\frac{k_m}{\rho\mu}-\left(\left(\frac{\gamma_c}{\gamma_d}\right)^2-1\right)4\gamma_d^2C_I^2h^{-1}\frac{k_m^2}{\mu^2}\right]\ge 0,
\tag{3.92}
$$

$$
\left[\left(\frac{2\gamma_c}{\gamma_d}-1\right)(\gamma_c+\gamma_d)\frac{k_f}{\rho\mu}-\left(\left(\frac{\gamma_c}{\gamma_d}\right)^2-1\right)4\gamma_d^2C_I^2h^{-1}\frac{k_f^2}{\mu^2}-\frac{\tilde{D}_t^2}{\rho^2}\left(\left(\frac{\gamma_c}{\gamma_d}\right)^2-1\right)\right]\ge 0,
\tag{3.93}
$$

which is equivalent to

$$0 < \left(\frac{\gamma_c}{\gamma_d} - 1\right)\left(2\frac{C_I^2}{h}\frac{k_m}{\nu}\gamma_d - 1\right) \le 1,$$
$$0 < \left(\frac{\gamma_c}{\gamma_d} - 1\right)\left(4\frac{C_I^2}{h}\frac{k_f}{\nu}\gamma_d + \tilde{D}_t^2\frac{\nu}{k_f}\frac{1}{\gamma_d} - 2\right) \le 1.$$

Then, from (3.91), (3.92) and (3.93), we have

$$\begin{aligned}
&\left\|\varepsilon_{d,h}^{N+1}\right\|_{L^2(\Gamma_{cd})}^2 + \left\|\varepsilon_{c,h}^{N+1}\right\|_{L^2(\Gamma_{cd})}^2 + (\gamma_c+\gamma_d)\frac{k_f}{\rho\mu}\left\|\nabla e_{f,h}^N\right\|_{L^2(\Omega_d)}^2 \\
&+2(\gamma_c+\gamma_d)\sum_{k=1}^{N}\left(\frac{\nu}{2}\left\|\mathbb{D}\left(\mathbf{e}_{u,h}^k\right)\right\|_{L^2(\Omega_c)}^2 + \frac{\alpha\nu\sqrt{\mathbf{d}}}{\sqrt{\operatorname{trace}\left(\prod\right)}}\left\|P_\tau\mathbf{e}_{u,h}^k\right\|_{L^2(\Gamma_{cd})}^2\right) \\
&+\left(\gamma_c^2-\gamma_d^2\right)\sum_{k=1}^{N}\left\|\mathbf{e}_{u,h}^k\cdot\mathbf{n}_{cd}\right\|_{L^2(\Gamma_{cd})}^2 + \frac{2\gamma_c}{\gamma_d}(\gamma_c+\gamma_d)\sum_{k=1}^{N}\frac{\sigma k_m}{\rho\mu}\left\|e_{m,h}^k - e_{f,h}^k\right\|_{L^2(\Omega_d)}^2 \\
&+\left[\frac{2\gamma_c}{\gamma_d}(\gamma_c+\gamma_d)\frac{k_m}{\rho\mu} - \left(\left(\frac{\gamma_c}{\gamma_d}\right)^2-1\right)4\gamma_d^2C_I^2h^{-1}\frac{k_m^2}{\mu^2}\right]\sum_{k=1}^{N}\left\|\nabla e_{m,h}^k\right\|_{L^2(\Omega_d)}^2 \\
&+\left[\left(\frac{2\gamma_c}{\gamma_d}-1\right)(\gamma_c+\gamma_d)\frac{k_f}{\rho\mu} - \left(\left(\frac{\gamma_c}{\gamma_d}\right)^2-1\right)4\gamma_d^2C_I^2h^{-1}\frac{k_f^2}{\mu^2} - \frac{1}{\rho^2}\left(\left(\frac{\gamma_c}{\gamma_d}\right)^2-1\right)\tilde{D}_t^2\right] \\
&\quad\sum_{k=1}^{N}\left\|\nabla e_{f,h}^k\right\|_{L^2(\Omega_d)}^2 \\
&\le \left(\frac{\gamma_c}{\gamma_d}\right)^2\left\|\varepsilon_{d,h}^1\right\|_{L^2(\Gamma_{cd})}^2 + \delta\left\|\varepsilon_{c,h}^1\right\|_{L^2(\Gamma_{cd})}^2 + (\gamma_c+\gamma_d)\frac{k_f}{\rho\mu}\left\|\nabla e_{f,h}^0\right\|_{L^2(\Omega_d)}^2,
\end{aligned} \tag{3.94}$$

which implies the convergence of $\mathbf{e}_{u,h}^k$, $e_{m,h}^k$ and $e_{f,h}^k$.

Next we derive a geometric convergence rate for Case 3. Plugging (3.34) into (3.35), using the inverse inequality (3.68) and trace inequality, and combining (3.47) and (3.48), we have

$$\begin{aligned}
&\left\|\varepsilon_{d,h}^{k+1}\right\|_{L^2(\Gamma_{cd})}^2 + \frac{1}{\rho^2}\left(\left(\frac{\gamma_c}{\gamma_d}\right)^2-1\right)\left\|e_{f,h}^{k-1}\right\|_{L^2(\Gamma_{cd})}^2 + \left(\gamma_c^2-\gamma_d^2\right)\left\|\mathbf{e}_{u,h}^k\cdot\mathbf{n}_{cd}\right\|_{L^2(\Gamma_{cd})}^2 \\
&= \left(\frac{\gamma_d}{\gamma_c}\right)^2\left\|\varepsilon_{d,h}^{k-1}\right\|_{L^2(\Gamma_{cd})}^2 + \left(\left(\frac{\gamma_c}{\gamma_d}\right)^2-\left(\frac{\gamma_d}{\gamma_c}\right)^2\right)\left\|\varepsilon_{d,h}^{k-1}\right\|_{L^2(\Gamma_{cd})}^2 \\
&\quad-\frac{2\gamma_c}{\rho}\left(1+\frac{\gamma_c}{\gamma_d}\right)\left(a_m\left(e_{m,h}^{k-1},e_{m,h}^{k-1}\right)+a_f\left(e_{f,h}^{k-1},e_{f,h}^{k-1}\right)\right. \\
&\quad\left.+\left(\frac{\sigma k_m}{\mu}\left(e_{m,h}^{k-1}-e_{f,h}^{k-1}\right),e_{m,h}^{k-1}-e_{f,h}^{k-1}\right)_{\Omega_d}\right) \\
&\quad-2(\gamma_c+\gamma_d)\left(c\left(\mathbf{e}_{u,h}^k,\mathbf{u}_h,\mathbf{e}_{u,h}^k\right)+c\left(\mathbf{u}_h,\mathbf{e}_{u,h}^k,\mathbf{e}_{u,h}^k\right)\right)-2(\gamma_c+\gamma_d)a_c\left(\mathbf{e}_{u,h}^k,\mathbf{e}_{u,h}^k\right) \\
&\quad-2(\gamma_c+\gamma_d)\frac{\alpha\nu\sqrt{\mathbf{d}}}{\sqrt{\operatorname{trace}\left(\prod\right)}}\left\langle P_\tau\left(\mathbf{e}_{u,h}^k+\frac{k_f}{\mu}\nabla e_{f,h}^{k-1}\right),P_\tau\mathbf{e}_{u,h}^k\right\rangle
\end{aligned}$$

$$
\begin{aligned}
&\leq \left(\frac{\gamma_d}{\gamma_c}\right)^2 \left\|\varepsilon_{d,h}^{k-1}\right\|_{L^2(\Gamma_{cd})}^2 + \left(\left(\frac{\gamma_c}{\gamma_d}\right)^2 - \left(\frac{\gamma_d}{\gamma_c}\right)^2\right) \left\|\varepsilon_{d,h}^{k-1}\right\|_{L^2(\Gamma_{cd})}^2 \\
&\quad - \frac{2\gamma_c}{\rho}\left(1+\frac{\gamma_c}{\gamma_d}\right)\left(\frac{k_m}{\mu}\|\nabla e_{m,h}^{k-1}\|_{L^2(\Omega_d)}^2 + \frac{k_f}{\mu}\|\nabla e_{f,h}^{k-1}\|_{L^2(\Omega_d)}^2\right. \\
&\quad \left. + \frac{\sigma k_m}{\mu}\left\|e_{m,h}^{k-1} - e_{f,h}^{k-1}\right\|_{L^2(\Omega_d)}^2\right) \\
&\quad - 2(\gamma_c+\gamma_d)\left(-\nu\left\|\mathbb{D}\left(\mathbf{e}_{u,h}^k\right)\right\|_{L^2(\Omega_c)}^2 + 2\nu\left\|\mathbb{D}\left(\mathbf{e}_{u,h}^k\right)\right\|_{L^2(\Omega_c)}^2\right) \\
&\quad - 2(\gamma_c+\gamma_d)\frac{\alpha\nu\sqrt{\mathbf{d}}}{\sqrt{\operatorname{trace}(\prod)}}\left\|P_\tau \mathbf{e}_{u,h}^k\right\|_{L^2(\Gamma_{cd})}^2 \\
&\quad - 2(\gamma_c+\gamma_d)\left(-\frac{\nu}{2}\left\|\mathbb{D}\left(\mathbf{e}_{u,h}^k\right)\right\|_{L^2(\Omega_c)}^2 - \frac{k_f}{2\rho\mu}\left\|\nabla e_{f,h}^{k-1}\right\|_{L^2(\Omega_d)}^2\right) \\
&\leq \left(\frac{\gamma_d}{\gamma_c}\right)^2 \left\|\varepsilon_{d,h}^{k-1}\right\|_{L^2(\Gamma_{cd})}^2 - \frac{2\gamma_c}{\rho}\left(1+\frac{\gamma_c}{\gamma_d}\right)\left(\frac{\sigma k_m}{\mu}\left\|e_{m,h}^{k-1} - e_{f,h}^{k-1}\right\|_{L^2(\Omega_d)}^2\right) \\
&\quad - 2(\gamma_c+\gamma_d)\frac{\alpha\nu\sqrt{\mathbf{d}}}{\sqrt{\operatorname{trace}(\prod)}}\left\|P_\tau \mathbf{e}_{u,h}^k\right\|_{L^2(\Gamma_{cd})}^2 \\
&\quad + \left(\left(\frac{\gamma_c}{\gamma_d}\right)^2 - \left(\frac{\gamma_d}{\gamma_c}\right)^2\right)\left[4\gamma_d^2 C_I^2 h^{-1}\left(\frac{k_m^2}{\mu^2}\left\|\nabla e_{m,h}^{k-1}\right\|_{L^2(\Omega_d)}^2 + \frac{k_f^2}{\mu^2}\left\|\nabla e_{f,h}^{k-1}\right\|_{L^2(\Omega_d)}^2\right)\right. \\
&\quad \left. + \frac{2\tilde{D}_t^2}{\rho^2}\left\|\nabla e_{f,h}^{k-1}\right\|_{L^2(\Omega_d)}^2\right] \\
&\quad - \frac{2\gamma_c}{\rho}\left(1+\frac{\gamma_c}{\gamma_d}\right)\left(\frac{k_m}{\mu}\|\nabla e_{m,h}^{k-1}\|_{L^2(\Omega_d)}^2\right) - \nu(\gamma_c+\gamma_d)\left\|\mathbb{D}\left(\mathbf{e}_{u,h}^k\right)\right\|_{L^2(\Omega_c)}^2 \\
&\quad - \frac{2\gamma_c}{\rho}\left(1+\frac{\gamma_c}{\gamma_d}\right)\frac{k_f}{\mu}\|\nabla e_{f,h}^{k-1}\|_{L^2(\Omega_d)}^2 + (\gamma_c+\gamma_d)\frac{k_f}{\rho\mu}\left\|\nabla e_{f,h}^{k-1}\right\|_{L^2(\Omega_d)}^2. \qquad (3.95)
\end{aligned}
$$

Then we have

$$
\begin{aligned}
&\left\|\varepsilon_{d,h}^{k+1}\right\|_{L^2(\Gamma_{cd})}^2 + \frac{1}{\rho^2}\left(\left(\frac{\gamma_c}{\gamma_d}\right)^2 - 1\right) \\
&\quad \left\|e_{f,h}^{k-1}\right\|_{L^2(\Gamma_{cd})}^2 + \left(\gamma_c^2 - \gamma_d^2\right)\left\|\mathbf{e}_{u,h}^k \cdot \mathbf{n}_{cd}\right\|_{L^2(\Gamma_{cd})}^2 + \nu(\gamma_c+\gamma_d)\left\|\mathbb{D}\left(\mathbf{e}_{u,h}^k\right)\right\|_{L^2(\Omega_c)}^2 \\
&\quad + \frac{2\gamma_c}{\rho}\left(1+\frac{\gamma_c}{\gamma_d}\right)\left(\frac{\sigma k_m}{\mu}\left\|e_{m,h}^{k-1} - e_{f,h}^{k-1}\right\|_{L^2(\Omega_d)}^2\right) + 2(\gamma_c+\gamma_d)\frac{\alpha\nu\sqrt{\mathbf{d}}}{\sqrt{\operatorname{trace}(\prod)}}\left\|P_\tau \mathbf{e}_{u,h}^k\right\|_{L^2(\Gamma_{cd})}^2 \\
&\leq \left(\frac{\gamma_d}{\gamma_c}\right)^2 \left\|\varepsilon_{d,h}^{k-1}\right\|_{L^2(\Gamma_{cd})}^2 \\
&\quad - \left[\frac{2\gamma_c}{\rho}\left(1+\frac{\gamma_c}{\gamma_d}\right)\frac{k_m}{\mu} - \left(\left(\frac{\gamma_c}{\gamma_d}\right)^2 - \left(\frac{\gamma_d}{\gamma_c}\right)^2\right)4\gamma_d^2\frac{C_I^2}{h}\frac{k_m^2}{\mu^2}\right]\left\|\nabla e_{m,h}^{k-1}\right\|_{L^2(\Omega_d)}^2
\end{aligned}
$$

$$-\left[\frac{2\gamma_c}{\rho}\left(1+\frac{\gamma_c}{\gamma_d}\right)\frac{k_f}{\mu}-\left(\left(\frac{\gamma_c}{\gamma_d}\right)^2-\left(\frac{\gamma_d}{\gamma_c}\right)^2\right)\left(4\gamma_d^2\frac{C_I^2}{h}\frac{k_f^2}{\mu^2}+\frac{2\tilde{D}_t^2}{\rho^2}\right)-(\gamma_c+\gamma_d)\frac{k_f}{\rho\mu}\right]\|\nabla e_{f,h}^{k-1}\|^2_{L^2(\Omega_d)}. \tag{3.96}$$

Assuming that

$$\left[\frac{2\gamma_c}{\rho}\left(1+\frac{\gamma_c}{\gamma_d}\right)\frac{k_m}{\mu}-\left(\left(\frac{\gamma_c}{\gamma_d}\right)^2-\left(\frac{\gamma_d}{\gamma_c}\right)^2\right)4\gamma_d^2\frac{C_I^2}{h}\frac{k_m^2}{\mu^2}\right]\geq 0, \tag{3.97}$$

$$\left[\frac{2\gamma_c}{\rho}\left(1+\frac{\gamma_c}{\gamma_d}\right)\frac{k_f}{\mu}-\left(\left(\frac{\gamma_c}{\gamma_d}\right)^2-\left(\frac{\gamma_d}{\gamma_c}\right)^2\right)\left(4\gamma_d^2\frac{C_I^2}{h}\frac{k_f^2}{\mu^2}+\frac{2\tilde{D}_t^2}{\rho^2}\right)-(\gamma_c+\gamma_d)\frac{k_f}{\rho\mu}\right]\geq 0, \tag{3.98}$$

which is equivalent to

$$0<\left(\frac{\gamma_c}{\gamma_d}-1\right)\left(2\frac{C_I^2}{h}\frac{k_m}{\nu}\gamma_d-\frac{\gamma_c^2}{\gamma_c^2+\gamma_d^2}\right)\leq\frac{\gamma_c^2}{\gamma_c^2+\gamma_d^2},$$

$$0<\left(\frac{\gamma_c}{\gamma_d}-1\right)\left(4\frac{C_I^2}{h}\frac{k_f}{\nu}\gamma_d+\tilde{D}_t^2\frac{\nu}{k_f}\frac{1}{\gamma_d}-2\frac{\gamma_c^2}{\gamma_c^2+\gamma_d^2}\right)\leq\frac{\gamma_c^2}{\gamma_c^2+\gamma_d^2}.$$

Then, considering (3.97) and (3.98) into (3.96), we obtain

$$\left\|\varepsilon_{d,h}^{k+1}\right\|^2_{L^2(\Gamma_{cd})}\leq\left(\frac{\gamma_d}{\gamma_c}\right)^2\left\|\varepsilon_{d,h}^{k-1}\right\|^2_{L^2(\Gamma_{cd})}$$

which implies the geometric convergence rate $\sqrt{\frac{\gamma_d}{\gamma_c}}$ for $\varepsilon_{d,h}^k$. The geometric convergence rate can be similarly obtained for the rest variables through same arguments at the end of proof in Theorem 3.4. □

Next, we deduce the possible range of Robin parameters which satisfy the restrictions (3.85)-(3.86) to ensure the convergence in the above theorem. From the first restriction (3.85), we can see that

$$\gamma_d\in\left[\frac{1}{2}\frac{h}{C_I^2}\frac{\nu}{k_m},+\infty\right)\text{ and }\gamma_c\in\left(\gamma_d,\frac{2\frac{C_I^2}{h}\frac{k_m}{\nu}\gamma_d}{2\frac{C_I^2}{h}\frac{k_m}{\nu}\gamma_d-1}\gamma_d\right]. \tag{3.99}$$

If γ_d is close to $\frac{1}{2}\frac{h}{C_I^2}\frac{\nu}{k_m}$, then γ_c will have a very wide range extended to $(\gamma_d,+\infty)$. In this situation, the range of the second restriction (3.86) is more decisive. It is easy to see that $4\frac{C_I^2}{h}\frac{k_f}{\nu}\gamma_d+\tilde{D}_t^2\frac{\nu}{k_f}\frac{1}{\gamma_d}-2$ has an extreme point on the positive semi-axis

$$\gamma_d=\sqrt{h}\frac{\tilde{D}_t}{2C_I}\frac{\nu}{k_f} \tag{3.100}$$

which also lies in the range of γ_d by (3.99) as $h\leq\frac{k_m^2}{k_f^2}C_I^2\tilde{D}_t^2$, and the corresponding minimum value is

$$\min_{\gamma_d>0}\left\{4\frac{C_I^2}{h}\frac{k_f}{\nu}\gamma_d+\tilde{D}_t^2\frac{\nu}{k_f}\frac{1}{\gamma_d}-2\right\}=4\frac{C_I\tilde{D}_t}{\sqrt{h}}-2 \tag{3.101}$$

which is positive for $h < 4C_I^2\tilde{D}_t^2$. Substituting the minimum value (3.101) into (3.86), we deduce

$$\frac{\gamma_c}{\gamma_d} - 1 \leq \frac{1}{4\frac{C_I^2}{h}\frac{k_f}{\nu}\gamma_d + \tilde{D}_t^2\frac{\nu}{k_f}\frac{1}{\gamma_d} - 2} \leq \frac{1}{4\frac{C_I\tilde{D}_t}{\sqrt{h}} - 2}. \tag{3.102}$$

Meanwhile, substituting the extreme point (3.100) into the term $2\frac{C_I^2}{h}\frac{k_m}{\nu}\gamma_d - 1$ in (3.85), we have

$$\frac{\gamma_c}{\gamma_d} - 1 \leq \frac{1}{2\frac{C_I^2}{h}\frac{k_m}{\nu}\gamma_d - 1} \leq \frac{\sqrt{h}}{\frac{k_m}{k_f}C_I\tilde{D}_t - \sqrt{h}}. \tag{3.103}$$

Then, for $\gamma_d > 0$, the range of γ_c is restricted by

$$\gamma_d \leq \gamma_c \leq \min\left\{\frac{4C_I\tilde{D}_t - \sqrt{h}}{4C_I\tilde{D}_t - 2\sqrt{h}}, \frac{\frac{k_m}{k_f}C_I\tilde{D}_t}{\frac{k_m}{k_f}C_I\tilde{D}_t - \sqrt{h}}\right\}\gamma_d. \tag{3.104}$$

Since $k_m \leq k_f$ in the Dual-Porosity model, the upper bound coefficient in (3.104) is actually

$$\min\left\{\frac{4C_I\tilde{D}_t - \sqrt{h}}{4C_I\tilde{D}_t - 2\sqrt{h}}, \frac{\frac{k_m}{k_f}C_I\tilde{D}_t}{\frac{k_m}{k_f}C_I\tilde{D}_t - \sqrt{h}}\right\} = \frac{4C_I\tilde{D}_t - \sqrt{h}}{4C_I\tilde{D}_t - 2\sqrt{h}} \tag{3.105}$$

for $h < \left(4 - \frac{k_m}{k_f}\right)^2 C_I^2\tilde{D}_t^2$. Finally, the range of Robin parameters decided by (3.85)-(3.86) is

$$\gamma_d \in \left[\frac{1}{2}\frac{h}{C_I^2}\frac{\nu}{k_m}, +\infty\right) \text{ and } \gamma_c \in \left(\gamma_d, \frac{4C_I\tilde{D}_t - \sqrt{h}}{4C_I\tilde{D}_t - 2\sqrt{h}}\gamma_d\right] \tag{3.106}$$

where $h \leq \frac{k_m^2}{k_f^2}C_I^2\tilde{D}_t^2$.

4 Numerical Examples

In this section, we will present three numerical experiments to verify the theoretical conclusions and demonstrate the features of the proposed model and method.

4.1 Convergence Tests

First we consider the model problem (2.1)-(2.8) on $\Omega = [0,1] \times [-0.25, 0.75]$ where the Dual-Porosity domain is $\Omega_d = [0,1] \times [0, 0.75]$ and the conduit domain is $\Omega_c = [0,1] \times [-0.25, 0]$. The interface between these two domains is $\Gamma_{cd} = (0,1) \times \{0\}$. The following exact solutions are used:

$$p_m = \left(y^2 - y^3\right)cos(x), \quad p_f = \left(e^y + e^{-y} - 2\right)sin(x), \quad (x,y) \in \Omega_d, \tag{4.1}$$

$$\mathbf{u} = \begin{pmatrix} \frac{k_f}{\mu}\left(\frac{1}{\pi}sin(2\pi y) - 2y\right)cos(x) \\ \frac{k_f}{\mu}\left(\frac{1}{\pi^2}sin^2(\pi y) - y^2\right)sin(x) \end{pmatrix}, \quad p = 0, \quad (x,y) \in \Omega_c. \tag{4.2}$$

Then the source terms and Dirichlet boundary conditions of the model are chosen such that the above functions are the exact solutions of the model. We use a uniform grid with grid size $h = 1/64$. The Taylor-Hood elements are used for the Navier–Stokes system and the quadratic finite elements are used for the Dual-Porosity system. The initial values of the iteration are randomly set between 0 and 1. The stopping criteria for the iteration is $\|\mathbf{u}_h^k - \mathbf{u}_h^{k-1}\|_{L^2(\Omega_c)} \leq 10^{-9}$ and the maximum iteration number is set to 20.

In this example, we present three tests with different model parameters to test the effect of Robin parameters on the convergence of domain decomposition method. In addition to the three cases $\gamma_c = \gamma_d$, $\gamma_c < \gamma_d$, and $\gamma_c > \gamma_d$ discussed in this paper, we also compare them with the optimized parameters which are just directly borrowed from the optimized Schwarz method for the steady-state Dual-Porosity-Stokes model with BJS condition (see more details in [52]). As mentioned in Remark 3.12, these parameters are not necessarily optimal for the Dual-porosity-Navier–Stokes model, and more refined future works are needed for this model, since this paper does not focus on the optimized Schwarz method.

We first investigate the performance of the proposed method for

test A $k_m = 10^{-3}, k_f = 10^{-1}, \mu = 1, \nu = 1, \rho = 1, \sigma = 0.5, \alpha = 1.$

In this case, the values of permeability k_f and viscosity ν are not small. According to Theorem 3.4 the choice of $\gamma_c < \gamma_d$ should be suitable and their constraints (3.39) and (3.40) are independent of mesh size. In this test, we consider two step sizes $h = 1/32,\ 1/64$. γ_c is set to 15 and γ_d is chosen to be one value in the set $\{5, 15, 30, 45\}$ for the comparison purpose. In this comparison, we also add the optimized Robin parameters from [52]: $\gamma_d = 201.0619$, $\gamma_c = 9.3302$ for $h = 1/32$ and $\gamma_d = 402.1239$, $\gamma_c = 9.3302$ for $h = 1/64$, which are computed through an optimal formula in [52] (see (3.48) in Theorem 3.5 of [52]). At each domain decomposition iteration step, the errors are computed between the finite element solution of the domain decomposition method and the coupled finite element solution. The L^2-norm convergence for the parallel scheme (Algorithm 3.1) with $h = 1/32$ is shown in Fig. 2. The figure for $h = 1/64$ is very similar, hence omitted here due to the page limitation. To compare the parallel scheme and the serial scheme (Algorithm 3.2), we correspondingly present the L^2-norm convergence of the serial scheme with $h = 1/32$ in Fig. 3. In this case, the serial scheme shows a little better convergence than the parallel scheme although they have similar convergence rate.

From these numerical results, we can see that the domain decomposition iterations are convergent to the conforming finite element solution as $\gamma_c \leq \gamma_d$. The optimized Robin parameters borrowed from [52] also work well for the Dual-Porosity-Navier–Stokes model in this case. In Fig. 4, we present the contour of the logarithm of error ratio $\|e_h^{20}\|_0/\|e_h^1\|_0$ computed by the parallel scheme with $(\gamma_c, \gamma_d) \in [0, 1000] \times [0, 1000]$. From the contour in Fig. 4, we see that for the relatively larger permeability and viscosity used in this case, $\gamma_c < \gamma_d$ does show better convergence, which is in accordance with the analysis in Theorem 3.4.

In Table 1, we also list the numerical results of $\gamma_d = 45,\ \gamma_c = 15$ at selected iteration steps to clearly compare the error and rate with different mesh sizes $h = 1/32,\ 1/64$. All the listed convergence rates are smaller than the corresponding theoretical geometric rate $\left(\sqrt{\frac{15}{45}}\right)^4 \approx 0.11$. Hence we observe that the geometric convergence rate is independent of mesh size as long as the convergence is guaranteed.

In order to test the robustness of the proposed method for small permeability, we consider

test B $k_m = 10^{-8}, k_f = 10^{-6}, \mu = 10^{-2}, \nu = 10^{-2}, \rho = 1, \sigma = 0.5, \alpha = 1.$

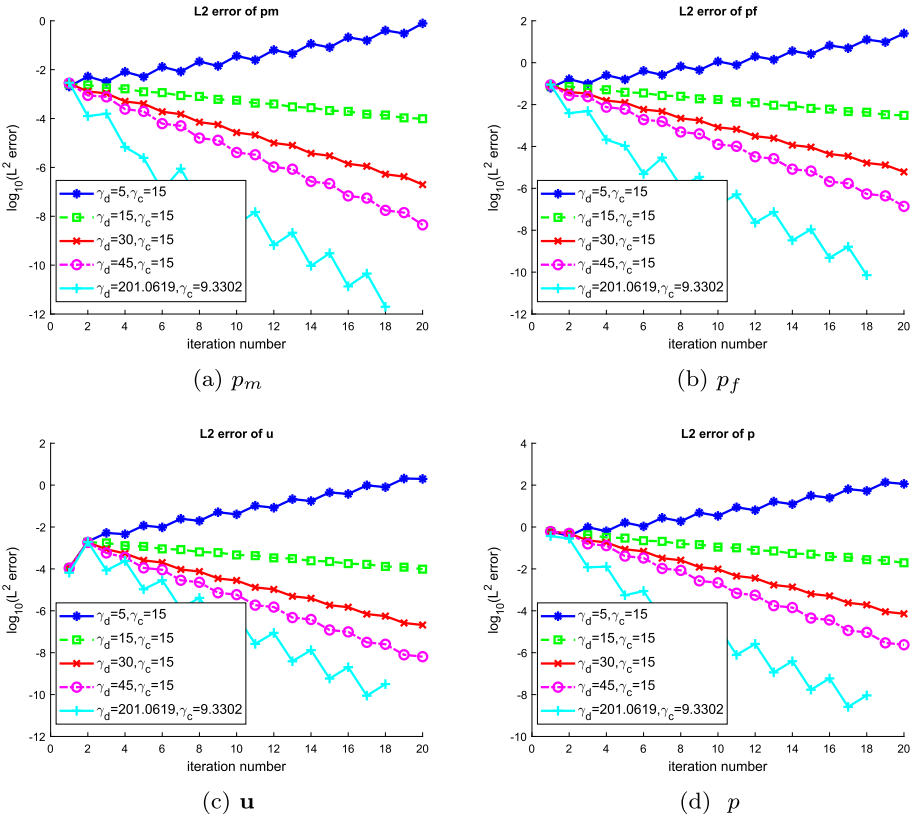

(a) p_m (b) p_f

(c) $\mathbf{u}$ (d) p

Fig. 2 Test A: L^2-norm errors of parallel DDM iterations with $h = 1/32$

Table 1 Test A: convergence error and rate of parallel DDM with $\gamma_c = 15$ and $\gamma_d = 45$

k	$\|\|e^k_{m,h}\|\|_1$	Rate	$\|\|e^k_{f,h}\|\|_1$	Rate	$\|\|\mathbf{e}^k_{u,h}\|\|_1$	Rate	$\|\|e^k_{p,h}\|\|_1$	Rate
Parallel DDM with $h = 1/64$								
8	1.5977e−5	–	4.9443e−4	–	2.3190e−5	–	8.5296e−3	–
12	1.0474e−6	0.0656	3.2414e−5	0.0656	1.5188e−6	0.0655	5.5927e−4	0.0656
16	6.8611e−8	0.0655	2.1233e−6	0.0655	9.9482e−8	0.0655	3.6637e−5	0.0655
20	4.4936e−9	0.0655	1.3907e−7	0.0655	6.5211e−9	0.0656	2.3998e−6	0.0655
Parallel DDM with $h = 1/32$								
8	1.5899e−5	–	4.9203e−4	–	2.3011e−5	–	8.5041e−3	–
12	1.0416e−6	0.0655	3.2235e−5	0.0655	1.5061e−6	0.0654	5.5734e−4	0.0655
16	6.8189e−8	0.0655	2.1103e−6	0.0655	9.8514e−8	0.0654	3.6486e−5	0.0655
20	4.4623e−9	0.0654	1.3810e−7	0.0654	6.4448e−9	0.0654	2.3876e−6	0.0654

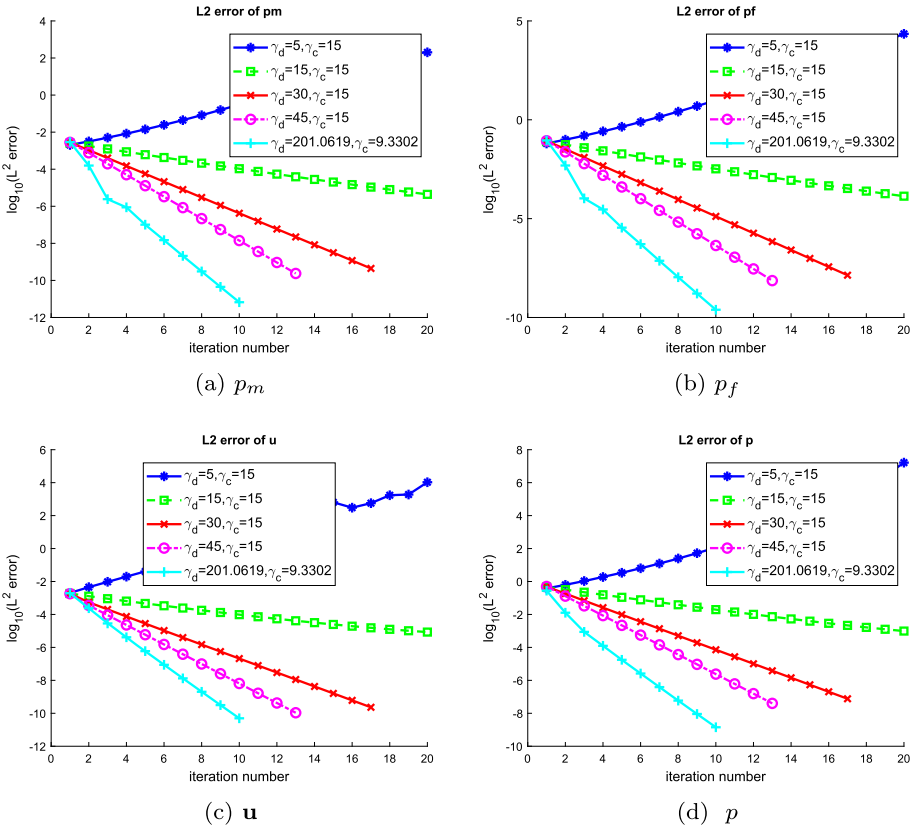

(a) p_m (b) p_f

(c) $\mathbf{u}$ (d) p

Fig. 3 Test A: L^2-norm errors of serial DDM iterations with $h = 1/32$

In this case, the value of permeability is much smaller than the previous case. According to Theorem 3.11, we consider $\gamma_c > \gamma_d$. To compare the parallel and serial schemes, the L^2-norm convergence with $h = 1/32$ are shown for them in Fig. 5. The parameter pair (γ_d, γ_c) is set to (10, 15), (50, 75), (100, 150), and (20, 450), respectively. Among these pair values, (20, 450) is very close to one of the local optimal parameters of the parallel scheme which can be observed in the contour of $\log\left(\|e_h^{20}\|_0\right)$ with $h = 1/32$ in Figs. 6.

From these numerical results, we can see the potential of the case $\gamma_c > \gamma_d$ for handling low permeability. By increasing the value of (γ_d, γ_c) from (10, 15) to (100, 150), the convergence of the parallel DDM is improved with the relatively bigger parameter (100, 150). This is consistent with the discussion in Remark 3.12 that a relatively large γ_d is more suitable in the case of small permeability. From the comparison between the parallel and serial schemes, it can be seen that the serial scheme does not necessarily have better convergence than the parallel scheme, and their local optimal parameters are quite different.

In Table 2, we list the numerical results of $\gamma_d = 100$, $\gamma_c = 150$ at selected iteration steps to compare the convergence error and rate of the parallel scheme under different mesh sizes $h = 1/32, 1/64$. All the listed convergence rates are smaller than or close to the corresponding theoretical geometric rate $\left(\sqrt{\frac{100}{150}}\right)^4 \approx 0.44$. Hence we observe that the geometric

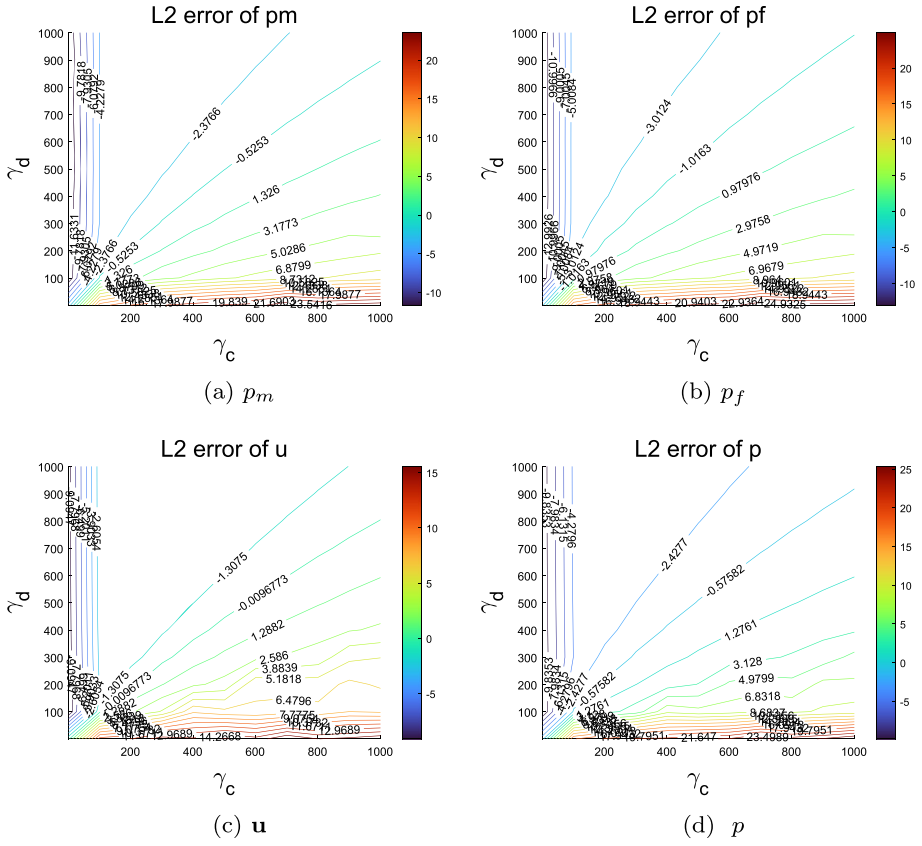

(a) p_m (b) p_f

(c) $\mathbf{u}$ (d) p

Fig. 4 Test A: contour of $\log\left(\|e_h^{20}\|_0/\|e_h^1\|_0\right)$ of parallel DDM with $(\gamma_c, \gamma_d) \in [0, 1000] \times [0, 1000]$

Table 2 Test B: convergence error and rate of parallel DDM with $\gamma_c = 150$ and $\gamma_d = 100$

k	$\|\|e^k_{m,h}\|\|_1$	rate	$\|\|e^k_{f,h}\|\|_1$	rate	$\|\|\mathbf{e}^k_{u,h}\|\|_1$	rate	$\|\|e^k_{p,h}\|\|_1$	rate
Parallel DDM with $h = 1/64$								
8	2.7133e−4	–	8.6401e−3	–	2.9091e−5	–	7.8258e−3	–
12	1.2180e−4	0.4489	3.8757e−3	0.4486	1.3122e−5	0.4511	3.4869e−3	0.4456
16	5.3510e−5	0.4393	1.7021e−3	0.4392	5.7994e−6	0.4420	1.5237e−3	0.4370
20	2.3071e−5	0.4312	7.3378e−4	0.4311	2.5209e−6	0.4347	6.5402e−4	0.4292
Parallel DDM with $h = 1/32$								
8	3.3616e−5	–	1.0866e−3	–	1.4904e−5	–	1.2930e−3	–
12	4.7847e−6	0.1423	1.5728e−4	0.1447	2.1549e−6	0.1446	1.8400e−4	0.1423
16	4.8739e−7	0.1019	1.7579e−5	0.1118	3.0823e−7	0.1430	1.8745e−5	0.1019
20	2.6241e−8	0.0538	2.0536e−6	0.1168	9.5615e−8	0.3102	1.0500e−6	0.0560

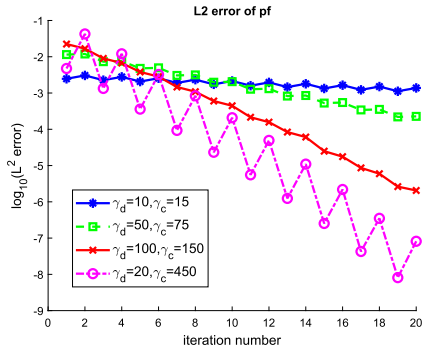

(a) parallel DDM: p_f

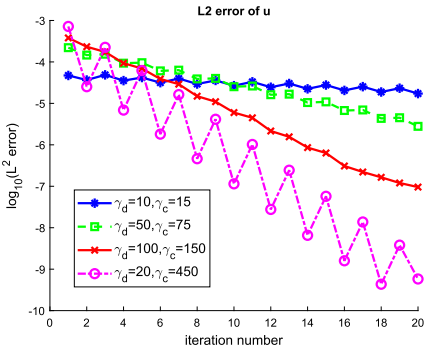

(b) parallel DDM: $\mathbf{u}$

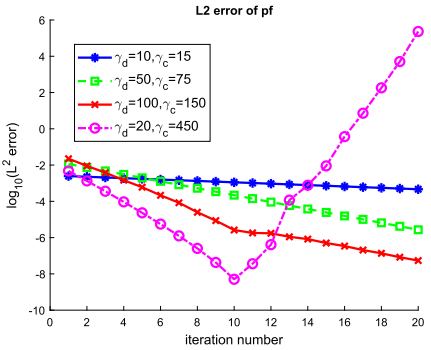

(c) serial DDM: p_f

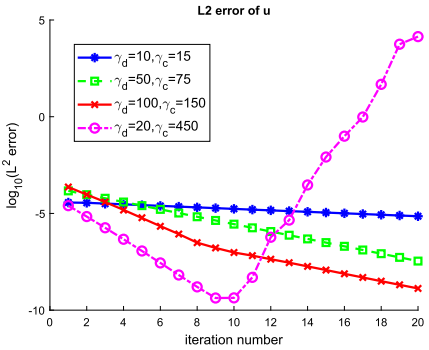

(d) serial DDM: $\mathbf{u}$

Fig. 5 Test B: L^2-norm errors of DDM iterations with $h = 1/32$

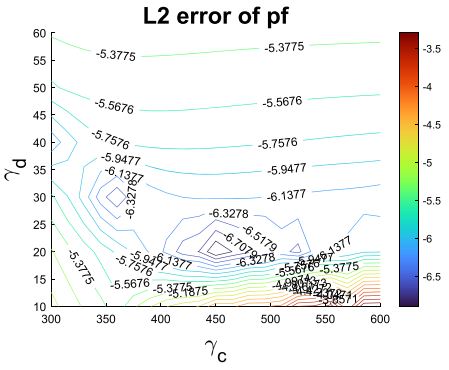

(a) p_f

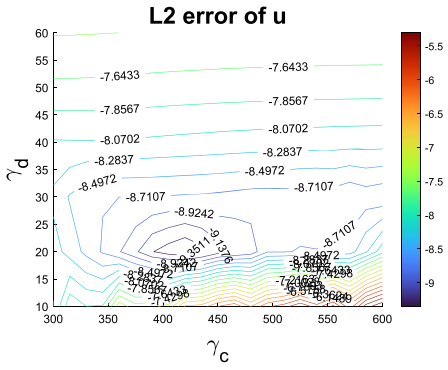

(b) $\mathbf{u}$

Fig. 6 Test B: contour of $\log\left(\|e_h^{20}\|_0\right)$ for parallel DDM to seek local optimal Robin parameters

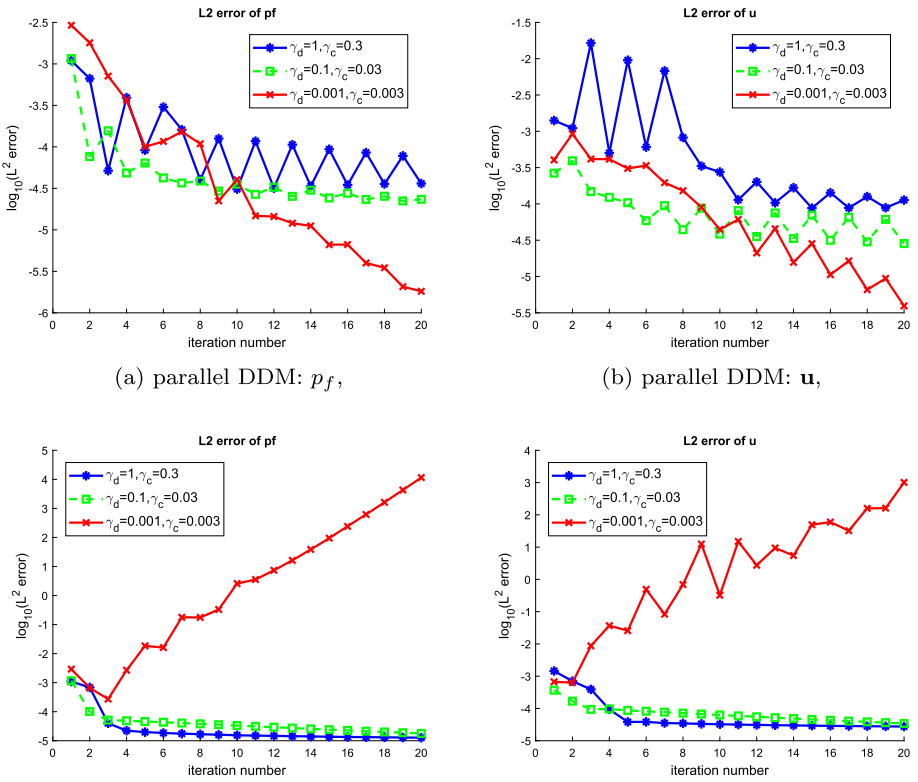

(a) parallel DDM: p_f, (b) parallel DDM: $\mathbf{u}$,

(c) serial DDM: p_f, (d) serial DDM: $\mathbf{u}$

Fig. 7 Test C: L^2-norm errors of parallel and serial DDM iterations with $h = 1/32$

convergence rate is independent of mesh size as long as the convergence is guaranteed. However, according to Remark 3.12, the constraints (3.85)-(3.88) in Theorem 3.11 depend on both the model parameters and the mesh size. Thus the range of suitable Robin parameters and the local optimal parameter values will change with different mesh sizes.

In the third case, we test the small viscosity $\nu = 10^{-6}$.

test C $k_m = 10^{-6}, k_f = 10^{-4}, \mu = 10^{-3}, \nu = 10^{-6}, \rho = 10^3, \sigma = 1, \alpha = 1.$

The pairs of (γ_d, γ_c) used in this case are set to $(1, 0.3)$, $(0.1, 0.03)$, $(0.001, 0.003)$. The mesh size is $h = 1/32$. The L^2-norm convergence for the parallel and serial schemes are given in Fig. 7. One can see that the convergence of the parallel DDM is gradually improved by reducing the value of Robin parameters. This is in accordance with the discussion in Remark 3.12 that a relatively small γ_d is more suitable for small ν. Meanwhile, the convergence of the serial DDM is not improved for the same group of parameters. This also indicates that the serial scheme does not necessarily have better convergence than the parallel scheme.

4.2 Cross-Flow Membrane Filtration Problem

In this example, we test the cross-flow membrane filtration problem [44, 52]. The contiguous domains are set to $\Omega_c = [0, 0.015] \times [0.0025, 0.0075]$ and $\Omega_d = [0.0035, 0.0105] \times$

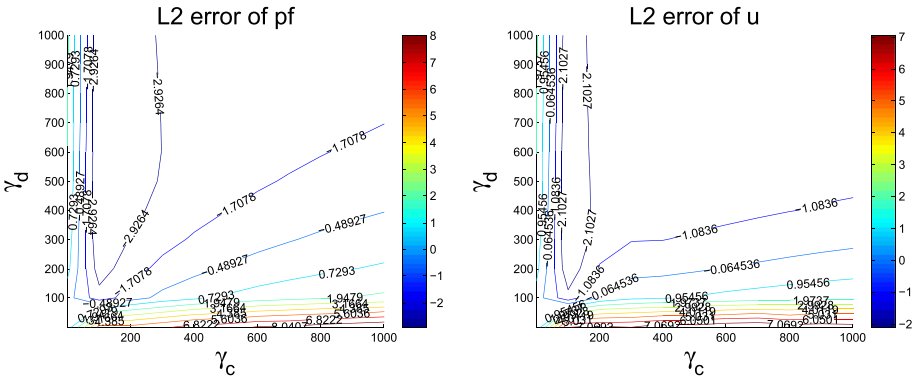

(a) p_f (b) $\mathbf{u}$

Fig. 8 Contour of $\log\left(\|e_h^{10}\|_0/\|e_h^1\|_0\right)$ with $(\gamma_c, \gamma_d) \in [0, 1000] \times [0, 1000]$

$[0, 0.0025]$, and the interface is $\Gamma_{cd} = [0.0035, 0.0105] \times 0.0025$. The boundary conditions are set as follows:

$$\mathbf{u} = (16000y^2 - 160y + 0.3, 0)^T \text{ on } \Gamma_c^{in} = \{0\} \times (0.0025, 0.0075), \tag{4.3}$$

$$\mathbb{T}(\mathbf{u}, p)\mathbf{n}_{cd} = 0 \text{ on } \Gamma_c^{out} = \{0.015\} \times (0.00625, 0.0075), \tag{4.4}$$

$$\mathbf{u} = 0 \text{ on } \partial\Omega_c \setminus (\Gamma_c^{in} \cup \Gamma_c^{out} \cup \Gamma_{cd}), \tag{4.5}$$

$$p_m = p_f = 0 \text{ on } \Gamma_d^b = (0.0035, 0.0105) \times \{0\}, \tag{4.6}$$

$$-\frac{k_m}{\mu}\nabla p_m \cdot (-\mathbf{n}_{cd}) = 0 \text{ on } \partial\Omega_c \setminus (\Gamma_d^b \cup \Gamma_{cd}), \tag{4.7}$$

$$-\frac{k_f}{\mu}\nabla p_f \cdot (-\mathbf{n}_{cd}) = 0 \text{ on } \partial\Omega_c \setminus (\Gamma_d^b \cup \Gamma_{cd}). \tag{4.8}$$

We use the following parameters in the simulation, $k_m = 10^{-9}$, $k_f = 10^{-7}$, $\mu = 10^{-2}$, $\rho = 1$, $\nu = 10^{-2}$, $\sigma = 0.5$, $\alpha = 0.1$. In Fig. 8, we present the contour of $\log\left(\|e_h^{10}\|_0/\|e_h^1\|_0\right)$ with $(\gamma_c, \gamma_d) \in [0, 1000] \times [0, 1000]$. From the numerical results, it can be seen that $\gamma_c < \gamma_d$ performs better than $\gamma_c = \gamma_d$ and $\gamma_c > \gamma_d$. In Fig. 9, we draw the velocities in conduit obtained by the domain decomposition method with two sets of Robin parameters that are opposite to each other, and compare with the velocity obtained by the coupled finite element (CFE) solution. Among the selected parameters, the velocity of the domain decomposition method with $\gamma_c = 100 < \gamma_d = 300$ is much closer to the velocity of the coupled finite element solution than that of the domain decomposition method with $\gamma_c = 300 > \gamma_d = 100$. The numerical results in Fig. 9 are compatible with the observations in Fig. 8.

4.3 Multistage Fractured Horizontal Wellbore

In this example, we simulate the flow around a five-stage fractured horizontal wellbore with cased hole completion, see [49] for the details of setup of geometries and interfac/boundary conditions. The simulation domain is the rectangle $[0, 10] \times [0, 6]$ and the horizontal wellbore is simplified as a smaller rectangle $[2.75, 7.25] \times [2.8, 3.2]$ embedded in this domain. The inhomogeneous Dirichlet boundary conditions are imposed on the outer boundaries of Ω_d, such that $p_{fh} = 100$ and $p_{mh} = 10$. The smallest spatial step size is about $h \approx 0.079$. The

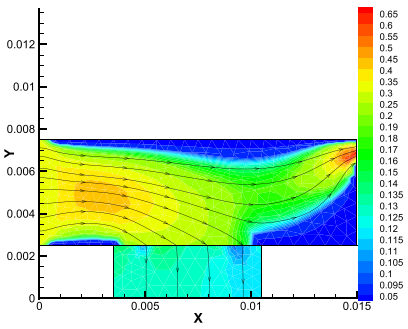

(a) CFE

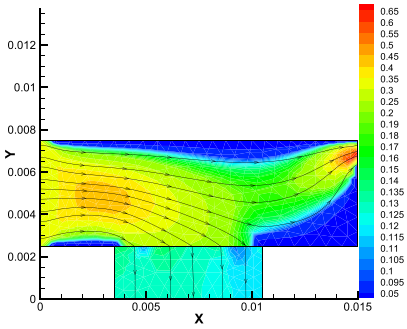

(b) DDM: $\gamma_c = 100$ $\gamma_d = 300$

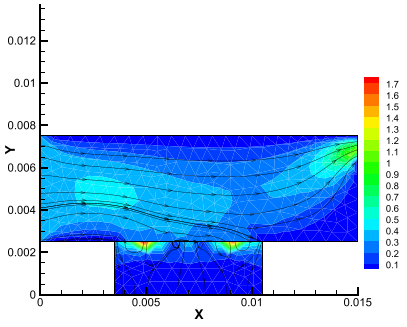

(c) DDM: $\gamma_c = 300$ $\gamma_d = 100$

Fig. 9 Comparison of velocities between CFE and DDM

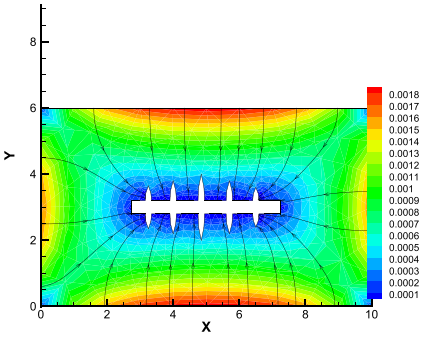

(a) velocity streamline in matrix

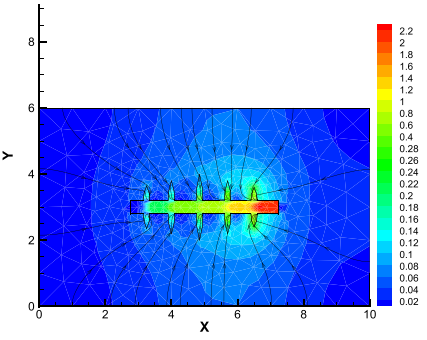

(b) velocity streamline in micro-fractures and conduits

Fig. 10 Velocities of DDM with $\gamma_c = 100$ and $\gamma_d = 200$

model parameters including rock and fluid properties used in the simulation are: permeability $k_m = 10^{-5}$, $k_f = 10^{-2}$, viscosity $\mu = 0.1, \nu = 0.1$, fluid density $\rho = 1$, and other parameters $\sigma = 0.1, \alpha = 1$.

The velocities solved by the domain decomposition method with $\gamma_c = 100$ and $\gamma_d = 200$ are draw in Fig. 10. The fluid in the matrix doesn't communicate with conduits but feeds the micro-fractures. The five-stage hydraulic fractures form attractions and the fluid in the micro-fractures can flow into the hydraulic fractures. The vertical wellbore is assumed

to be connected to the right end of horizontal wellbore, so the fluid in conduits does not communicate with the porous media but directly flows out of the horizontal well into the assumed vertical wellbore. With cased hole completion, the horizontal wellbore is only fed by the hydraulic fractures but does not directly communicate with the dual-porosity media flows. These results are physically valid and consistent with the investigation in [49].

5 Conclusions

In this article, we developed a parallel Robin–Robin domain decomposition method to numerically solve the Dual-Porosity-Navier–Stokes model with the Beavers–Joseph interface condition. This model describes the confined flow in porous media by the Dual-Porosity equations and the free flow in conduits by Navier-Stokes equation. And then the two flows are coupled through four physically valid interface conditions. The resulting coupled Dual-Porosity-Navier–Stokes model has higher fidelity than either the Dual-Porosity or Navier–Stokes systems on their own. However, coupling the two constituent models leads to a very complex system. Then the Robin–Robin domain decomposition method is constructed based on the interface conditions of Dual-Porosity-Navier–Stokes model. In both the theoretical analysis and the numerical experiments, we found that the Robin parameters depend on and are sensitive to the physical data. Both the analysis and numerical experiments demonstrate that with proper Robin parameters the domain decomposition solutions converge to the solution of the coupled system. The effect of Robin boundary on the convergence is investigated by considering different values of γ_c and γ_d in the examples.

Funding The first author is partially supported by NSFC grants 11701451 and 11931013. The third and fourth authors are partially supported by NSF grant DMS-1722647.

Data Availability The datasets generated during and/or analysed during the current study are available from the corresponding author on reasonable request.

Code Availability Custom code.

Declarations

Conflict of interest The authors have no conflicts of interest to declare that are relevant to the content of this article.

References

1. Discacciati, M.: Domain decomposition methods for the coupling of surface and groundwater flows. PhD thesis, Ecole Polytechnique Fédérale de Lausanne, Switzerland (2004)
2. Arbogast, T., Brunson, D.S.: A computational method for approximating a Darcy–Stokes system governing a vuggy porous medium. Comput. Geosci. **11**(3), 207–218 (2007)
3. Ervin, V.J., Jenkins, E.W., Sun, S.: Coupled generalized nonlinear Stokes flow with flow through a porous medium. SIAM J. Numer. Anal. **47**(2), 929–952 (2009)
4. Ambartsumyan, I., Khattatov, E., Wang, C., Yotov, I.: Stochastic multiscale flux basis for Stokes–Darcy flows. J. Comput. Phys. **401**, 109011 (2020)
5. Arbogast, T., Hesse, M.A., Taicher, A.L.: Mixed methods for two-phase Darcy–Stokes mixtures of partially melted materials with regions of zero porosity. SIAM J. Sci. Comput. **39**(2), B375–B402 (2017)
6. Çeşmelioğlu, A., Rivière, B.: Existence of a weak solution for the fully coupled Navier–Stokes/Darcy-transport problem. J. Differ. Equ. **252**(7), 4138–4175 (2012)

7. Chen, J., Sun, S., Wang, X.: A numerical method for a model of two-phase flow in a coupled free flow and porous media system. J. Comput. Phys. **268**, 1–16 (2014)
8. Chidyagwai, P., Rivière, B.: On the solution of the coupled Navier–Stokes and Darcy equations. Comput. Methods Appl. Mech. Eng. **198**(47–48), 3806–3820 (2009)
9. Diegel, A.E., Feng, X., Wise, S.M.: Analysis of a mixed finite element method for a Cahn–Hilliard–Darcy–Stokes system. SIAM J. Numer. Anal. **53**(1), 127–152 (2015)
10. Gao, Y., Han, D., He, X.-M., Rüde, U.: Unconditionally stable numerical methods for Cahn–Hilliard–Navier–Stokes–Darcy system with different densities and viscosities. J. Comput. Phys. **454**, 110968 (2022)
11. Gao, Y., He, X.-M., Mei, L., Yang, X.: Decoupled, linear, and energy stable finite element method for the Cahn–Hilliard–Navier–Stokes–Darcy phase field model. SIAM J. Sci. Comput. **40**(1), B110–B137 (2018)
12. Girault, V., Rivière, B.: DG approximation of coupled Navier–Stokes and Darcy equations by Beaver–Joseph–Saffman interface condition. SIAM J. Numer. Anal **47**(3), 2052–2089 (2009)
13. Han, D., Wang, X., Wu, H.: Existence and uniqueness of global weak solutions to a Cahn–Hilliard–Stokes–Darcy system for two phase incompressible flows in karstic geometry. J. Differ. Equ. **257**(10), 3887–3933 (2014)
14. He, X.-M., Jiang, N., Qiu, C.: An artificial compressibility ensemble algorithm for a stochastic Stokes–Darcy model with random hydraulic conductivity and interface conditions. Int. J. Numer. Meth. Eng. **121**(4), 712–739 (2020)
15. Jiang, N., Qiu, C.: An efficient ensemble algorithm for numerical approximation of stochastic Stokes–Darcy equations. Comput. Methods Appl. Mech. Eng. **343**, 249–275 (2019)
16. Shan, L., Hou, J., Yan, W., Chen, J.: Partitioned time stepping method for a dual-porosity-Stokes model. J. Sci. Comput. **79**, 389–413 (2019)
17. Yang, Z., Ming, J., Qiu, C., He, X.-M., Li, M.: A multigrid multilevel Monte Carlo method for Stokes–Darcy model with random hydraulic conductivity and Beavers–Joseph condition. J. Sci. Comput. **90**, 68 (2022)
18. Zhao, B., Zhang, M., Liang, C.: Global well-posedness for Navier–Stokes–Darcy equations with the free interface. Int. J. Numer. Anal. Mod. **18**, 569–619 (2021)
19. Al Mahbub, Md. A., He, X.-M., Nasu, N.J., Qiu, C., Zheng, H.: Coupled and decoupled stabilized mixed finite element methods for non-stationary dual-porosity-Stokes fluid flow model. Int. J. Numer. Meth. Eng. **120**(6), 803–833 (2019)
20. Armentano, M.G., Stockdale, M.L.: Approximations by mini mixed finite element for the Stokes–Darcy coupled problem on curved domains. Int. J. Numer. Anal. Mod. **18**, 203–234 (2021)
21. Ervin, V.J., Jenkins, E.W., Lee, H.: Approximation of the Stokes–Darcy system by optimization. J. Sci. Comput. **59**(3), 775–794 (2014)
22. Girault, V., Vassilev, D., Yotov, I.: Mortar multiscale finite element methods for Stokes–Darcy flows. Numer. Math. **127**(1), 93–165 (2014)
23. Boubendir, Y., Tlupova, S.: Domain decomposition methods for solving Stokes–Darcy problems with boundary integrals. SIAM J. Sci. Comput. **35**(1), B82–B106 (2013)
24. Cai, M., Mu, M., Xu, J.: Numerical solution to a mixed Navier–Stokes/Darcy model by the two-grid approach. SIAM J. Numer. Anal. **47**(5), 3325–3338 (2009)
25. Cao, Y., Gunzburger, M., He, X.-M., Wang, X.: Parallel, non-iterative, multi-physics domain decomposition methods for time-dependent Stokes–Darcy systems. Math. Comp. **83**(288), 1617–1644 (2014)
26. Chen, W., Gunzburger, M., Hua, F., Wang, X.: A parallel Robin–Robin domain decomposition method for the Stokes–Darcy system. SIAM. J. Numer. Anal. **49**(3), 1064–1084 (2011)
27. Discacciati, M., Miglio, E., Quarteroni, A.: Mathematical and numerical models for coupling surface and groundwater flows. Appl. Numer. Math. **43**(1–2), 57–74 (2002)
28. Layton, W.J., Schieweck, F., Yotov, I.: Coupling fluid flow with porous media flow. SIAM J. Numer. Anal. **40**(6), 2195–2218 (2002)
29. Qiu, C., He, X.-M., Li, J., Lin, Y.: A domain decomposition method for the time-dependent Navier–Stokes–Darcy model with Beavers–Joseph interface condition and defective boundary condition. J. Comput. Phys. **411**, 109400 (2020)
30. Zhang, Y., Zhou, C., Qu, C., Wei, M., He, X.-M., Bai, B.: Fabrication and verification of a glass–silicon–glass micro-nanofluidic model for investigating multi-phase flow in unconventional dual-porosity porous media. Lab Chip **19**, 4071–4082 (2019)
31. Barenblatt, G.E., Zheltov, I.P., Kochina, I.N.: Basic concepts in the theory of homogeneous liquids in fissured rocks. J. App. Math. Mech. **24**, 1286–1303 (1960)
32. Warren, J.E., Root, P.J.: The behavior of naturally fractured reservoirs. Soc. Petrol. Eng. J. **3**(3), 245–255 (1963)

33. Alahmadi, H.A.H.: A triple-porosity model for fractured horizontal wells. PhD thesis, Texas A&M University (2010)
34. Lim, K.T., Aziz, K.: Matrix-fracture transfer shape factors for dual-porosity simulators. J. Petrol. Sci. Eng. **13**, 169–178 (1995)
35. Pruess, K., Narasimhan, T.: A practical method for modeling fluid and heat flow in fractured porous media. SPE J. **25**, 14–26 (1985)
36. Dietrich, P., Helmig, R., Sauter, M., Hötzl, H., Köngeter, J., Teutsch, G.: Flow and Transport in Fractured Porous Media. Springer, Berlin (2005)
37. Bukač, M., Yotov, I., Zunino, P.: Dimensional model reduction for flow through fractures in poroelastic media. Esaim Math. Model. Numer. Anal. **51**(4), 1429–1471 (2017)
38. Ambartsumyan, I., Ervin, V.J., Nguyen, T., Yotov, I.: A nonlinear stokes–biot model for the interaction of a non-newtonian fluid with poroelastic media. Esaim Math. Model. Numer. Anal. **53**(6), 1915–1955 (2019)
39. Guo, C., Wang, J., Wei, M., He, X.-M., Bai, B.: Multi-stage fractured horizontal well numerical simulation and its application in tight shale reservoirs. SPE-176714, SPE Russian Petroleum Technology Conference, Moscow, Russia (2015)
40. Beavers, G., Joseph, D.: Boundary conditions at a naturally permeable wall. J. Fluid Mech. **30**, 197–207 (1967)
41. Hou, J., Qiu, M., He, X.-M., Guo, C., Wei, M., Bai, B.: A dual-porosity-Stokes model and finite element method for coupling dual-porosity flow and free flow. SIAM J. Sci. Comput. **38**(5), B710–B739 (2016)
42. Cao, Y., Gunzburger, M., Hu, X., Hua, F., Wang, X., Zhao, W.: Finite element approximation for Stokes–Darcy flow with Beavers–Joseph interface conditions. SIAM. J. Numer. Anal. **47**(6), 4239–4256 (2010)
43. Cao, Y., Gunzburger, M., Hua, F., Wang, X.: Coupled Stokes–Darcy model with Beavers–Joseph interface boundary condition. Comm. Math. Sci. **8**(1), 1–25 (2010)
44. Discacciati, M., Gerardo-Giorda, L.: Optimized Schwarz methods for the Stokes–Darcy coupling. IMA J. Numer. Anal. **38**(4), 1959–1983 (2018)
45. Discacciati, M., Quarteroni, A., Valli, A.: Robin-Robin domain decomposition methods for the Stokes–Darcy coupling. SIAM J. Numer. Anal. **45**(3), 1246–1268 (2007)
46. Gunzburger, M., He, X.-M., Li, B.: On Ritz projection and multi-step backward differentiation schemes in decoupling the Stokes–Darcy model. SIAM J. Numer. Anal. **56**(1), 397–427 (2018)
47. He, X.-M., Li, J., Lin, Y., Ming, J.: A domain decomposition method for the steady-state Navier–Stokes–Darcy model with Beavers–Joseph interface condition. SIAM J. Sci. Comput. **37**(5), S264–S290 (2015)
48. Liu, Y., Boubendir, Y., He, X.M., He, Y.: New optimized Robin-Robin domain decomposition methods using Krylov solvers for the Stokes–Darcy system. SIAM J. Sci. Comput. **44**(4), B1068–B1095 (2022)
49. Hou, J., Hu, D., He, X.M., Qiu, C.: Modeling and a Robin-type decoupled finite element method for dual-porosity-Navier–Stokes system with application to flows around multistage fractured horizontal wellbore. Comput. Meth. Appl. Mech. Eng. **388**, 114248 (2022)
50. Jäger, W., Mikelič, A,: On the interface boundary condition of Beavers, Joseph, and Saffman. SIAM J. Appl. Math. **60**(4), 1111–1127 (2000)
51. Saffman, P.: On the boundary condition at the interface of a porous medium. Stud. Appl. Math. **1**, 77–84 (1971)
52. Hou, J., Yan, W., Hu, D., He, Z.: Robin-Robin domain decomposition methods for the dual-porosity-conduit system. Adv. Comput. Math. **47**(7), 1–33 (2021)
53. Cao, Y., Gunzburger, M., He, X.-M., Wang, X.: Robin-Robin domain decomposition methods for the steady Stokes–Darcy model with Beaver–Joseph interface condition. Numer. Math. **117**(4), 601–629 (2011)
54. Liu, Y., He, Y., Li, X., He, X.-M.: A novel convergence analysis of Robin–Robin domain decomposition method for Stokes–Darcy system with Beavers–Joseph interface condition. Appl. Math. Lett. **119**, 107181 (2021)
55. Girault, V., Raviart, P. A.: Finite Element Methods for Navier–Stokes equations. Theory and algorithms, vol. 5 of Springer Series in Computational Mathematics. Springer-Verlag, Berlin (1986)
56. Gunzburger, M.: Finite Element Methods for Viscous Incompressible Flows. A Guide to Theory, Practice, and Algorithms.Computer Science and Scientific Computing. Academic Press, Boston (1989)
57. Temam, R.: Navier–Stokes Equations. Theory and Numerical Analysis. AMS Chelsea Publishing, Providence, RI, reprint of the 1984 edition (2001)
58. Qiu, M., Qing, F., Yu, X., Hou, J., Li, D., Zhao, X.: Finite element method for the stationary dual-porosity Navier–Stokes system with Beavers–Joseph interface conditions. Comput. Math. Appl. (2023). https://doi.org/10.1016/j.camwa.2023.01.015
59. Badea, L., Discacciati, M., Quarteroni, A.: Numerical analysis of the Navier–Stokes/Darcy coupling. Numer. Math. **115**(2), 195–227 (2010)

60. Çeşmelioğlu, A., Girault, V., Rivière, B.: Time-dependent coupling of Navier–Stokes and Darcy flows. ESAIM Math. Model. Numer. Anal. **47**(2), 539–554 (2013)
61. Brenner, S.C., Scott, L.R.: The Mathematical Theory of Finite Element Methods. Springer-Verlag, New York (1994)